HARVARD UNIVERSITY
Graduate School of Arts and Sciences

DISSERTATION ACCEPTANCE CERTIFICATE

The undersigned, appointed by the

Division of Medical Sciences

in the subject of Biological and Biomedical Sciences

have examined a dissertation entitled

Characterization and functional modulation of the cancer stem cell state in colorectal cancer

presented by Priscilla Cheung

candidate for the degree of Doctor of Philosophy and hereby certify that it is worthy of acceptance.

Signature: Alex Toker

Typed Name: Dr. Alex Toker

Signature: Yingzi Yang

Typed Name: Dr. Yingzi Yang

Signature: Ya-Chieh Hsu

Typed Name: Dr. Ya-Chieh Hsu

Signature:

Typed Name: Dr. Ophir Klein

Date: April 23, 2021

Characterization and functional modulation of the cancer stem cell state in colorectal cancer

A DISSERTATION PRESENTED

BY

PRISCILLA CHEUNG

TO

THE DIVISION OF MEDICAL SCIENCES

IN PARTIAL FULFILLMENT OF THE REQUIREMENTS

FOR THE DEGREE OF

DOCTOR OF PHILOSOPHY

IN THE SUBJECT OF

BIOLOGICAL AND BIOMEDICAL SCIENCES

HARVARD UNIVERSITY

CAMBRIDGE, MASSACHUSETTS

APRIL 2021

Dissertation Advisor: Professor Fernando Camargo Priscilla Cheung

Characterization and functional modulation of the cancer stem cell state in colorectal cancer

Abstract

Colorectal cancer (CRC) is the second leading cause of death among cancer patients in the United States and is characterized by a high degree of intratumor heterogeneity, which likely contributes to the difficulty in curative treatments and its common recurrence. Transplantation and lineage tracing studies have identified a subset of tumor cells, *Lgr5*+ cancer stem cells, as a driver of tumor progression in CRC, but recent studies suggest plasticity of the cancer stem cell state. Thus, the role of distinct tumor cell states in the progression of CRC remains unclear. Furthermore, no inhibitors against Wnt signaling, the most commonly mutated pathway driving CRC, have been approved for use in the clinic, underscoring the need for orthogonal approaches for the treatment of this disease. Studies have shown that activation of the Hippo transcriptional coactivator YAP inhibits Wnt in the intestine, but whether YAP behaves as a tumor suppressor in CRC by suppressing this pathway remains unknown. Here we demonstrate that activation of YAP through Hippo kinase inhibition reprograms intestinal stem cells into a wound-healing-like cell state that is low in Wnt and cannot self-renew. Leveraging this finding, we found that loss of the LATS1/2 Hippo kinases or activation of YAP is sufficient to reprogram colon cancer stem cells to this state and thereby suppress both tumor growth and initiation in organoids, patient-derived xenografts, and mouse models

of primary and metastatic CRC, establishing the role of YAP as a tumor suppressor in the adult colon. Complimentary to these genetic studies, we have developed small molecule inhibitors against LATS1/2, which we found to suppress the growth of CRC organoids. Altogether, this body of work provides a deeper understanding of the mechanistic underpinnings driving progression of colorectal malignancies, paving the way for the translation of these findings to novel therapeutics.

Table of Contents

Title Page i

Copyright Page ii

Abstract iii

Table of Contents v

Acknowledgements vii

Dedication x

1 Introduction 1

1.1 Overview of the intestine 2
1.2 Overview of colorectal cancer 4
1.3 Role of Hippo signaling in intestinal homeostasis and cancer 9
1.4 Outlook 15

2 Requirement of Hippo kinases in the maintenance of intestinal homeostasis 16

2.1 Abstract 17
2.2 Attributions 17
2.3 Introduction 18
2.4 Results 19
2.5 Discussion 32
2.6 Materials and Methods 35

3 YAP as a tumor suppressive program in metastatic colorectal cancer 47

3.1 Abstract 48
3.2 Attributions 48
3.3 Introduction 49
3.4 Results 50
3.5 Discussion 74
3.6 Materials and Methods 76
4 Pharmacological targeting of the LATS1/2 Hippo kinases in colorectal cancer 90
4.1 Abstract 91
4.2 Attributions 91
4.3 Introduction 92
4.4 Results 93
4.5 Discussion 97
4.6 Materials and Methods 99
5 Conclusion 103
5.1 Overview of Results 104
5.2 Discussion 104
5.3 Future Directions 108
5.4 Conclusion 110
References 111

Acknowledgements

The PhD journey (and science in general) is full of failures with short glimpses of success. My journey through this PhD would not have been possible without all the incredible people who have supported and mentored me over the years.

First, I would like to thank my thesis advisor Fernando Camargo for instilling in me a level of scientific rigor, intellectual curiosity, and drive to persevere. Thank you for giving me the opportunity to pursue my PhD in the lab, taking me on when I was a not-so-confident G2, giving me the freedom to try some cool things that did not end up in this dissertation, and supporting and encouraging me throughout.

I am grateful for all my mentors and advisors over the years. To members of my dissertation advisory committee Alex Toker, Carla Kim, and Omer Yilmaz for advising and guiding my scientific work. To my dissertation defense examiners Alex Toker, Yingzi Yang, Ya-Chieh Hsu, and Ophir Klein for taking the time to read my dissertation and being a part of this special time in my life. I would like to extend special thanks to Alex Toker for serving as chair of both committees.

I would also like to thank my mentors who played an important part in my scientific journey: first to Courtney Broaddus for taking me as a young undergraduate,

who knew next to nothing about science and my postdoc mentor in the lab Dario Barbone for believing in me; to Lin He for taking me as an undergraduate research assistant and giving me the opportunity to learn from two incredible postdocs Amy Li and Paul Lin; to Patrick Li for the career/life advice and friendship over the years; and to Em Ho for being my industry mentor.

I would like to extend special thanks to my collaborators Craig Thomas and Michele Ceribelli for all their work on the LATS1/2 inhibitors.

I am grateful for all the members of the Camargo laboratory, who have provided me with an intellectual and nurturing environment for me to grow as a scientist. I would like to extend special thanks to Jordi Xiol with whom I worked closely with for part of this dissertation and during the early years of my PhD. To Dejan Maglic for teaching me how to work with organoids during my rotation. To Wei-chien Yuan for teaching me many techniques and Michael Dill for reading all my fellowship proposals. I'd also like to thank all the other lab members past and present for their contributions, insights, and support -- Jianlong Sun, Dean Yimlamai, Constantina Christodoulou, Basanta Gurung, Riccardo Panero, Shelly Zing Chin Lum, Fernando Garcia-Osorio, Aubrey Plumb, Sarah Bowling, Alejo Rodriguez-Fraticelli, Sophia Shalhout, Li Li, Jacquelyn Russell, Walatta-Tseyon Mesquitta, Mark Ferreira, Edward Quach, and Qi Yu. To my fellow graduate students Brian Pepe-Mooney, Sachin Patel, and Debra Van Egeren for leading the way and sharing a part of this PhD journey together.

To all my friends near and far, with whom I have been fortunate to meet and grow together, thank you. Thank you for keeping me sane when science got hard. I would like to extend my thanks to those I have met during my time here at Harvard - my Elite fam: Qi Yu, Sarah Bowling, Aaron Moye, and Julio Sainz de Aja; my BBS PhD cohort; Atsushi

Taguchi, Rebeca Borges, Cristina Jayson, Steve Burger for all the game and wine nights; Manav Gupta and Shuchi Gupta for all the beers and travels; Brandon Sit and Maggie Chen for hotpot nights. A special thanks to Nishita Mohan, my first BBS friend, and Shikha Sheth, my 397 roommate of many years.

To Jonathan - thank you for all your encouragement and support. You were always there to cheer me on every step of the way. Thank you for all your selflessness, for helping me in any way that you can. I am excited for this next chapter of our life and am happy that I get to share it with you.

Finally, and above all, I would like to thank my family. To my brother Kevin for the joy of sharing our childhood together and teaching me about the real world outside of academia. To my parents for all your unconditional support and encouragement, your sacrifices in coming to a new country, and your selflessness in giving me and my brother the opportunity of an education. Thank you for letting me pursue my own dreams. I most certainly would not be here without you.

For my family.

1

Introduction

1.1 Overview of the intestine

The intestine is the major organ in the body that carries out essential absorptive, barrier, and endocrine functions, continuously withstanding insults from the external environment (Gehart & Clevers, 2019). To counteract these stresses, the intestine constantly renews its epithelial lining to regenerate all the diverse intestinal cell types important for homeostatic functions. Key to balancing the intestine's absorptive and barrier functions is its crypt-villus structure and high proliferation.

Containing millions of crypt-villus units, the intestine is composed of villi, which are finger-like protrusions out of the intestinal epithelium surrounded by multiple invaginations called crypts of Lieberkühn (Gehart & Clevers, 2019). These villi along the intestinal tract increase the surface area and thereby the absorptive capacity of the intestine (Gehart & Clevers, 2019). However, this structure also exposes the intestinal epithelium to harsh environmental stresses, resulting in the epithelium getting turned over every 3-5 days (Darwich et al., 2014; Peterson & Artis, 2014). Core to this cellular turnover is the highly proliferative *Lgr5*+ intestinal stem cells (ISCs) found at the bottom of these crypts (Barker et al., 2007), a positioning which protects the stem cells from the hazardous digestive environment above (Gehart & Clevers, 2019). They can self-renew and give rise to short-lived progenitors called transit amplifying (TA) cells, which may then differentiate into many of the absorptive (enterocytes) or secretory (goblet, enteroendocrine, and Paneth cells) mature cell types as the TA cells move out of the crypt (Gehart & Clevers, 2019). ISCs require high levels of Wnt signaling to maintain their stemness, signals which are produced by the Paneth or deep crypt secretory cells in the niche of the small intestine or colon, respectively (Sasaki et al., 2016; Sato et al., 2011). Indeed, embryonic deletion of the Wnt transcription factor TCF4 prevents development

of crypts in mice (Korinek et al., 1998). Wnt antagonists (Kuhnert et al., 2004; Ordóñez-Morán et al., 2015; Pinto et al., 2003) as well as conditional deletion of Wnt signals through β-catenin (Fevr et al., 2007) or the TCF4 transcription factor (van Es et al., 2012) lead to loss of proliferative crypts. Because Wnt signals do not travel far beyond the niche, a gradient of Wnt signaling forms along this crypt-villus axis (Gregorieff & Clevers, 2005), which causes the ISCs to differentiate into mature intestinal cell types as they get pushed out of the crypt. Thus, maintaining this gradient of Wnt signaling is essential for normal crypt structure and ISC function.

1.1.1 Wnt signaling and cancer

Wnt signaling is mediated by the transcriptional activity of β-catenin. In the absence of Wnt signals, β-catenin is bound to the β-catenin destruction complex, which consists of the scaffolding protein Axin, two serine/threonine kinases CK1 and GSK3α/β, and the tumor suppressor APC (Behrens et al., 1998; Kimelman & Xu, 2006). In this complex, β-catenin is sequentially phosphorylated by CK1 and GSK3α/β at the N-terminus (Amit et al., 2002; Liu et al., 2002), which targets β-catenin for proteasomal degradation by the E3 ubiquitin ligase β-TrCP (Aberle et al., 1997; Hart et al., 1999). In the presence of Wnt ligands, which bind to the Frizzled and LRP5/6 receptor complex (Bhanot et al., 1996; Pinson et al., 2000; K Tamai et al., 2000; Wehrli et al., 2000), the scaffolding protein Dishevelled is recruited to the receptor (Tauriello et al., 2012; Wallingford & Habas, 2005), which leads to a series of phosphorylation events on the cytoplasmic tail of LRP and sequestration of Axin away from the β-catenin destruction complex (MacDonald et al., 2009; Keiko Tamai et al., 2004). These events altogether stabilize β-catenin and allow it to translocate to the nucleus, where it can displace the

transcriptional repressor Groucho and bind to the TCF family of transcription factors, activating downstream target genes associated with proliferation and stemness (Behrens et al., 1996; Cavallo et al., 1998; Clevers, 2006; Molenaar et al., 1996; Roose et al., 1998). R-spondin, a secreted Wnt agonist, can potentiate Wnt signaling by binding to LGR receptors and inducing phosphorylation of LRP6 and clearance of the E3 ligases RNF43/ZNRF3, which target Frizzled and LRP6 for proteasomal degradation (Carmon et al., 2011; de Lau et al., 2011; Hao et al., 2012; Koo et al., 2012).

Dysregulation of Wnt leads to colorectal cancer initiation and progression in humans. In particular, inactivation of the gene *APC* is found in 50-70% of sporadic colon cancer patients and results in stabilization of β-catenin and constitutive activation of Wnt signaling (Cancer Genome Atlas Network, 2012; Walther et al., 2009). Thus, targeting Wnt could be a therapeutic strategy for treatment of these cancers. However, due to the role of Wnt in tissue homeostasis and regeneration in many organs, there are currently no Wnt inhibitors approved for use in the clinic (Kahn, 2014). Furthermore, many of the Wnt inhibitors target upstream of APC, which would limit their use in patients with *APC* mutant colon tumors (Kahn, 2014). As such, approaches targeting β-catenin or orthogonal inhibition through crosstalk with another pathway are needed for the treatment of CRC (Kahn, 2014).

1.2 Overview of colorectal cancer

Colorectal cancer (CRC) is the second leading cause of cancer-related deaths in the United States with an estimated 150,000 new cases diagnosed and estimated 50,000 deaths in 2021 (Siegel, Miller, Goding Sauer, et al., 2020). While the incidence of CRC has been declining for several decades due to early screening and removal of colon polyps and

improvements in treatments, an estimated 20% of patients present with metastatic disease and 50% of patients with localized disease develop metastases (Siegel, Miller, & Jemal, 2020). Once diagnosed with metastatic disease, the five-year survival rate for these patients is 14% (Siegel, Miller, Goding Sauer, et al., 2020), underscoring the need to develop better targeted therapies.

CRC develops in a stepwise manner though an accumulation of genetic and epigenetic changes in oncogenes and tumor suppressors that drive the transformation of a benign colon polyp to an adenocarcinoma (Fearon, 2011; Fearon & Vogelstein, 1990). This progression, termed the adenoma-carcinoma sequence, posits that tumor initiation and distinct stages of tumor progression are driven by particular driver events. About 90% of CRCs are initiated by mutations that result in hyperactivation of the Wnt signaling pathway, predominantly through mutations or loss of heterozygosity in the tumor suppressor APC (Cancer Genome Atlas Network, 2012; Fearon, 2011; Fearon & Vogelstein, 1990; Gerstung et al., 2020). This is often followed by mutations that cause oncogenic activation of the MAPK pathway and inactivation of TGFβ signaling and TP53 (Fearon, 2011; Fearon & Vogelstein, 1990; Gerstung et al., 2020). Because this stepwise accumulation of mutations is thought to be responsible for driving colon polyps to advanced stage cancers, growth within a tumor has been suggested to be driven by fitness selection and clonal expansion (Nowell, 1976).

1.2.1 Intratumor heterogeneity in colorectal cancer

However, this sequential clonal evolution does not describe the extensive intratumor heterogeneity evident in CRC (Punt et al., 2016), which is the variability in cellular phenotypes and function between subpopulations of tumor cells within the same

tumor (Almendro et al., 2013; Marusyk et al., 2012; McGranahan & Swanton, 2015). This heterogeneity was first identified over 25 years ago with the finding that clones of different ploidies were present within the same tumor (Wersto et al., 1991). In recent years, sequencing studies have revealed an additional layer of genetic heterogeneity at a spatial level (T. M. Kim et al., 2015; Sottoriva et al., 2015). CRC cells of the same genetic background were demonstrated to exhibit functional variability in proliferation, persistence, and chemotherapeutic response (Kreso et al., 2013). Furthermore, cancer stem cells, a rare population of "stem-like" cells within the tumor (P Dalerba et al., 2007; O'Brien et al., 2007; Ricci-Vitiani et al., 2007), have been suggested to contribute to phenotypic heterogeneity through multilineage differentiation processes (Piero Dalerba et al., 2011).

This variability in the histology, transcriptional signatures, genetic background (Heitzer et al., 2013; C. Yu et al., 2014), and metastatic and proliferative potential has many important implications, especially for advanced stage cancers. Because tumors are heterogeneous, individual biopsies taken from a tumor may not be representative of the entire tumor, preventing the study and treatment of cancer. Different cancer cells will also have varied responses to therapy, and thus treatment may leave behind microscopic residual disease and lead to relapse (Siravegna et al., 2015). As such, understanding the biology of CRC development, in particular which tumor cells are fated to contribute to disease progression and the mechanisms underlying their contributions to tumor growth, will help better inform future therapeutic strategies.

1.2.2 Colon cancer stem cells

Numerous studies have identified a subset of tumor cells in CRC to drive tumor progression. Based on the seminal study in acute myeloid leukemia establishing the idea of cancer stem cells (Lapidot et al., 1994), serial transplantation assays first identified $CD133^+$ colon tumor cells to have the capacity to form tumors following subcutaneous injection of these cells into immunocompromised mice (O'Brien et al., 2007; Ricci-Vitiani et al., 2007). Subsequent studies identified additional markers, including $EpCAM^{high}/CD44^+/CD166^+$ (P Dalerba et al., 2007), $ALDH^+$ (E. H. Huang et al., 2009), $EphB2^{high}$ (Merlos-Suárez et al., 2011), and *Lgr5*$^+$ (Cortina et al., 2017; Kemper, Prasetyanti, et al., 2012), to mark cancer stem cells in CRC. However, these xenotransplantation studies are artificial as cancer cells are isolated from their host environment and introduced into a new hostile environment, where cancer cells might need to adapt to engraft and initiate new tumors. Furthermore, these markers such as CD133 may not be reliable or specific and can change in different genetic and epigenetic contexts (P Dalerba et al., 2007; Jeon et al., 2010; Kemper, Versloot, et al., 2012; Shmelkov et al., 2008).

Lineage tracing studies subsequently validated the existence of cancer stem cells in CRC to arise *de novo* and propagate tumors. In murine intestinal and colonic adenomas and CRC, stem cell activity was shown to lie within certain subpopulations of cells within the tumor (De Sousa E Melo et al., 2017; Goto et al., 2019; Nakanishi et al., 2013; Roper et al., 2017; Schepers et al., 2012). Molecular clocks and lineage tracing methods in human adenomas and CRC have also revealed stem cell activity (Cortina et al., 2017; Goto et al., 2019; Humphries et al., 2013; Shimokawa et al., 2017; Siegmund & Marjoram, 2009; Sottoriva et al., 2013). Furthermore, targeting of these populations appeared to inhibit

tumor growth and, in some studies, metastasis (De Sousa E Melo et al., 2017; Goto et al., 2019; Shimokawa et al., 2017), suggesting that these cancer stem cells could be clinically relevant. Unexpectedly in the studies that targeted the *Lgr5*+ population, this tumor regression was found to be temporary as the differentiated tumor cells were able to regenerate the cancer stem cell population once *Lgr5*+ cell depletion therapy was discontinued (De Sousa E Melo et al., 2017; Shimokawa et al., 2017). Another study also found that the cancer cells disseminating to the liver were *Lgr5*- and once in the liver re-established the *Lgr5* differentiation hierarchy (Fumagalli et al., 2020), indicating that this cell state is plastic.

Furthermore, other works indicate that the cancer stem cell state in CRC is also microenvironmentally defined. Wnt activity was found to characterize the cancer stem cell population and observed to mark tumor cells near the stroma (Vermeulen et al., 2010). These and other signals from the stroma were demonstrated to induce stem cell properties in the differentiated tumor cell population (Lotti et al., 2013; Todaro et al., 2014; Vermeulen et al., 2010). Recent lineage tracing studies showed that tumor expansion is driven by cancer cells at the edge of the tumor irrespective of expression of stem cell markers, which was found to be influenced by secreted factors from cancer associated fibroblasts (Lamprecht et al., 2017; Lenos et al., 2018). Most recently, colorectal cancer cells were found to be hierarchically organized by their protein synthesis activity and in zones with those in close proximity to the stroma with high biosynthetic capacity and Wnt activity (Morral et al., 2020), supporting the idea that targeting properties of the cancer stem cell phenotype and plasticity is of greater importance than candidate populations themselves (Piskol & de Sousa e Melo, 2020). Because of these

different factors affecting cancer stem cells, the role of distinct tumor cell states in the progression of CRC remains unclear.

1.3 Role of Hippo signaling in intestinal homeostasis and cancer

1.3.1 Overview of Hippo signaling

A major pathway known to interact with Wnt in the intestine is the Hippo signaling pathway, a highly conserved signaling cascade important in organ size control. This signaling pathway was first discovered in *D. melanogaster* in a series of mosaic genetic screens, which identified the Hippo pathway components Hippo (Hpo) (Harvey et al., 2003; Jia et al., 2003; Pantalacci et al., 2003; Udan et al., 2003; Wu et al., 2003), Salvador (Sav) (Kango-Singh, 2002; Tapon et al., 2002), and Warts (Wts) (Justice et al., 1995; Xu et al., 1995) when perturbed to be associated with tissue overgrowth phenotypes characterized by increased cell proliferation and reduced cell death. Subsequent work established that Hpo together with its partner Sav phosphorylates and activates Wts and its partner Mats (Harvey et al., 2003; Lai et al., 2005; Pantalacci et al., 2003; Udan et al., 2003; Wei et al., 2007; Wu et al., 2003), which in turn phosphorylate and inactivate the major downstream effector of the pathway Yorkie (Yki) (J. Huang et al., 2005; Wu et al., 2008). Phosphorylation of Yki causes it to be sequestered in the cytoplasm, where it cannot bind to the transcription factor Scalloped (Sd) and promote transcription of genes involved in cell proliferation (J. Huang et al., 2005; Thompson & Cohen, 2006; Wu et al., 2008).

The corresponding orthologs were identified to be highly conserved in mammals. Like in *Drosophila*, the mammalian Hippo pathway consists of a core kinase cascade MST1/2 (homologs of Hpo) and LATS1/2 (homologs of Wts), which act to regulate the

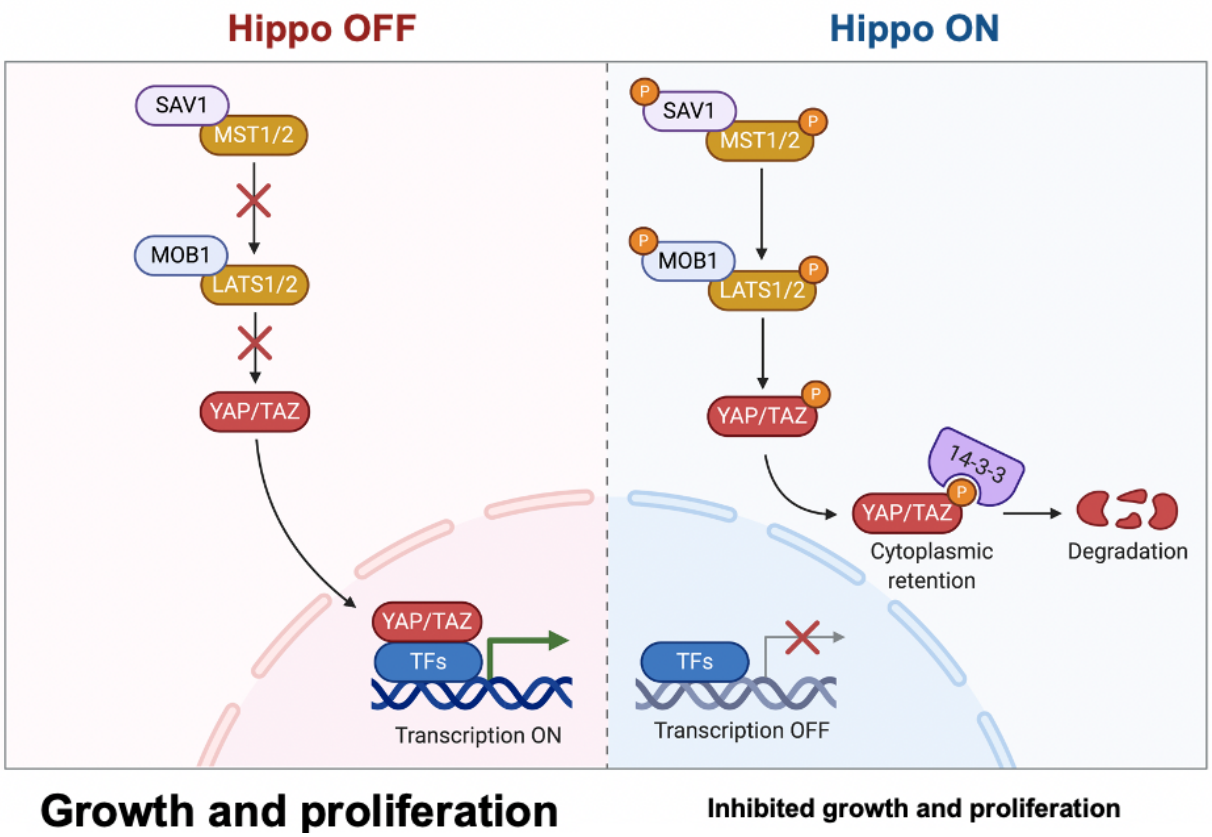

Figure 1.2. YAP/TAZ as downstream effectors of the Hippo pathway. Left, When Hippo signaling is off, YAP/TAZ can translocate into the nucleus and activate transcription of target genes through TEAD1-4 binding and concomitant chromatin remodeling. **Right,** When Hippo signaling is active, the kinase cascade phosphorylates YAP/TAZ, causing their cytoplasmic retention and eventual degradation.

major downstream transcriptional effectors of the pathway YAP (YAP1) and its paralog TAZ (WWTR1) (both homologues of Yki). When the Hippo pathway is on through a number of external signals, MST1/2 together with SAV1 phosphorylate MOB1A/B (homologues of Mats) and LATS1/2 (Callus et al., 2006; Chan et al., 2005; Praskova et al., 2008; Tapon et al., 2002; Wu et al., 2003), which in turn phosphorylate and inhibit the activity and stability of YAP/TAZ through cytoplasmic sequestration via 14-3-3 and interaction with the E3 ligase $SCF^{\beta\text{-}TRCP}$ (Dong et al., 2007; Lei et al., 2008; Zhao et al., 2007) (**Figure 1.2 Right**). YAP is directly phosphorylated by LATS1/2 at 5 consensus HXRXXS motifs (Zhao et al., 2007, 2010) - when the serines are mutated to alanines, YAP cannot be phosphorylated and is active, with the 5SA mutant being more active than the single S127A mutant (Zhao et al., 2009). When these sites are non-phosphorylated, YAP/TAZ can enter the nucleus and displace VGLL4, preventing its inhibition of the TEAD family of transcription factors (Jiao et al., 2014; W. Zhang et al., 2014) (**Figure 1.2 Left**). They bind to proximal promoters and distal enhancers of target genes, recruiting other factors and remodeling chromatin to activate transcription of genes involved in cell proliferation, cell adhesion, and cell migration (Galli et al., 2015; Lian et al., 2010; Stein et al., 2015; Zanconato et al., 2015). Indeed, these signaling components have been shown to regulate organ size in mammals—activation of *Yap* expression or inactivation of upstream components in mice leads to an abnormal, dramatic expansion of many organs, including liver (Camargo et al., 2007; Dong et al., 2007; Yin et al., 2013; N. Zhang et al., 2010; Zhou et al., 2009) and heart (Del Re et al., 2013; Heallen et al., 2011; Lin et al., 2014; von Gise et al., 2012; Xin et al., 2011, 2013).

1.3.2 Role of Hippo signaling in intestinal homeostasis

In the intestine, YAP is expressed in the nucleus of cells at the bottom of the crypt whereas YAP is more cytoplasmic in the villi (Barry et al., 2013; Camargo et al., 2007; Zhou et al., 2011), indicating a role of YAP in the regulation of intestinal stem cells. Early work suggested that YAP activation through ubiquitous overexpression of the S127A mutant or developmental deletion of Mst1/2 or Sav1 via *Villin-Cre* leads to expansion of the intestinal stem cell compartment and defects in differentiation through potentiation of Wnt signaling (Cai et al., 2010; Zhou et al., 2009), suggesting a role for YAP in proliferation and expansion of progenitors in the intestine. Barry et al. on the other hand observed loss of proliferative crypts and downregulation of Wnt target gene expression upon intestinal-specific YAP expression (Barry et al., 2013), confirmed separately by Gregorieff et al. in YAP-expressing organoids (Gregorieff et al., 2015). Furthermore, YAP loss results in Wnt hypersensitivity to R-spondin1, a potent secreted Wnt agonist that promotes crypt proliferation (Barry et al., 2013; K. A. Kim et al., 2005; Ootani et al., 2009), indicating a growth suppressive function of YAP. Interestingly, intestinal-specific deletion of YAP has no effect on the intestine (Barry et al., 2013; Cai et al., 2010; Zhou et al., 2011), suggesting that YAP is dispensable for normal homeostasis. These opposing observations are likely due to differences in experimental models used and the timing of YAP activation.

On the other hand, YAP is indispensable and required for mucosal regeneration in different models of intestinal and colonic injury. Many groups observed that YAP levels are upregulated during tissue repair following dextran sulfate sodium (DSS)-induced colitis or irradiation (Cai et al., 2010; Gregorieff et al., 2015; Yui et al., 2018). Following DSS treatment, mice with intestinal-specific YAP deletion experience crypt loss and

increased mortality compared to that of wildtype (Cai et al., 2010). A similar reduction in crypt proliferation was also observed in Yap knockout mice 3 days following irradiation (Gregorieff et al., 2015), which is in contrast to the crypt hyperplasia observed at 7 days post irradiation (Barry et al., 2013). In the short term, YAP knockout leads to Wnt-driven differentiation of Paneth cells and loss of intestinal stem cells following injury but induces hyperplasia in the long term due to excessive Wnt signaling (Hong et al., 2016). These findings indicated that YAP plays divergent roles at different time points after injury depending on the cellular processes involved as regeneration is known to occur in different phases (Hong et al., 2016). Further studies revealed that YAP mediates regeneration by remodeling stem cells (Gregorieff et al., 2015), activating expression of a fetal intestinal program (Yui et al., 2018), and expanding quiescent stem cells (Ayyaz et al., 2019) that accompany the loss of intestinal stem cells and Paneth cells and drop in Wnt signaling upon injury (Nusse et al., 2018). Following intestinal organoid growth *in vitro*, Serra et al. observed a switch from nuclear YAP in the early stages after seeding, mimicking regeneration, to variable YAP subcellular localization at later stages of organoid formation, which drives the formation of the first Paneth cell (Serra et al., 2019). These observations may provide a model for how the regenerating epithelium is able to restore proliferative crypts from a Wnt low state that is induced by injury.

1.3.3 Hippo-Wnt crosstalk

All these studies above indicate that Hippo signaling is highly interconnected with the Wnt pathway to regulate intestinal homeostasis and regeneration. Early studies suggested that YAP potentiates Wnt signaling as evidenced by increased levels of nuclear β-catenin and expression of Wnt target genes upon YAP overexpression or MST1/2

knockout (Camargo et al., 2007; Zhou et al., 2009). Other studies reported a role for cytoplasmic YAP in inhibiting Wnt signaling. YAP/TAZ was shown to be a part of the APC destruction complex and help retain β-catenin in the cytoplasm, facilitating its degradation by β-TrCP (Azzolin et al., 2014; Imajo et al., 2012). YAP/TAZ was also found to interact with Dishevelled, a Wnt positive regulator, thereby inhibiting Wnt signaling (Barry et al., 2013; Varelas et al., 2010). Reciprocally, both canonical and non-canonical Wnt signaling can also induce YAP/TAZ activity (Azzolin et al., 2012, 2014; Konsavage et al., 2012; Park et al., 2015). From these studies, the interaction between the Hippo and Wnt signaling pathways is quite complex and is yet to be fully appreciated.

1.3.4 Role of Hippo signaling in colorectal cancer

As Wnt signaling is commonly hyperactivated in CRC, crosstalk with the Hippo pathway could have tremendous implications on the progression of the disease. Intestinal-specific deletion of upstream Hippo components MST1/2 or Sav1 was found to lead to adenoma formation (Cai et al., 2010; Zhou et al., 2011). Furthermore, in both the Apc^{Min} and intestinal-specific Cre or CreERT2 $Apc^{fl/fl}$ mouse models, YAP deletion in these mice abolished adenoma formation (Azzolin et al., 2014; Cai et al., 2015; Gregorieff et al., 2015), suggesting a possible oncogenic role for YAP in CRC. Indeed, studies of human patient CRC samples revealed that YAP/TAZ levels are positively correlated with advanced stage cancer and poor prognosis (Lam-Himlin et al., 2006; Steinhardt et al., 2008; Wang et al., 2013; Yuen et al., 2013; Zhou et al., 2011). In a number of human colon cancer cell lines, knockdown of YAP inhibited their proliferation, metastasis, and invasion (Konsavage et al., 2012; Rosenbluh et al., 2012; Wang et al., 2013; Zhou et al., 2011). Barry et al. revisited these results found that YAP expression suppressed tumor growth in

xenograft experiments, and loss of YAP expression in a subset of human CRC was associated with poor prognosis and high grade disease (Barry et al., 2013). Further work discovered that the function of LATS1/2 in cancer cell growth is cell type-dependent - knockout of LATS1/2 in the murine MC38 colon cancer cell line inhibited its growth in contrast to the pro-proliferative effect observed in other cell lines (Pan et al., 2019). Taken together, these contrasting findings suggest that the role of YAP in the initiation and progression of CRC is still a subject of debate.

1.4 Outlook

As is evident from numerous studies, there is clear interaction between the Hippo and Wnt signaling pathways in the intestine. However, the conflicting results on YAP as a tumor suppressor or as an oncogene in this context preclude the use of therapeutically activating YAP for the treatment of CRC. Herein I describe my contributions to efforts to inhibit the Hippo signaling pathway genetically and pharmacologically in intestinal homeostasis and tumor progression. These findings will pave way for clinical translation of these results for the 90% of CRCs driven by aberrant Wnt signaling.

2

Requirement of Hippo kinases in the maintenance of intestinal homeostasis

2.1 Abstract

The intestine, which carries out the body's vital functions of nutrient digestion and absorption, serves as a critical barrier to the external environment and thus has a remarkable capacity to regenerate itself following injury. This process is intricately regulated by crosstalk between the Hippo and Wnt signaling pathways, the cross-regulation of which is still a subject of debate. Here we demonstrate that the Hippo kinases LATS1/2 and MST1/2, which inhibit YAP activity, are required for maintaining Wnt signaling and canonical stem cell function. Hippo inhibition induces a distinct epithelial cell state marked by low Wnt signaling, a wound healing response, and transcription factor *Klf6* expression. Using organoid-forming assays and lineage tracing, we found that induction of this cell state via YAP impairs intestinal stem cell self-renewal. Finally, we demonstrate that this cell state has a physiological equivalent in two models of colonic injury and repair. Collectively, our results identify a role for YAP in reprogramming stem cells to a wound-healing like cell state in the intestine.

2.2 Attributions

The work described in this chapter is adapted from the following manuscript:

> **Cheung P***, Xiol J*, Dill MT, Yuan WC, Panero R, Roper J, Osorio FG, Maglic D, Li Q, Gurung B, Calogero RA, Yilmaz ÖH, Mao J, Camargo FD. Regenerative Reprogramming of the Intestinal Stem Cell State via Hippo Signaling Suppresses Metastatic Colorectal Cancer. ***Cell Stem Cell***. 2020 Oct 1;27(4):590-604.e9.
>
> * Equal contribution

J.X. and F.D.C. conceived of the study. F.D.C. supervised the study. J.X. designed and performed the *in vivo* Lats1/2, Mst1/2, and colonic injury experiments. P.C. designed and performed all *in vitro* and *in vivo* tetO-Yap^{S127A} experiments and bulk RNA-sequencing. F.G.O. assisted with the scRNA-seq experiments. Q.L. provided the Lats1/2 KO mice and performed the LATS1/2 KO lineage tracing experiment under supervision of J.M. B.G. provided experimental support. P.C. carried out computational analyses with assistance from R.P., D.M., and R.A.G. P.C., J.X., and F.D.C. wrote the manuscript with critical reading and feedback from the other co-authors.

2.3 Introduction

The gut epithelium is organized in a monolayer of cells that carries out essential absorptive, barrier, and endocrine functions (Peterson & Artis, 2014). Cellular turnover is sustained by highly proliferative *Lgr5*+ stem cells found at the bottom of intestinal and colonic crypts (Barker et al., 2007), and the presence of an active Wnt signaling pathway acts as a defining property for these stem cells. Wnt agonists are secreted by neighboring cells, forming the niche, and as cells move up the crypt, they undergo differentiation (Gehart & Clevers, 2019). Thus, regulated control of this pathway is essential for maintaining normal crypt structure and function.

The transcriptional co-activator YAP, which is negatively regulated by the Hippo kinases MST1/2 and LATS1/2, plays an important role in maintaining intestinal homeostasis. It has been shown to mediate epithelial repair following injury (Cai et al., 2010; Gregorieff et al., 2015; Yui et al., 2018), but the molecular events that follow YAP activation remain controversial. We previously have shown that YAP overexpression in the intestine leads to Wnt inhibition and crypt degeneration (Barry et al., 2013), but

subsequent reports on the effects of YAP on Wnt signaling have been contradictory (Azzolin et al., 2014; Cai et al., 2015; Gregorieff et al., 2015).

Here, we use multiple genetic models and single-cell RNA-sequencing to uncover a role for YAP in reprogramming gut epithelial cells into a state distinct from those found in steady-state intestine. This state is characterized molecularly by a wound healing signature, expression of Krüppel-like factor 6 (*Klf6*), and low levels of Wnt signaling. Using organoid and lineage tracing assays, we demonstrate that this *Klf6*+ cell state induced by overexpression of YAP or loss of LATS1/2 cannot self-renew. Finally, the overlap in gene expression profile between this cell state and that of colonic regeneration indicates that the cellular state induced by knockout of LATS1/2 represents the physiological equivalent of a transiently repairing cell state.

2.4 Results

2.4.1 YAP reprograms intestinal epithelial cells into a wound healing state

Our previous data show that overexpression of an active version of YAP in the mouse intestine leads to Wnt inhibition and degeneration of intestinal crypts (Barry et al., 2013). To explore fully the cellular and molecular consequences of YAP dysregulation in the intestinal mucosa, we studied additional models of YAP activation via deletion of its upstream negative regulatory kinases LATS1/2 and MST1/2. First, we used a *Lrig1-CreERT2* driver to delete the LATS1/2 kinases in mouse intestinal stem cells (ISCs) (hereafter referred to as *Lats1/2* cKO) and transcriptionally profiled single cells isolated from the small intestine of these mice seven days after one dose of tamoxifen injection (**Figures 2.1A-B**) (Powell et al., 2012). Unsupervised clustering followed by uniform manifold approximation and projection (UMAP) representation of the single-cell gene

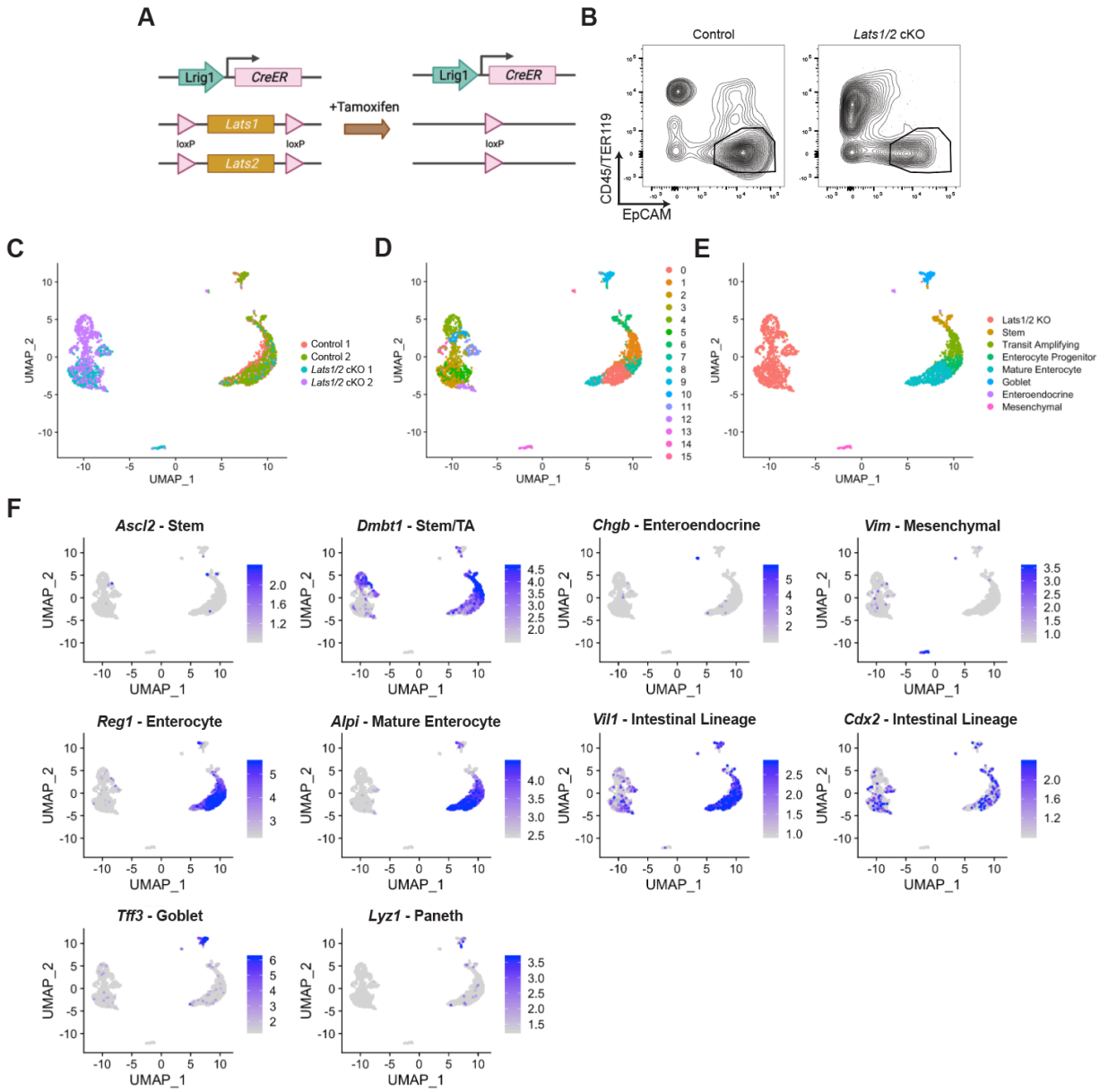

Figure 2.1. (A) Genetics of *Lrig1-CreERT2 Lats1*$^{fl/fl}$ *Lats2*$^{fl/fl}$ mice before and after injection with tamoxifen. (B) Gating strategy for isolation of intestinal epithelial cells by FACS. Cells from control and *Lats1/2* cKO mice were sorted on forward scatter and side scatter and subsequently by EpCAM+, Lin- (CD45, TER119), and DAPI-. Sorted cells were encapsulated for scRNA-seq. (C) UMAP representation of scRNA-seq data of intestinal epithelial cells from 2 control and 2 *Lats1/2* cKO animals in the indicated colors. (D) Unsupervised clustering of control and *Lats1/2* cKO cells. (E) UMAP representation of single cell transcriptome profiles of intestinal epithelial cells from 2 *Lats1*$^{fl/fl}$ *Lats2*$^{fl/fl}$ (control) and 2 *Lrig1-CreERT2 Lats1*$^{fl/fl}$ *Lats2*$^{fl/fl}$ (*Lats1/2* cKO) animals 7 days after tamoxifen induction. Clusters are annotated by cell type based on expression of known marker genes. (F) UMAP showing expression of cell-type specific markers.

expression profiles reveals a distinct clustering of the *Lats1*/2 knockout cells from the control cells (**Figure 2.1C**) (McInnes et al., 2018). While the cells in the controls could be identified by markers of normal intestinal cell states, the *Lats1/2* knockout cells could not be assigned to any known intestinal cell type (**Figures 2.1D-F**). The *Lats1/2* knockout cells lack expression of characteristic markers of normal intestinal states but still belong to the intestinal lineage as seen by expression of *Villin* and *Cdx2* (**Figure 2.1F**), thus defining a distinct cell type not present in the homeostatic intestinal epithelium. Upregulated genes in *Lats1/2* knockout cells relative to control cells are overrepresented in gene ontology (GO) terms involved in wound healing and actin reorganization, which have been associated with YAP activation (Cai et al., 2010; Dupont et al., 2011; Zhao et al., 2007, 2011, 2012), and those downregulated are overrepresented in terms related to intestinal absorption and villus organization (**Figure 2.2A**). Gene set enrichment analysis (GSEA) confirms that the *Lats1/2* knockout cells are highly enriched for two previously published YAP gene signatures and reveals that they are negatively enriched for intestinal β-catenin targets compared to the stem cells (**Figures 2.2B-D**) (Barry et al., 2013; Fevr et al., 2007; Gregorieff et al., 2015). Upregulated genes include known targets of YAP, such as *AmotL2*, and fetal marker *Ly6a*/*Sca1*, which has been identified to label a cell state induced after damage or infection (**Figure 2.2E**) (Nusse et al., 2018; Yui et al., 2018). Interestingly, these cells are also marked by high expression of the transcription factor *Klf6*, which has been characterized as an immediate-early gene in response to injury and implicated to be a tumor suppressor in CRC (Inuzuka et al., 1999; Kojima et al., 2000; Ratziu et al., 1998; Reeves et al., 2004). These findings altogether suggest a role for YAP in molecularly reprogramming epithelial cells into a distinct transcriptional state that is not present in steady-state intestine.

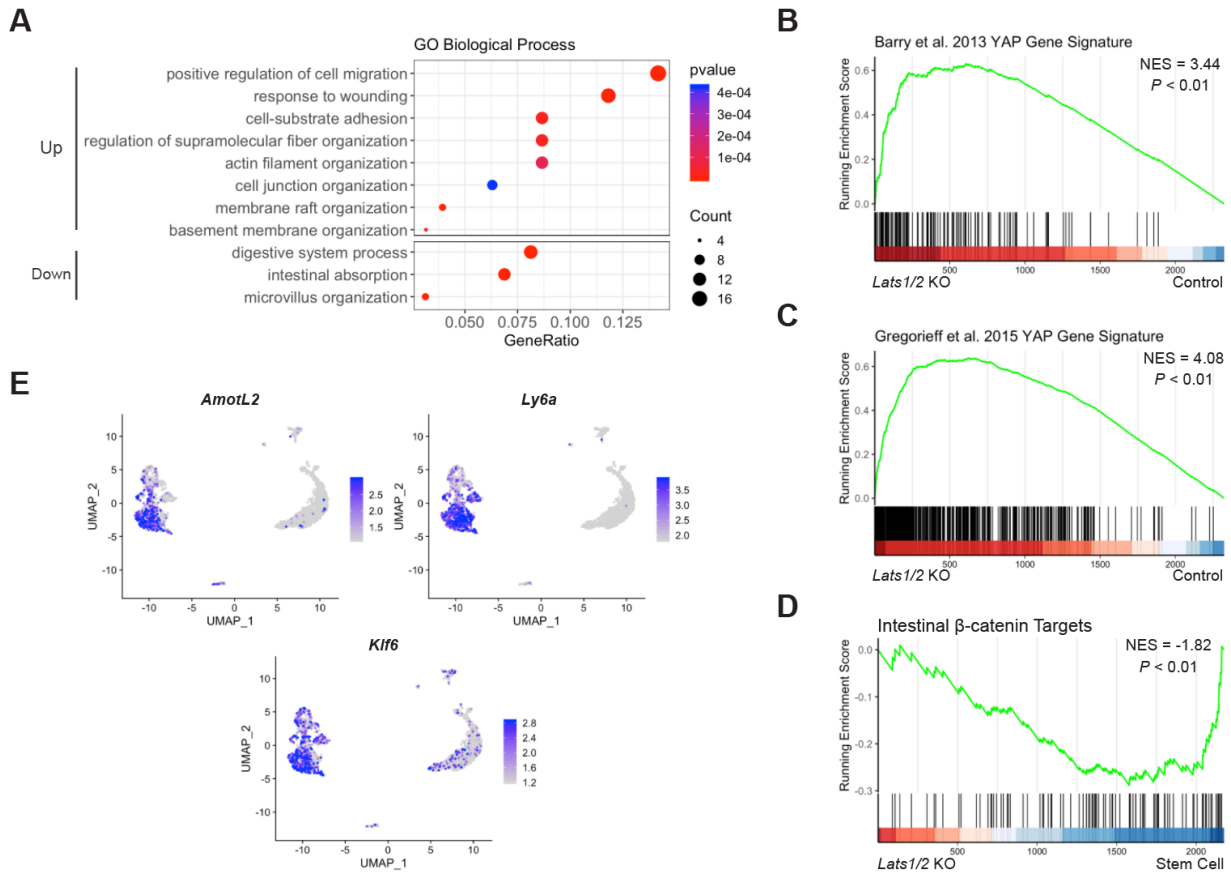

Figure 2.2. (A) GO enrichment analysis of upregulated and downregulated genes in *Lats1/2* KO cells compared to control cells, excluding the mesenchymal population. (B) GSEA of a YAP gene signature from Barry et al., 2013 in *Lats1/2* KO cells compared to control cells. (C) GSEA of a YAP gene signature from Gregorieff et al., 2015 in *Lats1/2* KO cells compared to control cells. (D) GSEA of intestinal β-catenin targets in *Lats1/2* KO cells compared to the stem cells. (E) Normalized expression of the indicated genes overlaid on the UMAP plots.

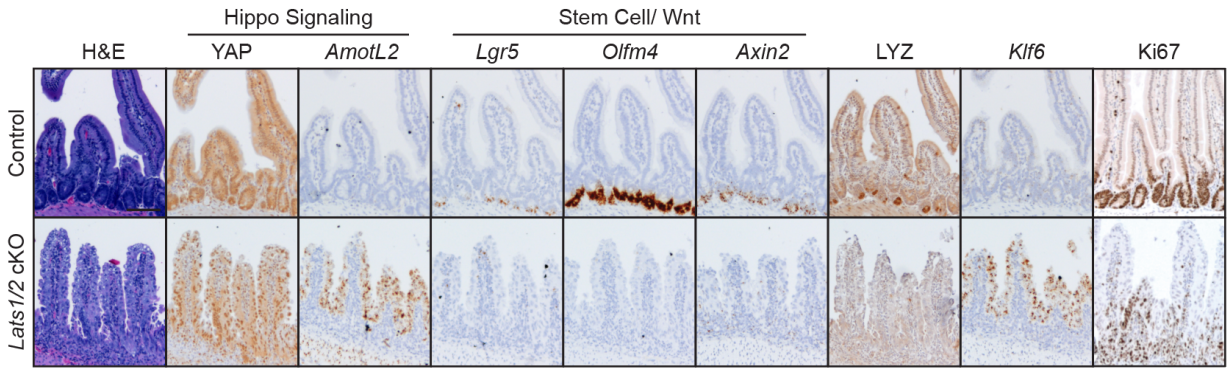

Figure 2.3. (A) Histological analysis of control and *Lats1/2* cKO duodenal samples 7 days after tamoxifen induction: H&E stains, IHC for YAP, LYZ, and Ki67, and RNA-ISH for *Amotl2, Lgr5, Olfm4*, *Axin2*, and *Klf6*. Scale bar, 100 μm.

To validate these results, we performed immunohistochemistry analysis of the intestine from *Lats1/2* cKO mice seven days post tamoxifen treatment. This analysis reveals an accumulation of YAP in the nucleus and expression of the YAP target gene *AmotL2* (**Figure 2.3**). Consistent with the single-cell RNA-sequencing (scRNA-seq) data, charact.ristic markers of normal intestinal cell states are not present, such as those associated with ISCs (*Lgr5* and *Olfm4*), secretory cells (LYZ), and targets of the Wnt signaling pathway (*Axin2*). *Lats1/2* knockout cells retain their proliferative capacity as observed by staining with Ki67 and show marked increase in *Klf6* levels, corroborating our scRNA-seq findings of YAP-mediated induction of a distinct *Klf6*+ cell state.

This loss of typical intestinal cellular organization was confirmed in additional models for activation of endogenous YAP through knockout of the MST1/2 kinases in *Mst1*$^{-/-}$ *Mst2*$^{fl/fl}$ mice via an intestinal specific, developmental *Villin-Cre* driver and the adult-inducible *Villin-CreERT2* driver (hereafter referred to as *Mst1/2* cKO) (El Marjou et al., 2004; Madison et al., 2002; Zhou et al., 2011). In both models, we observed loss of ISC markers and Wnt targets accompanied by YAP activation (**Figures 2.4A and B**). Altogether, our results point to a requirement for Hippo kinases in maintaining Wnt signaling in ISCs and suggest that persistent YAP activation cannot sustain normal homeostasis.

2.4.2 Activation of YAP leads to loss of canonical stem cell properties

As YAP-expressing cells are transcriptionally distinct from normal ISCs, we examined their capacity to form intestinal organoids. To test the effect of YAP activation in organoids, we generated a colon organoid line that would allow for inducible overexpression of YAP^{S127A}, a transcriptionally active mutant form of YAP (hereafter

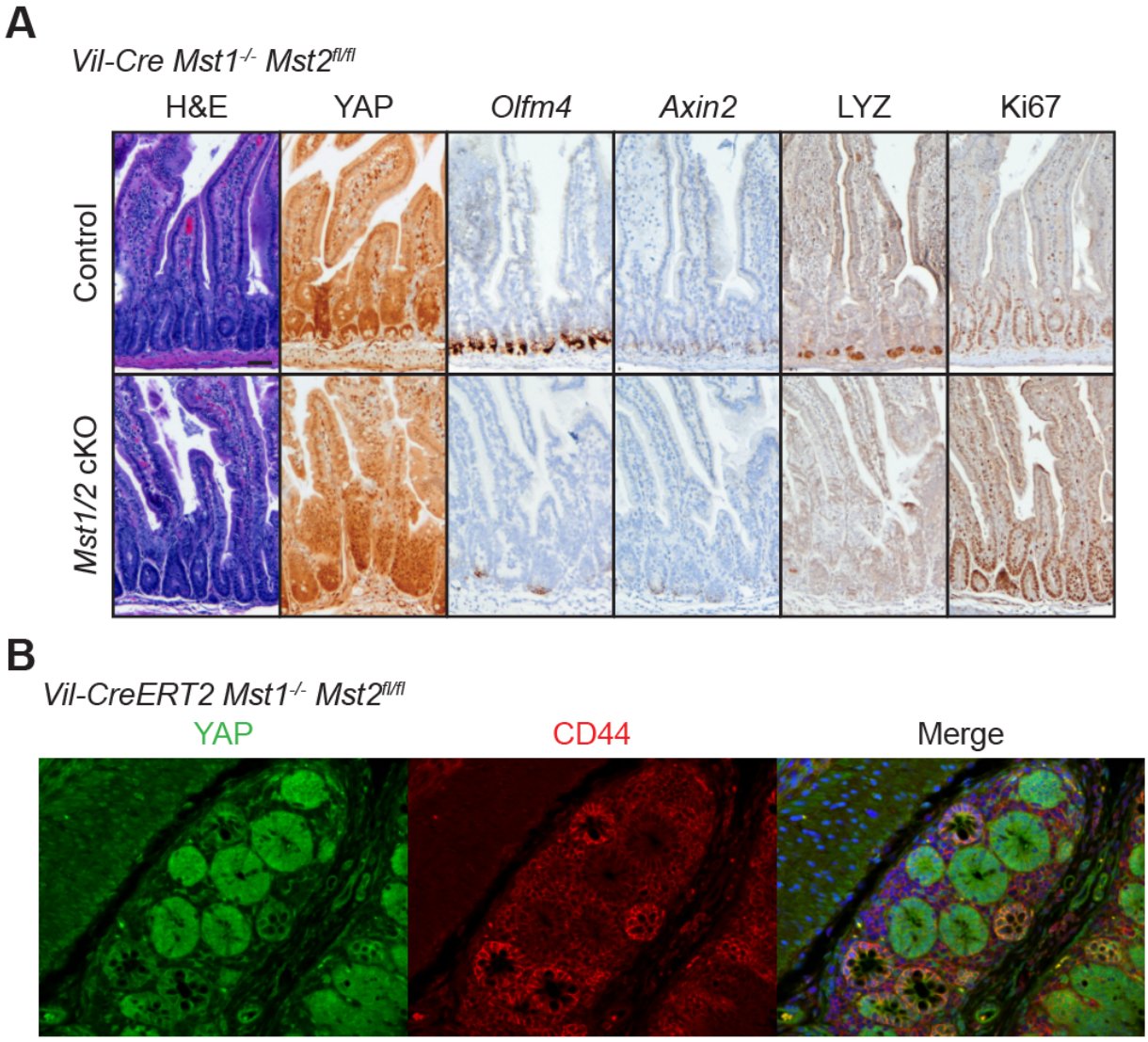

Figure 2.4. (A) Histological analysis of *Mst1*$^{-/-}$ *Mst2*$^{fl/fl}$ (control) and *Vil-Cre Mst1*$^{-/-}$ *Mst2*$^{fl/fl}$ (*Mst1/2* cKO) samples: IHC for YAP, LYZ, and Ki67 and RNA-ISH for *Olfm4* and *Axin2*. Scale bar, 50 μm. (B) Immunofluorescence (IF) for YAP (green) and CD44 (red) in crypts of *Vil-CreERT2 Mst1*$^{-/-}$ *Mst2*$^{fl/fl}$ mice 1 month after tamoxifen injection. Sections were counterstained with DAPI (blue).

Figure 2.5. (A) Schematic for generating *tetO-YAP^{S127A} rtTA* organoids. (B) Brightfield images of *tetO-YAP^{S127A} rtTA* organoids on the indicated days in the presence or absence doxycycline. The organoids were split on day 4. Scale bar, 200 μm. (C) Brightfield images of *Lrig1-CreERT2 Lats1$^{fl/fl}$ Lats2$^{fl/fl}$* organoids 7 days after plating in the presence of 4-OHT for 24 hours. Scale bar, 200 μm. (D) Bright-field images of wild-type colon organoids five days after treatment with 4-OHT for 24 hours. Scale bar, 200 μm. (E-F) RT-qPCR analysis of the indicated genes in *tetO-YAP^{S127A} rtTA* organoids 2 days after induction with doxycycline. Data are represented as mean ± SEM; n = 3 biological and 2 technical replicates. ****$P < 0.001$. (G) RTq-PCR analysis of the indicated genes in *Lrig1-CreERT2 Lats1$^{fl/fl}$ Lats2$^{fl/fl}$* organoids 2 days after treatment with 4- OHT for 24 hours. Data are represented as mean ± SEM; n = 2 biological and 2 technical replicates. *$p < 0.05$ and ***$p < 0.001$. (H) Histological analysis of *tetO-YAP^{S127A} rtTA* organoids 3 and 4 days after induction with doxycycline: H&E stains, IHC for YAP and Ki67, and RNA-ISH for *AmotL2, Lgr5, Axin2*, and *Klf6*. Scale bar, 50 μm.

Figure 2.5 (Continued)

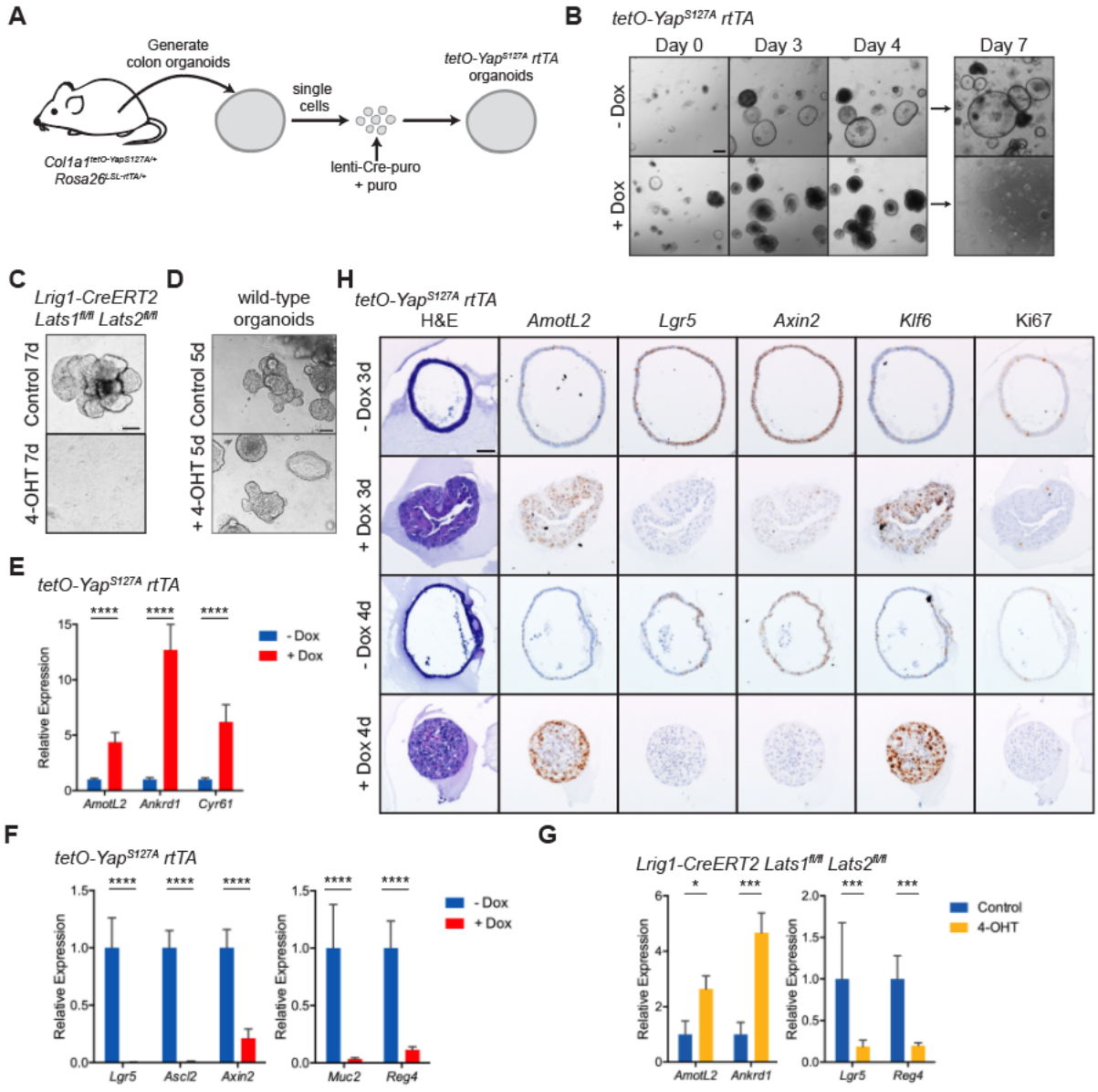

referred to as *tetO-YAP rtTA*) (**Figure 2.5A**) (Yimlamai et al., 2014; Zhao et al., 2007). Induction of YAP expression by doxycycline for 48 hours causes the organoids to lose single cell, columnar organization and prevents them from growing or forming spheroids upon passage (**Figure 2.5B**). *Lats1/2* cKO colon organoids upon 4-OHT treatment also exhibit a similar phenotype of not being able to grow or form 3D structures (**Figure 2.5C**), which is not due to 4-OHT toxicity (**Figure 2.5D**). In both contexts of YAP activation, we observed upregulation of mRNA levels of YAP targets and downregulation of ISC and secretory cell markers and the Wnt target *Axin2* (**Figures 2.5E-G**). Histological analysis confirms these results and reveals a progressive loss of the monolayer structure, upregulation of *Klf6* expression, and proliferation arrest (**Figure 2.5H**). These results collectively suggest that this Wnt-low, *Klf6*-high state induced by YAP is incompatible with organoid growth *in vitro*.

To determine whether these YAP-expressing cells have functional stem cell activity *in vivo*, we leveraged lineage tracing in *Lgr5-CreERT2* knock-in mice to trace *Lgr5*+ ISCs with and without activation of YAP (Barker et al., 2007; Huch et al., 2013). We induced YAP activation and tdTomato expression by intraperitoneal injection of tamoxifen and doxycycline in *Lgr5-IRES-CreERT2* $Col1a1^{tetO\text{-}YapS127A/+}$ $Rosa26^{LSL\text{-}rtTA/LSL\text{-}Tomato}$ mice (**Figure 2.6A**). Compared to the homogeneous Tomato labeling in uninduced crypts 5 days post induction, crypts with YAP-activated ISCs exhibit mosaic Tomato labeling in the small intestine (**Figure 2.6B**), indicating that YAP expression in ISCs negatively affects their ability to contribute to intestinal lineages. Indeed, these YAP-activated ISCs are pushed out of intestinal crypts and villi over the course of 10 days (**Figure 2.6C**), suggesting that these mutant cells are quickly replaced by wildtype ISCs. Similarly, lineage tracing in *Lgr5-CreERT2* $Lats1^{fl/fl}$ $Lats2^{fl/fl}$ $Rosa26^{mT/mG}$ mice reveals progressive

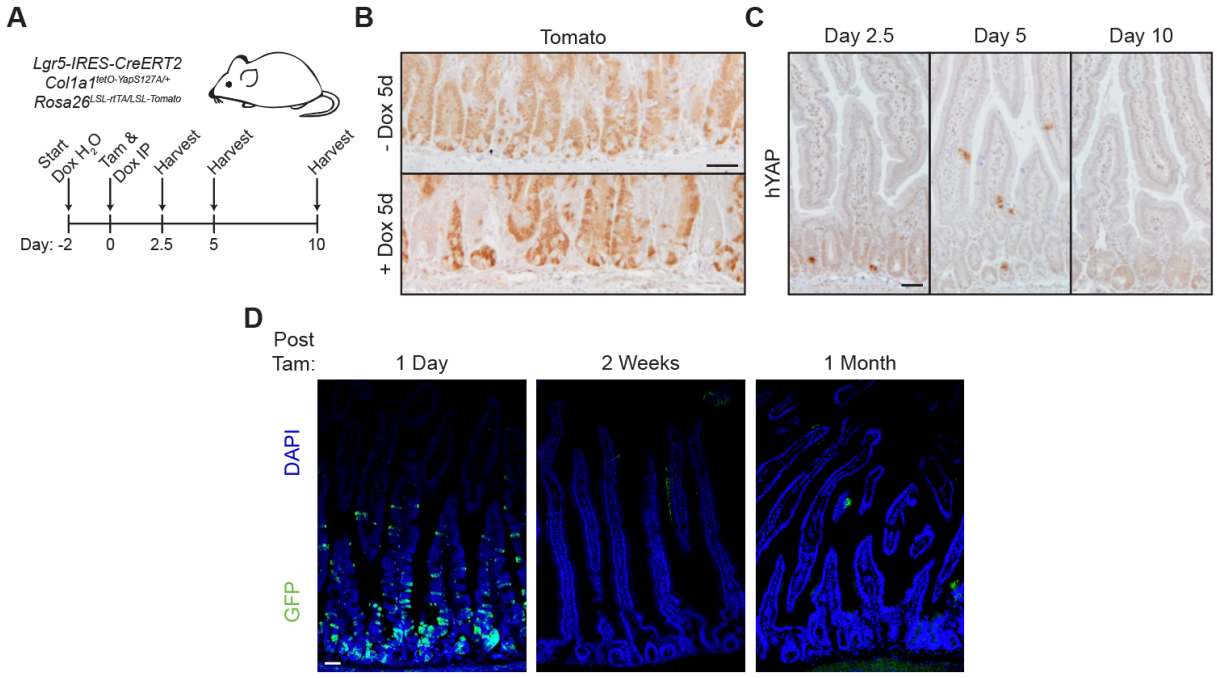

Figure 2.6. (A) Schematic of *Lgr5* lineage tracing, including timeline of doxycycline administration, doxycycline and tamoxifen injections, and tissue collection. (B) IHC for Tomato in the small intestine of *Lgr5-IRES-CreERT2 Col1a1*$^{tetO\text{-}YapS127A/+}$ *Rosa26*$^{LSL\text{-}rtTA/LSL\text{-}Tomato}$ mice 5 days after tamoxifen injection with or without administration of doxycycline. Scale bar, 50 μm. (C) IHC for human YAP in the small intestine of *Lgr5-IRES-CreERT2 Col1a1*$^{tetO\text{-}YapS127A/+}$ *Rosa26*$^{LSL\text{-}rtTA/LSL\text{-}Tomato}$ mice on the indicated days after tamoxifen and doxycycline administration. Scale bar, 50 μm. (D) IF for GFP and DAPI in the small intestine of *Lgr5-CreERT2 Lats1*$^{fl/fl}$ *Lats2*$^{fl/fl}$ *Rosa26*$^{mT/mG}$ at the indicated times after the second injection with tamoxifen.

loss of GFP+ ISCs at 2 weeks and 1 month after induction (**Figure 2.6D**). Altogether, these models suggest that YAP activation within ISCs leads to loss of normal stem cell function *in vivo*.

2.4.3 A YAP gene signature is activated during mucosal healing

The activation of YAP previously has been shown to be required for mucosal regeneration in different models of intestinal and colonic injury (Cai et al., 2010; Gregorieff et al., 2015). Thus, we investigated whether such physiological activation of YAP via injury induces reprogramming of intestinal epithelial cells to this Wnt-low, *Klf6*+ state that we described above. To characterize epithelial cells during wound healing, we induced a punch lesion in mice by colonoscopy and collected samples from injured animals after six days (Seno et al., 2009). Histological analysis reveals an increased accumulation of YAP in the nucleus of epithelial cells at sites of wound healing and concomitant upregulation of *Klf6* and the YAP target *AmotL2* when compared to uninjured controls (**Figure 2.7A**). Intriguingly, these areas are also depleted of *Lgr5*+ ISCs and *Reg4*+ deep crypt secretory (DCS) cells, suggesting that physiological regeneration activates a transcriptional state similar to that which we observed in *Lats1/2* cKO and *Mst1/2* cKO animals.

In a second model of colonic injury, we induced acute inflammation in adult mice by supplementing drinking water with 3.5% dextran sulfate sodium (DSS) for five days (**Figure 2.7B**), which leads to a loss of colonic crypts and immune cell infiltration (**Figure 2.7C**). Three days after DSS washout, crypts in inflamed areas of the colon show marked activation of YAP, increased *Klf6* expression, and loss of *Lgr5* and *Reg4* markers

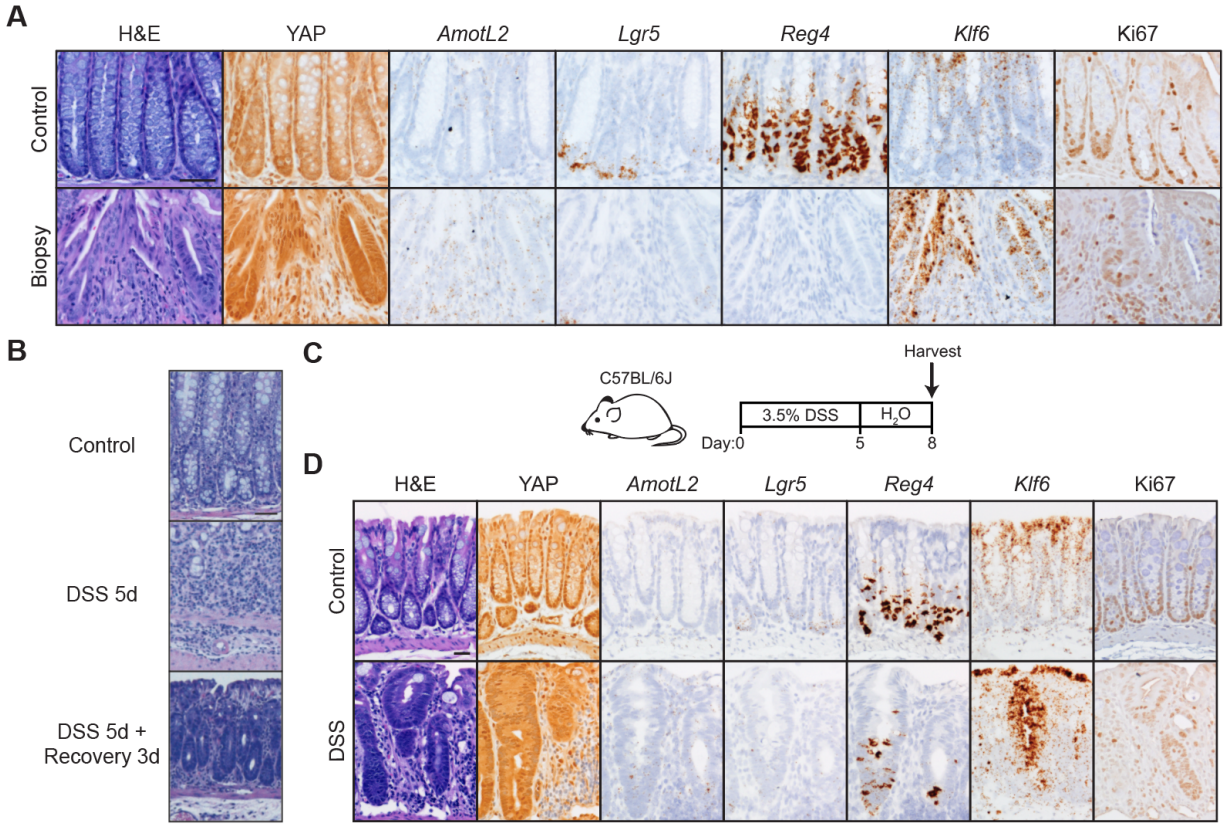

Figure 2.7. (A) Histological analysis of colon samples from mice 6 days after inducing a punch biopsy: H&E stains, IHC for YAP and Ki67, and RNA-ISH for *AmotL2, Lgr5, Reg4,* and *Klf6*. Scale bar, 50 μm. (B) H&E stains of colonic samples from mice following DSS treatment with or without recovery. Scale bar, 50 μm. (C) Schematic of colonic injury and regeneration by dextran sulfate sodium (DSS), including timeline of DSS administration and tissue collection. (D) Histological analysis of colon samples from mice after a 5-day DSS treatment and 3-day recovery: H&E stains, IHC for YAP and Ki67, and RNA-ISH for *AmotL2, Lgr5, Reg4,* and *Klf6*. Scale bar, 25 μm.

(**Figure 2.7D**). These data altogether suggest that YAP activation is a general and specific response to injury in the colon during regeneration.

To characterize the molecular changes in the colonic epithelium during regeneration, we performed scRNA-seq on epithelial cells isolated from DSS-treated and control mice (**Figure 2.8A**). UMAP representation of the transcriptomic profiles reveals that the DSS-treated cells, despite being distinct from control cells (**Figure 2.8B**), maintain some features of normal colonic cells and could be assigned to known colonic cell types by marker expression (**Figures 2.8C-E**). As reported previously (Yui et al., 2018), the DSS sample presents with upregulation of *Ly6a/Sca1* transcript levels (**Figure 2.8F**). Differentially expressed genes between DSS and control are positively enriched for wound healing response, cell-cell contact pathways, and YAP gene signatures and negatively enriched for a previously published ISC gene signature (**Figures 2.8H-J**) (Barry et al., 2013; Gregorieff et al., 2015; Muñoz et al., 2012). Remarkably, this DSS injury signature is highly enriched in the transcriptomes of *Lats1/2* knockout cells (**Figure 2.8K**). Collectively, these data suggest that the cellular state induced by knockout of *Lats1/2* or activation of YAP likely represents the physiological equivalent of a transiently repairing cell state.

2.5 Discussion

YAP is known to play an important role during mucosal healing and has been proposed to remodel stem cells, activate expression of a fetal program, or expand quiescent stem cells upon injury (Ayyaz et al., 2019; Gregorieff et al., 2015; Yui et al., 2018). Using scRNA-seq, we elucidate a role for YAP in reprogramming colon cells into a cell type marked by high *Klf6* expression that is unique to the repairing epithelium and

Figure 2.8. (A) Gating strategy for isolation of colon epithelial cells by FACS. Cells from control and DSS-treated mice, following a 3-day recovery period, were sorted on forward scatter and side scatter and subsequently by EpCAM+, Lin- (CD45, TER119), and DAPI-. Sorted cells were encapsulated for scRNA-seq. (B) UMAP representation of scRNA-seq data of colonic epithelial cells from control and DSS-treated mice, following a 3-day recovery period, in the indicated colors. (C) Unsupervised clustering of the DSS and control samples. (D) UMAP showing cell types in the indicated colors by the treatment group. (E) UMAP showing expression of cell-type specific markers. (F) UMAP showing expression of *Ly6a/Sca1* in control and DSS samples. (G) GSEA of KEGG pathways in the DSS sample compared to control. (H) GSEA of a *Lgr5* ISC gene signature in the DSS sample compared to control. (I) GSEA of a YAP gene signature from Barry et al., 2013 in DSS compared to control. (J) GSEA of a YAP gene signature from Gregorieff et al., 2015 in DSS compared to control. (K) Expression of the DSS injury signature, characterized by genes upregulated at least 2-fold in stem cells, progenitors, goblet cells, or colonocytes in DSS versus control samples, overlaid onto the UMAP of *Lats1/2* cKO scRNA-seq.

Figure 2.8 (Continued)

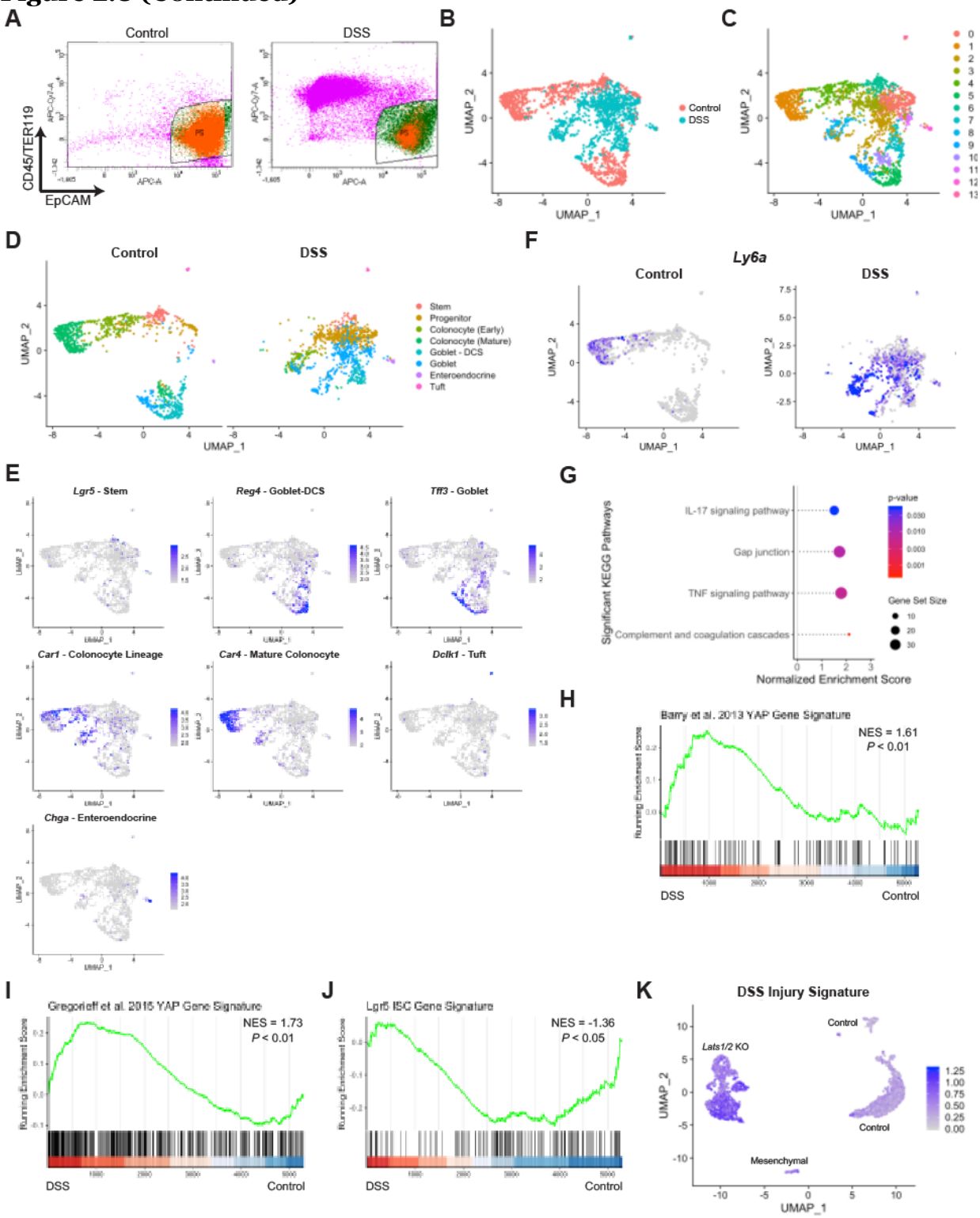

distinct from all cell types present during homeostasis. This state is characterized by the expression of injury-associated genes and a low Wnt signature, which confirms our earlier finding that YAP inhibits Wnt signaling in the intestine (Barry et al., 2013). Our work is in agreement with a recent scRNA-seq study identifying a stem cell type enriched in YAP target genes (Ayyaz et al., 2019). In contrast to this work, our data suggest that this YAP-driven cell state does not exist in homeostasis, and it instead arises from the reprogramming of traditional intestinal stem cells. As we observed overlap in the transcriptomes between that of LATS1/2 inhibition and colonic regeneration, we propose that this cell state is the physiological equivalent of a transiently repairing cell type.

This cross-regulation between the Wnt and Hippo signaling pathways has been a subject of debate - in some contexts, YAP potentiates Wnt signaling; in others, YAP suppresses Wnt (Azzolin et al., 2014; Barry et al., 2013; Cai et al., 2015; Gregorieff et al., 2015). Our data demonstrate that YAP overexpression or Hippo inhibition is incompatible with intestinal stem cell function. YAP activation not only prevents colonic organoids from re-forming following passage but also results in their loss from the intestinal epithelium. As Wnt is aberrantly regulated in a majority of colorectal cancers, these findings have tremendous implications for the treatment of this disease.

2.6 Materials and Methods

2.6.1 Mice

All animal protocols and procedures were approved by the respective local animal institutional committees. All mice used for this study were on a C57BL/6J background unless indicated otherwise.

Models of YAP activation: *Lats1*$^{fl/fl}$ *Lats2*$^{fl/fl}$ (controls) and their *Lrig1-CreERT2* *Lats1*$^{fl/fl}$ *Lats2*$^{fl/fl}$ littermates were injected intraperitoneally with 2 mg of tamoxifen and harvested on the days indicated for single cell RNA sequencing and histology experiments. The intestine and colon of *Villin-Cre Mst1*$^{-/-}$ *Mst2*$^{fl/fl}$ mice and their *Mst1*$^{-/-}$ *Mst2*$^{fl/fl}$ littermates were collected at the indicated ages for histological analysis. *Villin-CreERT2 Mst1*$^{-/-}$ *Mst2*$^{fl/fl}$ mice and their *Mst1*$^{-/-}$ *Mst2*$^{fl/fl}$ littermates were injected intraperitoneally with 2 mg of tamoxifen and harvested 1 month after for histology experiments.

Lineage tracing experiments: 2-4 months old *Lgr5-IRES-CreERT2 Col1a1*$^{tetO\text{-}YapS127A/+}$ *Rosa26* $^{LSL\text{-}rtTA/LSL\text{-}Tomato}$ mice were administered doxycycline (2 mg/ml with 0.5% sucrose) in drinking water ad libitum two days prior to intraperitoneal injection with 3 mg of tamoxifen and 25 μg/g doxycycline and were harvested on the indicated days for histology experiments (*Lgr5-IRES-CreERT2* mice were a kind gift of Meritxell Huch). 2-month-old *Lgr5-CreERT2 Lats1*$^{fl/fl}$ *Lats2*$^{fl/fl}$ *Rosa26*$^{mT/mG}$ mice were injected intraperitoneally with 120 mg/kg tamoxifen for two consecutive days and harvested on the indicated days for immunofluorescence.

2.6.2 Punch biopsy

Colorectal injuries were created using the Storz endoscopic system as described previously (Seno et al., 2009). Briefly, mice were anesthetized, and a colonoscope was inserted to the mid-descending colon. 3 French flexible biopsy forceps were inserted through the working channel of the scope and used to create 3–5 discrete, oval-shaped wounds in the mucosal lining of the distal colon.

2.6.3 Experimental colitis

Colitis was induced in 2-month-old female C57BL/6 mice by administration of 3.5% DSS in drinking water for 5 days followed by normal water for 3 days.

2.6.4 Mouse colon organoid isolation and culturing

For colon epithelial cell isolation for organoid culture, a 2 cm piece of distal colon was extracted from 2-month-old mice and incubated in 4 mM EDTA in PBS with mild agitation for 45 min at 4°C. The colon pieces were cut open, and colon crypts were scraped from the tissue with a coverslip. After washing with cold PBS and centrifugation at 1000 g for 5 min, crypts were resuspended in Matrigel and plated in 24-well plates (50 μL Matrigel/well). The Matrigel was allowed to solidify for 15-30 min in a 37°C incubator. 500 μL of organoid culture media was then overlaid onto the Matrigel and changed every 2-3 days. The organoid cultures were maintained at 37°C in fully humidified chambers containing 5% CO_2.

Colon organoids were prepared from animals with the following genotypes: *Col1a1*$^{tetO\text{-}YapS127A/+}$ *Rosa26*$^{LSL\text{-}rtTA/+}$ and *Lrig1-CreERT2 Lats1*$^{fl/fl}$ *Lats2*$^{fl/fl}$. Organoids were grown in conditioned media containing Wnt3a, R-Spondin, and noggin, generated as described previously from L-WRN cells (Miyoshi & Stappenbeck, 2013) and diluted 1:1 with Advanced DMEM/F-12 containing 1x N-2, 1x B-27, 1% Pen/Strep, and 2 mM L-glutamine. The growth media also contained 50 ng/mL EGF, 0.1 mg/mL primocin, 1 μM N-acety-L-cysteine, 10 mM HEPES, and 10 μM Y-27632 (added only upon passaging). Induction of *Lats1/2* knockout was performed by addition of 100 nM 4-OHT overnight whereas Yap overexpression was induced with 1 μg/mL doxycycline in the media.

To generate *tetO-Yap*^{S127A} *rtTA* organoids, organoids derived from *Col1a1*$^{tetO\text{-}YapS127A/+}$ *Rosa26*$^{LSL\text{-}rtTA/+}$ mice were transduced with a lentivirus expressing Cre recombinase (generated from Cre-IRES-PuroR, a gift from Darrell Kotton) to activate rtTA expression (Somers et al., 2010). Three days after infection, organoids were selected by adding 1 μg/mL puromycin.

2.6.5 Organoid transfection and infection

2-3 days prior to transfection or infection, organoids were treated with 10 mM nicotinamide. Organoids were washed with PBS and treated with dispase to dissolve the Matrigel. They were passaged through a 25G syringe three times, spun down for 5 min at 1000 g and resuspended in 450 μL of culture media. The cell suspension was transferred to a 48-well plate, and 10 μL of a lentivirus solution (titer approximately 10^7 pfu/mL) or 50 μL of lipofectamine-DNA complex were added to the well. Cells were spinoculated for 1 hr at 30°C at 600 g. After a 4-6 h recovery at 37°C, the cells were resuspended, centrifuged in an Eppendorf tube, resuspended in 50 μL Matrigel, and cultured as described above.

2.6.6 Lentivirus production

Lentiviruses were generated in 293X cells by transfecting backbone and packaging plasmids using TransIT reagent following manufacturer's instructions. 293X cells were maintained in DMEM (+10% FBS, 2 mM L-glutamine, 1% Pen/Strep). The supernatant containing the virus was collected 48 and 60-72 hours after transfection, concentrated by

ultracentrifugation at 16,000 rpm for 90 min at 4°C, and resuspended in the remaining supernatant.

2.6.7 Histology

Intestine and colon samples were fixed overnight in 10% formalin, washed with PBS and 70% ethanol, and embedded in paraffin. Organoids grown in Matrigel were fixed in 4% paraformaldehyde/PBS, washed extensively with PBS and encapsulated in Histogel prior to embedding in paraffin. The paraffin blocks were cut into 5 μm sections using a microtome.

For immunohistochemistry, antigen retrieval for most epitopes was performed with citric-acid based pH 6.0 Antigen Unmasking Solution at 95°C in a pressure cooker for 1 hr. For epitopes requiring high pH, antigen retrieval was performed with tris-based pH 9.0 Antigen Unmasking Solution at 37°C for 10 min. The slides were blocked with 0.3% hydrogen peroxide and subsequently 2.5% donkey serum in PBS and incubated with primary antibody in blocking buffer overnight at 4°C. After washing with PBS three times, slides were incubated with biotinylated secondary antibodies in PBS for 1 hr. The signal was amplified with VectaStain ABC Reagent and developed with DAB. Harris modified hematoxylin was used to counterstain nuclei and subsequently slides were washed, dehydrated, and mounted using VectaMount.

For immunofluorescence, following antigen retrieval, blocking, and primary antibody incubation, slides were incubated with appropriate fluorescent antibodies and 1 μg/ml DAPI for 1 hour and then mounted with Prolong Gold antifade with DAPI.

For RNA *in situ* hybridization, we used the RNAScope Brown HD 2.5 kit according to the manufacturer's instructions.

IHC and RNAScope images were taken using a Zeiss Axio Scope. IF images were obtained on a Zeiss AxioObserver Z1.

2.6.8 RNA isolation and RT-qPCR

RNA from organoids was extracted using Trizol reagent. cDNA was obtained using the cDNA Synthesis Kit and diluted 1:40 for RT-qPCR if starting from 500 ng of RNA. RT-qPCR was performed on a One Step plus Sequence Detection System (Applied Biosystems) using Fast SYBR® Green Master Mix (Life Technologies), and gene expression data was quantified using the DeltaDeltaCt method and normalized to *Gapdh*/*GADPH*.

2.6.9 Fluorescence-activated cell sorting

For isolation of intestinal and colonic epithelial cells for fluorescence-activated cell sorting (FACS), a piece of intestine was extracted from mice and incubated in 4 mM EDTA in PBS with gentle rocking for 40 min at 4°C. The small intestine was shaken to dissociate epithelial cells whereas the colon was cut open and scraped with a coverslip to dissociate the crypts. The smooth muscle layer was removed, and the remaining supernatant was centrifuged and incubated in 3 mg/mL collagenase/dispase in PBS for 6 min at 37°C with repeated up and down pipetting. The single cells were then placed on ice, centrifuged, filtered through 70 μm strainers, and stained in 2% FBS/PBS with fluorescent conjugated EpCAM, CD45, and TER119 antibodies diluted 1:100 for 30 min at 4°C.

All sorting was performed on a BD FACSAria II, using a 100 μm nozzle, and FlowJo (Tree Star) software was used for all flow cytometry analysis. The following combinations were used to isolate each of the respective populations: intestinal/colonic epithelial cells:

EpCAM+CD45-TER119-; tumor epithelial cells: EpCAM+CD45-TER119-CD11b-. For all sorts, 4', 6-diamidino-2-phenylindole (DAPI) was used to eliminate dead cells.

2.6.10 Single-cell RNA sequencing and analysis

InDrop-v2 (1CellBio) encapsulation protocol was performed following manufacturer's instructions found at the company's website. 5,000 cells were encapsulated per library and condition. Whole-transcriptome libraries were prepared as previously described (Zilionis et al., 2017) and sequenced on an Illumina NextSeq 500 using paired-end 75 cycles v2 kits (Read 1: 36 cycles; Index Read: 6 cycles; Read 2: 50 cycles). The fastq to counts conversion was performed using the indropIndex and the indropCounts functions, which are part of the rCASC framework (Alessandrì et al., 2019). The indropCounts function, which invokes the inDrop pipeline v20170126 (https://github.com/indrops/indrops), was used with the following options: M=10, U=2, D=400, and low.complexity.mask="False" and the following packages: Bowtie v1.1.1.1, Samtools v1.3.1, RSEM v1.3.0, and Java v1.8.0 (Langmead et al., 2009; B. Li & Dewey, 2011; H. Li et al., 2009).

To visualize the single cell data, we used Seurat (v3.1.3 with default parameters except where indicated) (Butler et al., 2018). In both datasets, cells that had more than 15% of the total UMIs in mitochondrial genes were filtered out, and those with a log10(number of genes per UMI) greater than 0.8 were kept. We also set a minimum threshold of UMIs/cell and genes/cell: 600 UMIs/cell and 250 genes/cell in both the control and *Lats1/2* cKO samples and 300 UMIs/cell and 300 genes/cell in the colon control and DSS sample. For each experiment, the number of cells were down sampled to the sample with the fewest cells to obtain an equal number of cells per condition for

downstream analysis. Next, sctransform was used to normalize UMI counts and find variable features for dimensionality reduction (Hafemeister & Satija, 2019). Dimensionality reduction was performed using RunPCA to generate points for embedding, which were then used to construct UMAP plots (RunUMAP) and find neighbors for clustering (FindNeighbors). For all relevant functions, 40 principal components were used. FindClusters (resolution=1.4) was used to run the Louvain clustering algorithm.

For differential expression analysis, the bimod test (McDavid et al., 2013) implemented in Seurat was used to find the differentially expressed genes between the *Lats1/2* KO cells and control cells, excluding the mesenchymal population, or stem cells in the *Lats1/2* cKO scRNA-seq and between the same cell type in the DSS versus control in the DSS scRNA-seq. For the *Lats1/2* cKO scRNA-seq, gene ontology enrichment analysis was performed on genes with an adjusted p-value < 0.05 and a log2FC > 1 or < -1 in the *Lats1/2* knockout cells versus control using enrichGO in the clusterProfiler R package to identify significant GO biological processes overrepresented (G. Yu et al., 2012). For both datasets, gene set enrichment analysis (GSEA) was performed on the ranked average log fold change of the differentially expressed genes using the fgsea R package to identify significant KEGG pathways enriched (Sergushichev, 2016). The GSEA function in clusterProfiler was used to perform GSEA of previously published gene signatures. The intestinal β-catenin signature is derived from the supplementary table of downregulated genes in intestinal crypt cells upon deletion of β-catenin (Fevr et al., 2007). The *Lgr5* ISC gene signature is derived from the "mRNA stem cell signature" in the supplementary table of Muñoz et al., 2012. For the YAP gene signatures, the Barry et al., 2013 signature is derived from the supplementary table of genes upregulated upon

transgenic YAP overexpression in mouse crypts whereas the Gregorieff et al., 2015 signature is derived from the supplementary table of YAP activated genes with a log2 fold change < -1. To generate the DSS injury signature, we kept all genes with adjusted p-value < 0.05 and log2FC > 1 and plotted this injury signature onto the UMAP of control and *Lats1/2* cKO cells by taking the average of the normalized expression values of the signature genes for each cell and plotting the log2 + 1 of these values.

2.6.11 Bulk RNA sequencing and analysis

RNA was isolated from organoids using the NucleoSpin RNA XS kit. The libraries for the RNA-seq analysis were prepared with 100 ng of RNA using the TruSeq RNA Library Preparation Kit v2 (Illumina) according to the manufacturer's protocol. All of the libraries were sequenced on an Illumina HiSeq 4000 using paired end 150 cycles kits at Novogene. Raw sequencing reads were aligned to a reference transcriptome generated from the Ensembl v98 database with Salmon v0.14.1 using options "--seqBias --useVBOpt --gcBias --numBootstraps 30 --validateMappings" (Patro et al., 2017). Length-scaled transcripts per million were acquired using the tximport function, and log2 fold changes and false discovery rates were determined by DESeq2 in R (Love et al., 2014; Soneson et al., 2015). Shrunken log2 fold changes were determined with DESeq2, which were used to rank genes for GSEA of significant KEGG pathways by fgsea or of previously published gene signatures using the GSEA function (Kanehisa, 2000). In cases where there were duplicate gene symbols or Entrez IDs, the more significant gene was kept for the ranking. To identify the transcription factors differentially expressed, the differentially expressed genes at 72 hours with adjusted p-value < 0.05 and absolute log2 fold change > 1 were overlapped with the CIS-BP v2.00 database of mouse transcription factors (Weirauch et

al., 2014). enrichGO in the clusterProfiler R package was used to identify significant GO biological processes overrepresented (G. Yu et al., 2012).

2.6.12 Quantification and statistical analysis

Data represented are expressed as mean ± standard error of mean unless otherwise specified. Data were analyzed using Prism Software 6.0 (GraphPad). Technical and biological replicates are specified for each experiment in the figure legends. P-values were determined by a two-tailed t test with Welch's correction unless otherwise indicated whereas p-values for the Kaplan-Meier survival curve were determined with the log rank test. The p-values are presented as follows: $*P < 0.05$, $**P < 0.01$, $***P < 0.001$, $****P < 0.0001$.

2.6.13 Data and code availability

The datasets generated in this study are available in the NCBI GEO database under GSE152376. Code to reproduce the analyses of the single-cell and bulk RNA-seq datasets can be found at https://github.com/cheungpriscilla/CellStemCell_2020.

2.6.14 Antibodies

Antibody	Source	Identifier
Rabbit monoclonal anti-YAP (clone D8H1X)	Cell Signaling Technology	Cat#14074; RRID: AB_2650491
Rabbit polyclonal anti-human Lysozyme	Dako	Cat#A0099; RRID: AB_2341230
Rabbit monoclonal anti-Ki67 (clone SP6)	GeneTex	Cat#GTX16667; RRID: AB_422351

Rat monoclonal anti-mouse CD44	BD Biosciences	Cat#550538; RRID: AB_393732
Goat polyclonal anti-mCherry (tdTomato)	Sicgen	Cat#AB0040-200; RRID: AB_2333092
Rat monoclonal anti-Ki67 (clone SolA15)	Invitrogen	Cat#14-5698-82; RRID: AB_10854564
Rabbit monoclonal non-phospho (active) β-catenin (Ser33/37/Thr41) (clone D13A1)	Cell Signaling Technology	Cat#8814; RRID: AB_11127203
Rabbit monoclonal anti-phospho-histone H3 (Ser10) (clone E173)	Millipore	Cat#04-1093; RRID: AB_1977262
Rabbit monoclonal anti-HA-tag (clone C29F4)	Cell Signaling Technology	Cat#3724; RRID: AB_1549585
Rabbit monoclonal anti-GAPDH (clone 14C10) (HRP conjugated)	Cell Signaling Technology	Cat#3683; RRID: AB_1642205
APC rat monoclonal anti-mouse CD326 (Ep-CAM)	BioLegend	Cat#118214; RRID: AB_1134102
APC/Cy7 rat monoclonal anti-mouse TER-119	BioLegend	Cat#116223; RRID: AB_2137788
APC/Cy7 rat anti-mouse CD45 (clone 30-F11)	BD Biosciences	Cat#557659; RRID: AB_396774
APC/Cy7 rat anti-CD11b (clone M1/70)	BD Biosciences	Cat#557657; RRID: AB_396772
Biotinylated goat anti-rabbit IgG	Vector Laboratories	Cat#BA-1000; RRID: AB_2313606
Biotinylated goat anti-rat IgG	Vector Laboratories	Cat#BA-9400; RRID: AB_2336202
Donkey anti-rabbit IgG, Alexa Fluor 488	Thermo Fisher Scientific	Cat#A-21206; RRID: AB_2535792
Donkey anti-rat IgG, Alexa Fluor 594	Thermo Fisher Scientific	Cat#A-21209; RRID: AB_2535795

2.6.15 RT-qPCR primers

Gene	Direction	Sequence 5' to 3'	Source
Mouse AmotL2	Forward	TGGAGACTGTACTGAGGGAGAA	Galli et al., 2015
	Reverse	GAGCCGCTGGATTTCATTTTCC	
Mouse Ankrd1	Forward	CATGATGCTGTGAGGCTGAAC	Galli et al., 2015
	Reverse	CATGATGCTGTGAGGCTGAAC	
Mouse Axin2	Forward	GCCAAGTGTCTCTACCTCATTT	This paper
	Reverse	TCCAGCTCCAGTTTCAGTTTC	
Mouse Cyr61	Forward	AGGTCTGCGCTAAACAACTCA	Galli et al., 2015
	Reverse	ATATTCACAGGGTCTGCCTTCT	
Mouse Gapdh	Forward	AGGTCGGTGTGAACGGATTTG	This paper
	Reverse	TGTAGACCATGTAGTTGAGGTCA	
Mouse Lgr5	Forward	CCTACTCGAAGACTTACCCAGT	This paper
	Reverse	GCATTGGGGTGAATGATAGCA	
Mouse Muc2	Forward	AGGGCTCGGAACTCCAGAAA	This paper
	Reverse	CCAGGGAATCGGTAGACATCG	
Mouse Reg4	Forward	CTGGAATCCCAGGACAAAGAGTG	Sasaki et al., 2016

2.6.16 RNAscope probes

Probe Name	Source	Identifier
RNAscope probe-Mm-AmotL2	Advanced Cell Diagnostics	Cat#515181
RNAscope probe-Mm-Lgr5	Advanced Cell Diagnostics	Cat#312171
RNAscope probe-Mm-Olfm4	Advanced Cell Diagnostics	Cat#311831
RNAscope probe-Mm-Axin2	Advanced Cell Diagnostics	Cat#400331
RNAscope probe-Mm-Reg4	Advanced Cell Diagnostics	Cat#409601
RNAscope probe-Mm-Klf6	Advanced Cell Diagnostics	Cat#426901

3

YAP as a tumor suppressive program in metastatic colorectal cancer

3.1 Abstract

Although the Hippo transcriptional coactivator YAP is considered oncogenic in many tissues, its role in colorectal cancer (CRC) remains controversial. Recently, we found that inhibition of the LATS1/2 Hippo kinases, which activates YAP, reprograms intestinal stem cells to a wound-healing like cell state characterized by low Wnt activity and reduced stemness. Here we demonstrate loss of LATS1/2 or overexpression of YAP is sufficient to reprogram *Lgr5*+ cancer stem cells to this state, thereby suppressing tumor growth and initiation in organoids, patient-derived xenografts, and mouse models of primary and metastatic CRC. We further show that genetic deletion of YAP and its paralog TAZ promotes the growth of these tumors. Collectively, our results establish the role of YAP as a tumor suppressor in the adult colon and implicate Hippo kinases as therapeutic vulnerabilities in colorectal malignancies.

3.2 Attributions

The work described in this chapter is adapted from the following manuscript:

> **Cheung P***, Xiol J*, Dill MT, Yuan WC, Panero R, Roper J, Osorio FG, Maglic D, Li Q, Gurung B, Calogero RA, Yilmaz ÖH, Mao J, Camargo FD. Regenerative Reprogramming of the Intestinal Stem Cell State via Hippo Signaling Suppresses Metastatic Colorectal Cancer. ***Cell Stem Cell***. 2020 Oct 1;27(4):590-604.e9.
>
> * Equal contribution

J.X. and F.D.C. conceived of the study. F.D.C. supervised the study. J.X. designed and performed the *Apc*$^{-/-}$ *Lats1/2* KO, AKP primary tumor experiments, and *Yap/Taz* tumor deletion experiments. P.C. designed and performed all *Apc*$^{-/-}$ *tetO-Yap*^{S127A} experiments,

bulk RNA-sequencing, cancer stem cell assays, and metastasis experiments. M.T.D. assisted with the AKP colonoscopy injection experiments. W.C.Y. assisted with the metastasis experiments. J.R. assisted with the *Yap/Taz* tumor deletion experiments under supervision of O.H.Y. F.G.O. assisted with the scRNA-seq experiments. Q.L. provided the Lats1/2 KO mice under supervision J.M. B.G. provided experimental support. P.C. carried out computational analyses with assistance from R.P., D.M., and R.A.G. P.C., J.X., and F.D.C. wrote the manuscript with critical reading and feedback from the other co-authors.

3.3 Introduction

Colorectal cancer (CRC) is the second leading cause of cancer related deaths in the United States and develops in a stepwise manner through in accumulation of mutations (Fearon, 2011; Fearon & Vogelstein, 1990; Siegel, Miller, & Jemal, 2020). The most common event that triggers formation of colon tumors is the acquisition of mutations that constitutively activates Wnt signaling, which is thought to be the first step in the sequence that leads to malignant transformation of colon epithelial cells. The growth of colon tumors is driven by cancer stem cells that are labeled by the Wnt receptor *Lgr5* as in healthy tissue (Merlos-Suárez et al., 2011; Schepers et al., 2012). As targeting the Wnt pathway for the treatment of CRC has been historically challenging, the recent discovery that depletion of *Lgr5*+ cancer stem cells can arrest tumor growth and prevent metastasis in preclinical models has opened the door for developing strategies to specifically target this cell population (De Sousa E Melo et al., 2017; Shimokawa et al., 2017).

A major pathway known to interact with Wnt in the intestine is the Hippo signaling pathway by mediating epithelial repair following injury (Cai et al., 2010; Gregorieff et al.,

2015; Yui et al., 2018). Recently, we found that Hippo inhibition or YAP activation reprograms intestinal stem cells into a distinct cell state with features of wound healing, low Wnt signature, and reduced stemness. Due to conflicting reports on the role of YAP in the progression of CRC, whether crosstalk between the Hippo and Wnt signaling pathways could serve as a potential therapeutic window for the treatment of CRC remains unclear (Azzolin et al., 2014; Barry et al., 2013; Cai et al., 2015; Gregorieff et al., 2015).

Using mouse and human models of CRC, we show that YAP is capable of reprogramming cancer stem cells into a low Wnt, non-proliferative state, which leads to tumor regression in primary and metastatic disease. In addition, deletion of YAP favors growth of focally induced colonic tumors, further supporting the notion that YAP acts as a tumor suppressor in the colon and that targeting the Hippo kinases represents a novel therapeutic approach for combatting CRC.

3.4 Results

3.4.1 YAP can reprogram *Lgr5*+ stem cells in the presence of constitutively active Wnt signaling

The fact that YAP remodels stem cells *in vitro* even in the presence of exogenous Wnt signals prompted us to analyze the effect of YAP in the context of constitutively active Wnt. To assess the role of YAP in this process, we introduced an *Apc* mutation via CRISPR/Cas9 into *tetO-YAP rtTA* colon organoids (**Figure 3.1A**). Strikingly, *Apc*$^{-/-}$ organoids lose their characteristic spheroid structure as early as three days after doxycycline induction and could not grow after passage (**Figure 3.1B**). *Lrig1-CreERT2*-mediated deletion of *Lats1/2* in *Apc* mutant organoids results in a similar growth inhibition upon plating (**Figure 3.1C**). As in *Apc* wildtype organoids, YAP targets and

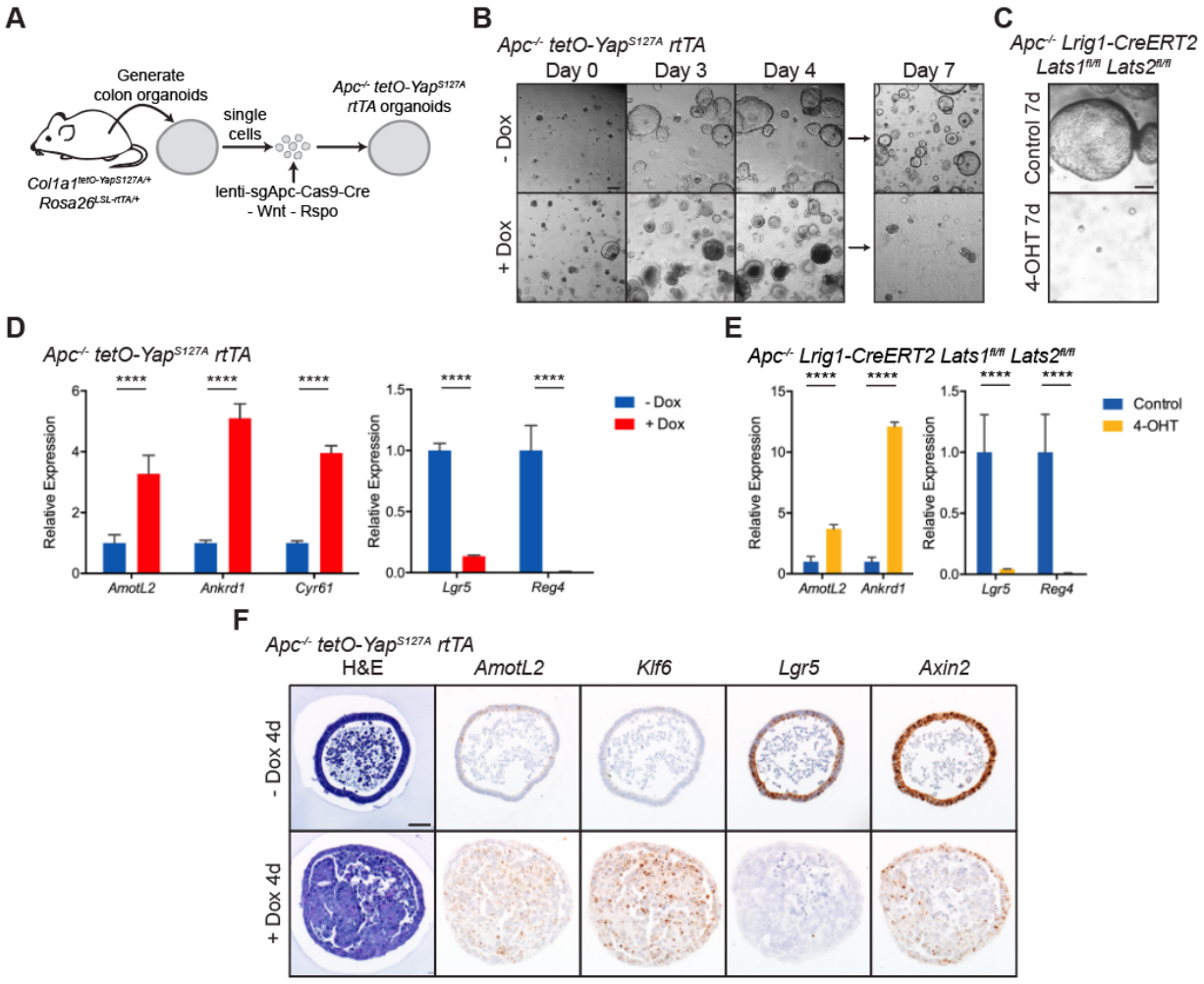

Figure 3.1. (A) Schematic for generating *Apc*$^{-/-}$ *tetO-YAP*^{S127A} *rtTA* organoids. (B) Brightfield images of *Apc*$^{-/-}$ *tetO-YAP*^{S127A} *rtTA* organoids on the indicated days in the presence or absence of doxycycline. The organoids were split on day 4. Scale bar, 200 µm. (C) Brightfield images of *Apc*$^{-/-}$ *Lrig1-CreERT2 Lats1/2*$^{fl/fl}$ organoids 7 days after plating in the presence of 4-OHT for 24 hours. Scale bar, 200 µm. (D) RT-qPCR analysis of the indicated genes in *Apc*$^{-/-}$ *tetO-YAP*^{S127A} *rtTA* organoids 1.5 days after induction with doxycycline. Data are represented as mean ± SEM; n = 3 biological and 3 technical replicates. ****$P < 0.0001$. (E) qRT-PCR analysis of the indicated genes in *Apc*$^{-/-}$ *Lrig1-CreERT2 Lats1/2*$^{fl/fl}$ organoids 2 days after treatment with 4-OHT for 24 hours. Data are represented as mean ± SEM; n = 2 biological and 2 technical replicates. ****p < 0.0001. (F) Histological analysis of *Apc*$^{-/-}$ *tetO-YAP*^{S127A} *rtTA* organoids 4 days after induction with doxycycline: H&E stains and RNA-ISH for *AmotL2*, *Klf6*, *Lgr5*, and *Axin2*. Scale bar, 50 µm.

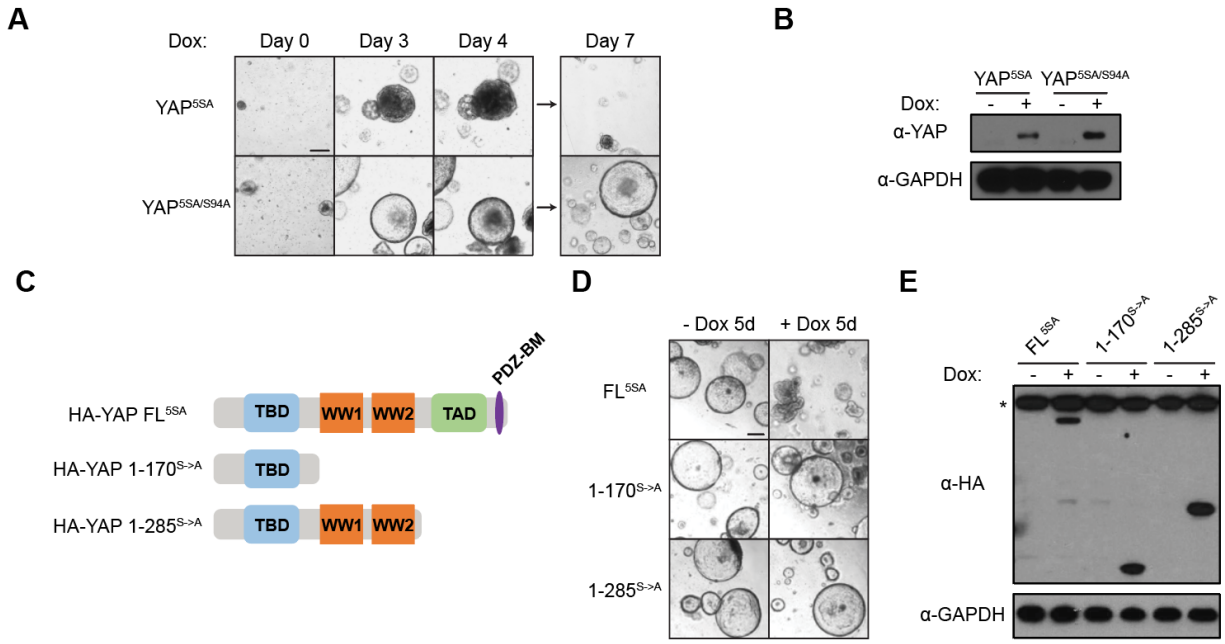

Figure 3.2. (A) Bright-field images of *Apc*$^{-/-}$ *CAGs-rtTA3* organoids expressing doxycycline-inducible Yap^{5SA} or YAP$^{5SA/S94A}$ on the indicated days in the presence of doxycycline. The organoids were split on day 4. Scale bar, 200 μm. (B) Western blot analysis of *Apc*$^{-/-}$ *CAGs-rtTA3* organoids expressing inducible YAP^{5SA} or YAP$^{5SA/S94A}$ after 2 days on doxycycline. Antibodies are indicated. (C) Schematic of the domain architecture of HA-tagged Yap^{5SA}: full-length (FL), amino acids 1-170, and amino acids 1-285. TBD = TEAD binding domain, WW = WW domain, TAD = transcription activation domain, PDZ-BM = PDZ-binding motif. (D) Bright-field images of *Apc*$^{-/-}$ *CAGs-rtTA3* organoids expressing inducible deletion versions of HA-tagged Yap^{5SA} for 5 days. Scale bar, 200 μm. (E) Western blot analysis of *Apc*$^{-/-}$ *CAGs-rtTA3* organoids expressing inducible deletion versions of HA-tagged YAP^{5SA} after 2 days on doxycycline. Antibodies are indicated. The asterisk indicates a non-specific band.

Klf6 are upregulated along with concomitant downregulation of ISC, DCS, and Wnt markers (**Figures 3.1D-F**). These results show that YAP is able to suppress Wnt and the colonic stem cell program even in the presence of constitutive Wnt signaling caused by the deletion of *Apc*.

To determine whether this reprogramming is mediated through YAP's transcriptional or cytoplasmic function, we generated *Apc*$^{-/-}$ *CAGs-rtTA3* organoids, carrying inducible expression of either YAP^{5SA} or YAP$^{5SA/S94A}$ (see STAR Methods) (Premsrirut et al., 2011). YAP^{5SA}, which cannot be phosphorylated by LATS1/2, is therefore nuclear and constitutively active while YAP^{S94A} cannot bind TEAD and is unable to activate transcription of target genes (Zhao et al., 2007, 2008). Only YAP^{5SA} expression is able to arrest organoid growth (**Figures 3.2A-B**), suggesting that binding to TEAD is required for YAP to prevent growth of *Apc*$^{-/-}$ organoids. We next determined whether YAP's transcription activation domain, which mediates recruitment of transcription machinery (Yagi et al., 1999), is required to mediate this phenotype. Expression of HA-tagged deletion versions of YAP^{5SA} in *Apc*$^{-/-}$ *CAGs-rtTA3* organoids reveals that only full-length YAP is able to induce proliferation arrest despite comparable levels of expression among the variants (**Figures 3.2C-E**). Collectively, these data suggest that YAP causes the loss of stem cell properties through TEAD-dependent transcriptional activity.

To gain further insight into the molecular changes underlying this change in cell fate, we performed RNA-seq analysis at sequential time points in *Apc*$^{-/-}$ *tetO-Yap rtTA* organoids upon YAP activation (**Figure 3.3A**). This analysis reveals an overall distinct transcriptional state of treated cells (**Figure 3.3B**), suggesting a global transcriptional reprogramming. This data also validate the immediate activation of YAP targets, substantiated by the enrichment of the Hippo signaling pathway and two published YAP

Figure 3.3. (A) Schematic of RNA-seq time course analysis in *Apc*$^{-/-}$ *tetO-YAP*^{S127A} *rtTA* organoids. (B) Heatmap of YAP downstream target genes, genes involved in Wnt signaling, and injury response genes over the time course of doxycycline induction in *Apc*$^{-/-}$ *tetO-YAP*^{S127A} *rtTA* organoids. (C) Principal component analysis of whole transcriptome profiles of *Apc*$^{-/-}$ *tetO-YAP*^{S127A} *rtTA* organoids at the indicated hours following doxycycline treatment. (D) GSEA of a YAP gene signature from Barry et al., 2013 in *Apc*$^{-/-}$ *tetO-YAP*^{S127A} *rtTA* organoids after 24 hours on doxycycline compared to 0 hours. (E) GSEA of a YAP gene signature from Gregorieff et al., 2015 in *Apc*$^{-/-}$ *tetO-YAP*^{S127A} *rtTA* organoids after 24 hours on doxycycline compared to 0 hours. (F) GSEA of KEGG pathways in *Apc*$^{-/-}$ *tetO-YAP*^{S127A} *rtTA* organoids after 24 hours on doxycycline compared to 0 hours. (G) GSEA of a *Lgr5* ISC gene signature in *Apc*$^{-/-}$ *tetO-YAP*^{S127A} *rtTA* organoids after 72 hours on doxycycline compared to 0 hours. (H) Heatmap of Wnt signaling pathway nuclear co-factors over the time course of doxycycline treatment in *Apc*$^{-/-}$ *tetO-YAP*^{S127A} *rtTA* organoids. (I) GSEA of KEGG pathways in *Apc*$^{-/-}$ *tetO-YAP*^{S127A} *rtTA* organoids after 72 hours on doxycycline compared to 0 hours. (J) GO overrepresentation analysis of upregulated transcription factors (adjusted p-value < 0.05 and $\log_2$ fold change > 1) in *Apc*$^{-/-}$ *tetO-YAP*^{S127A} *rtTA* organoids after 72 hours on doxycycline compared to 0 hours. (K) GSEA of intestinal β-catenin targets in differentially expressed transcription factors in *Apc*$^{-/-}$ *tetO-YAP*^{S127A} *rtTA* organoids after 72 hours on doxycycline compared to 0 hours.

Figure 3.3 (Continued)

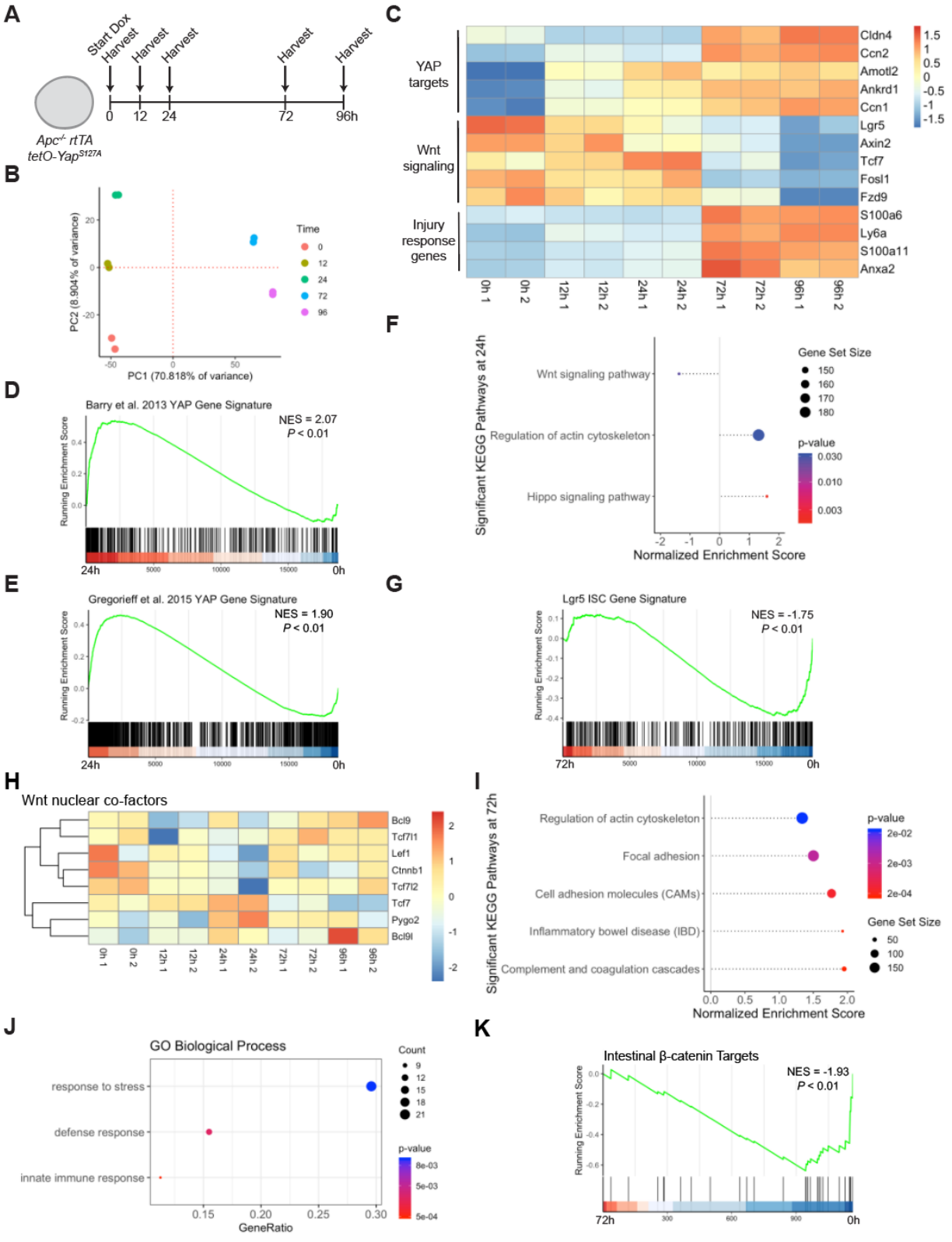

gene signatures by GSEA (**Figures 3.3C-F**), and the downregulation of Wnt and ISC gene signatures, which predominantly occurs between 24 and 72 hours (**Figures 3.3C, 3.3F, and 3.3G**) (Barry et al., 2013; Gregorieff et al., 2015; Muñoz et al., 2012). Interestingly, Wnt nuclear co-factors are not downregulated over the course of YAP activation with the exception of *Tcf7*, which is also a target of the Wnt pathway (**Figure 3.3H**), suggesting that downregulation of Wnt signaling upon YAP activation may be due to post-translational modifications or changes in protein interaction partners of these factors unrelated to transcript levels. Additionally, injury signature genes, such as *Anxa2*, *Ly6a/Sca1*, *S100A6*, and *S100A11*, are concomitantly upregulated, and pathways related to cell-cell contact, actin cytoskeleton, and response to injury are significantly enriched at 72 hours (**Figures 3.3C and 3.3I**). These enriched pathways are also recapitulated in GO overrepresentation analysis and GSEA of the transcription factors differentially expressed at 72 hours (**Figures 3.3J-K**), underscoring their role in mediating this cell fate change. Altogether, these findings substantiate the transcriptional activity of YAP in driving a complete reprogramming of intestinal cells even in the context of an *Apc* deletion.

3.4.2 Activation of YAP induces loss of cancer stem cells and tumor regression

We next tested whether YAP expression could also induce similar molecular changes in colon organoids carrying mutations associated with malignant colon cancer disease. In order to do so, we generated $Apc^{-/-}$ $Kras^{G12D}$ $p53^{-/-}$ (AKP) cancer organoids with inducible YAP^{5SA} overexpression (**Figure 3.4A**). Overexpression of YAP^{5SA} by addition of doxycycline to the culture media leads to death of AKP organoids by seven days after induction (**Figure 3.4B**). As in wild-type and $Apc^{-/-}$ organoids, ISC marker *Lgr5* and DCS

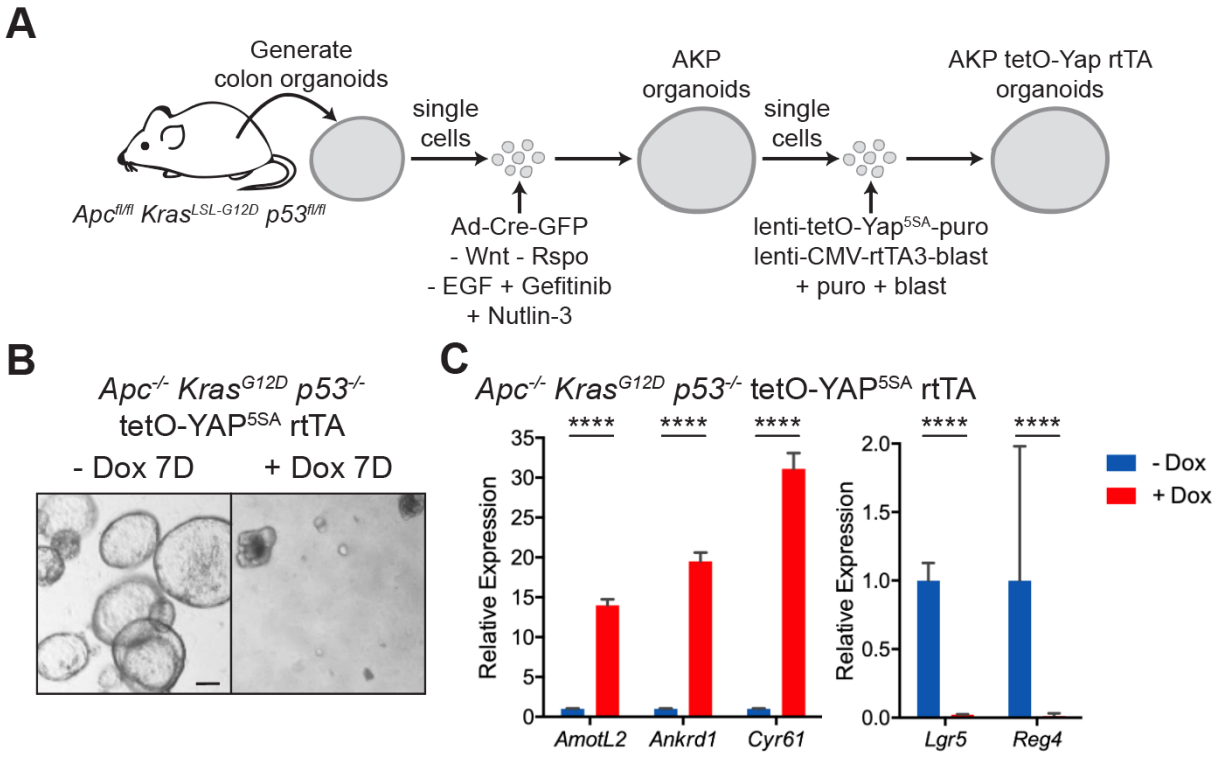

Figure 3.4. (A) Schematic for generating *Apc*$^{-/-}$ *Kras*^{G12D} *p53*$^{-/-}$ tetO-YAP^{5SA} rtTA organoids. (B) Brightfield images of *Apc*$^{-/-}$ *Kras*^{G12D} *p53*$^{-/-}$ tetO-YAP^{5SA} rtTA organoids after 7 days in the presence or absence of doxycycline. The organoids were split on day 4. Scale bar, 200 μm. (C) RT-qPCR analysis of the indicated genes in *Apc*$^{-/-}$ *Kras*^{G12D} *p53*$^{-/-}$ tetO-YAP^{5SA} rtTA organoids 3 days after induction with doxycycline. Data are represented as mean ± SEM; n = 3 biological and 2 technical replicates. ****$P < 0.0001$.

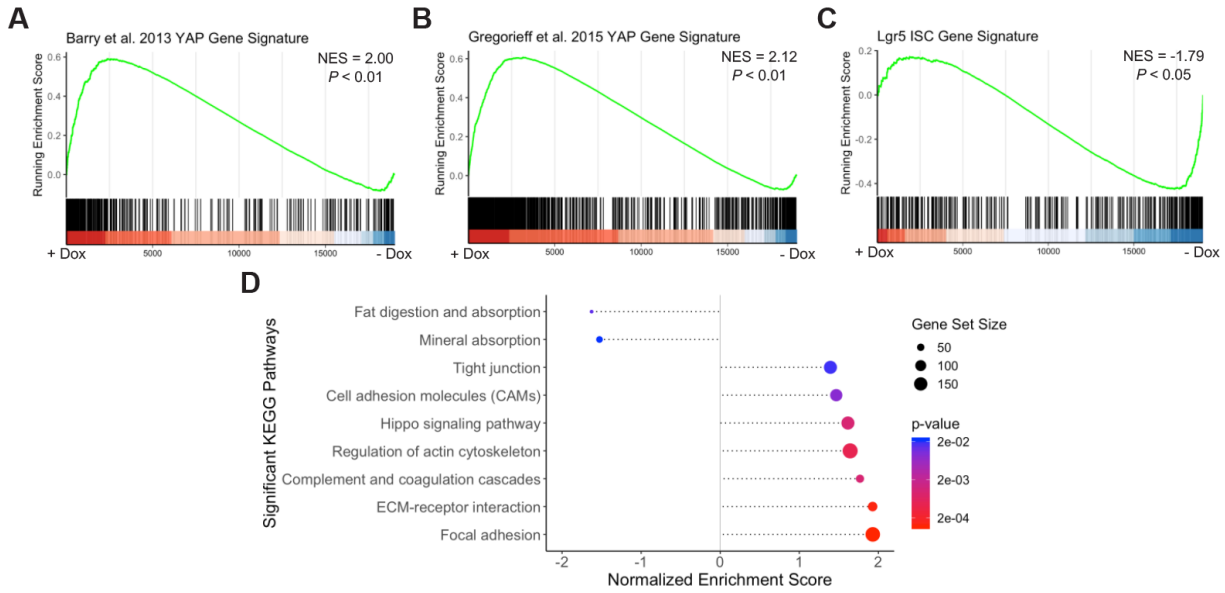

Figure 3.5. (A) GSEA of a YAP gene signature from Barry et al., 2013 in *Apc*$^{-/-}$ *Kras*^{G12D} *p53*$^{-/-}$ tetO-YAP^{5SA} rtTA organoids 3 days after induction with doxycycline. (B) GSEA of a YAP gene signature from Gregorieff et al., 2015 in *Apc*$^{-/-}$ *Kras*^{G12D} *p53*$^{-/-}$ tetO-YAP^{5SA} rtTA organoids 3 days after treatment with doxycycline. (C) GSEA of KEGG pathways in *Apc*$^{-/-}$ *Kras*^{G12D} *p53*$^{-/-}$ tetO-YAP^{5SA} rtTA organoids 3 days after induction with doxycycline. (D) GSEA of a *Lgr5* ISC gene signature in *Apc*$^{-/-}$ *Kras*^{G12D} *p53*$^{-/-}$ tetO-YAP^{5SA} rtTA organoids 3 days after induction with doxycycline.

marker *Reg4* are downregulated after doxycycline induction (**Figure 3.4C**). Similar to other contexts, RNA-seq analysis of these organoids at 72 hours post doxycycline reveals significant enrichment of previously published YAP gene signatures and pathways involving cell-cell contact, actin cytoskeleton, and response to injury and negative enrichment of those related intestinal absorption and the *Lgr5* ISC gene signature (**Figures 3.5A-D**) (Barry et al., 2013; Gregorieff et al., 2015; Muñoz et al., 2012), confirming our previous findings that YAP is reprogramming these cancer cells to a low Wnt, wound healing-like state.

To test if YAP is capable of reprogramming AKP cells *in vivo*, where the cells are exposed to additional niche factors, we injected AKP organoids in the colon of NSG mice (**Figure 3.6A**). Two weeks after injection, YAP^{5SA} overexpression was induced by adding doxycycline to drinking water. Strikingly, histological analysis shows that tumor cells 4 days post doxycycline present with a different morphology, with an enlarged cytoplasm and loss of the characteristic columnar shape (**Figure 3.6B**). Expression of *Lgr5* is completely lost, and β-catenin is dislocated from the nucleus to the cytoplasm (**Figures 3.6B-C**). Further supporting the notion that these cells lack active Wnt signaling, expression of *Axin2* is greatly reduced. These YAP-overexpressing cells are also not proliferative, and as a consequence, YAP induction by doxycycline confers a survival advantage in these transplants (**Figure 3.6D**). To quantify tumor growth, we injected AKP organoids in the flanks of nude mice and confirmed that YAP-overexpressing cells in this model undergo the same phenotypic and molecular changes as cells growing in the colon (**Figure 3.7A-B**). Remarkably, YAP overexpression induces loss of cellularity and tumor regression (**Figures 2.7C-D**).

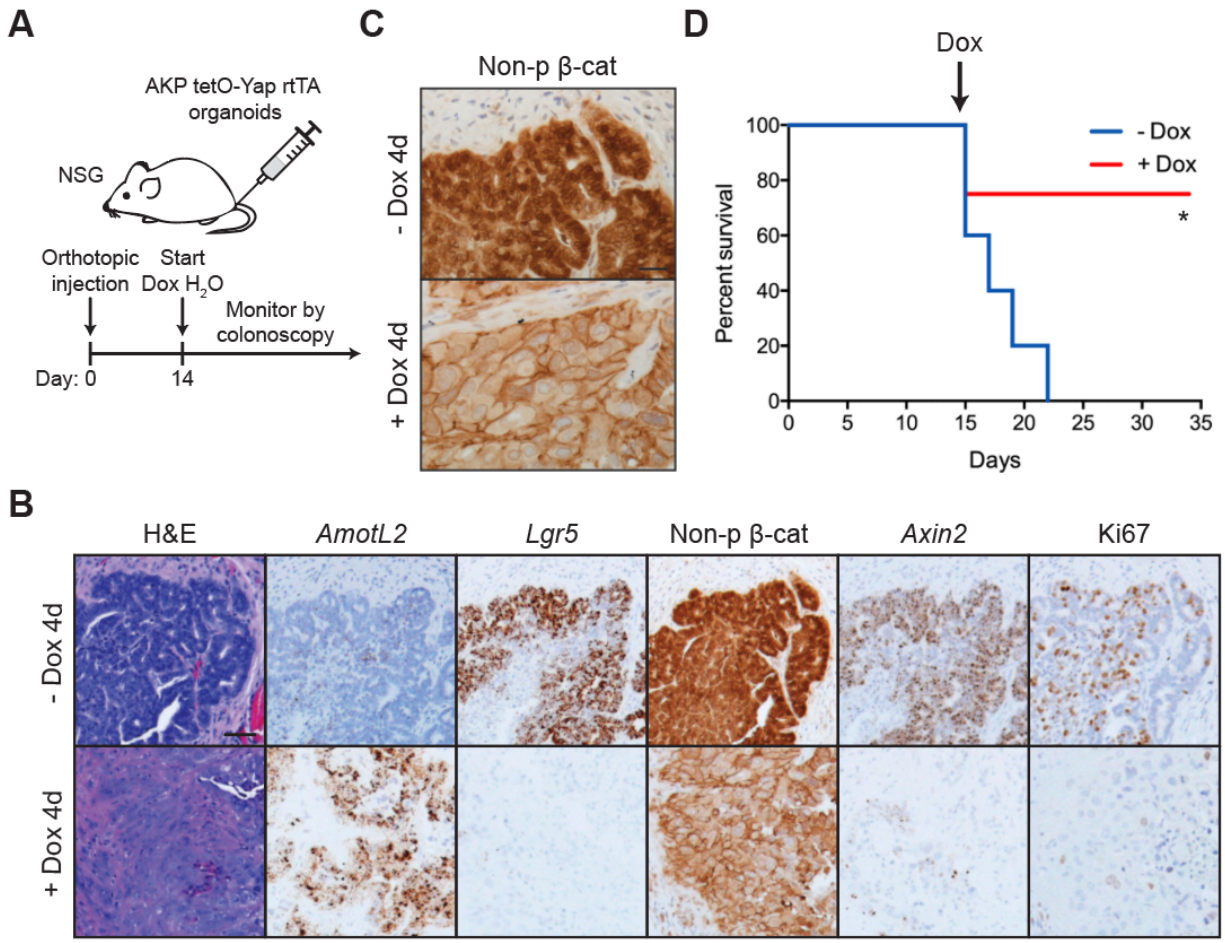

Figure 3.6. (A) Schematic of timeline for orthotopic injection of *Apc*$^{-/-}$ *Kras*^{G12D} *p53*$^{-/-}$ tetO-YAP^{5SA} rtTA organoids in the colons of NSG mice and doxycycline administration. (B) Histological analysis of orthotopic tumors from *Apc*$^{-/-}$ *Kras*^{G12D} *p53*$^{-/-}$ tetO-YAP^{5SA} rtTA organoids 4 days after doxycycline administration: H&E stains, IHC for non-phosphorylated (active) β-catenin and Ki67, and RNA-ISH for *AmotL2*, *Lgr5,* and *Axin2*. Scale bar, 50 μm. (C) IHC for non-phosphorylated β-catenin from *Apc*$^{-/-}$ *Kras*^{G12D} *p53*$^{-/-}$ rtTA tetO-YAP^{5SA} orthotopic tumors 4 days after doxycycline administration. Scale bar, 50 μm. (D) Kaplan-Meier survival curve of mice injected orthotopically with *Apc*$^{-/-}$ *Kras*^{G12D} *p53*$^{-/-}$ tetO-YAP^{5SA} rtTA organoids. Doxycycline treatment was started 14 days after injection as indicated with the arrow. - dox: n = 5, + dox: n = 4. *$P < 0.05$.

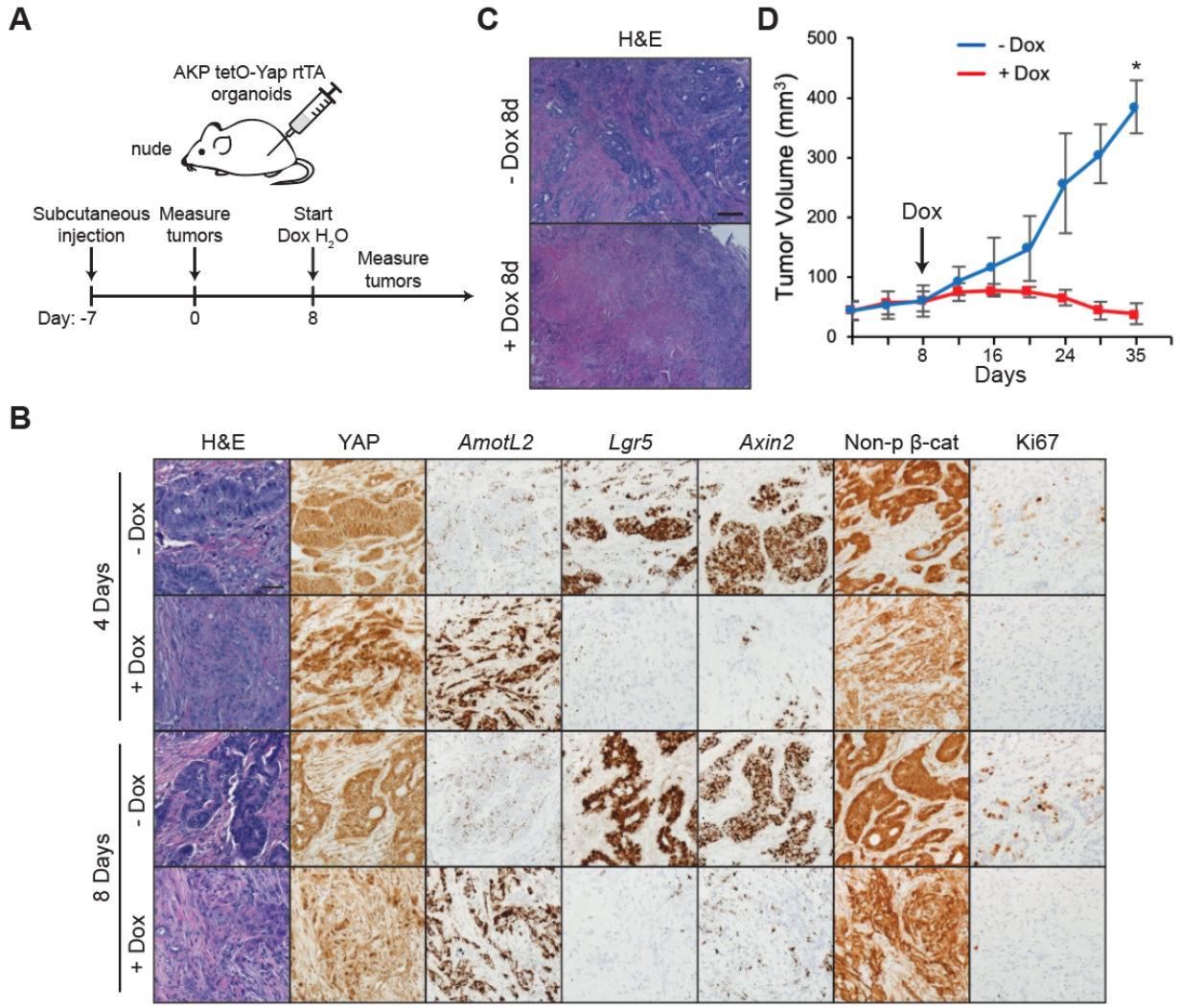

Figure 3.7. (A) Schematic of timeline for subcutaneous injection of *Apc*$^{-/-}$ *Kras*^{G12D} *p53*$^{-/-}$ tetO-YAP^{5SA} rtTA organoids in the flanks of nude mice, tumor measurements, and doxycycline administration. (B) Histological analysis of *Apc*$^{-/-}$ *Kras*^{G12D} *p53*$^{-/-}$ tetO-YAP^{5SA} rtTA subcutaneous tumors on the indicated days following doxycycline administration: H&E stains, IHC for YAP, non-phosphorylated β-catenin, and Ki67, and RNA-ISH for *AmotL2, Lgr5*, and *Axin2*. Scale bar, 50 μm. (C) H&E stains of *Apc*$^{-/-}$ *Kras*^{G12D} *p53*$^{-/-}$ tetO-YAP^{5SA} rtTA subcutaneous tumors 8 days after doxycycline administration. Scale bar, 200 μm. (D) Growth curve of subcutaneous tumors from *Apc*$^{-/-}$ *Kras*^{G12D} *p53*$^{-/-}$ tetO-YAP^{5SA} rtTA organoids injected in the flanks of nude mice. Measurements were started one week after injection (shown as day 0 on the plot). The arrow indicates the day doxycycline treatment was started. Data are represented as mean ± SD. **P* < 0.05.

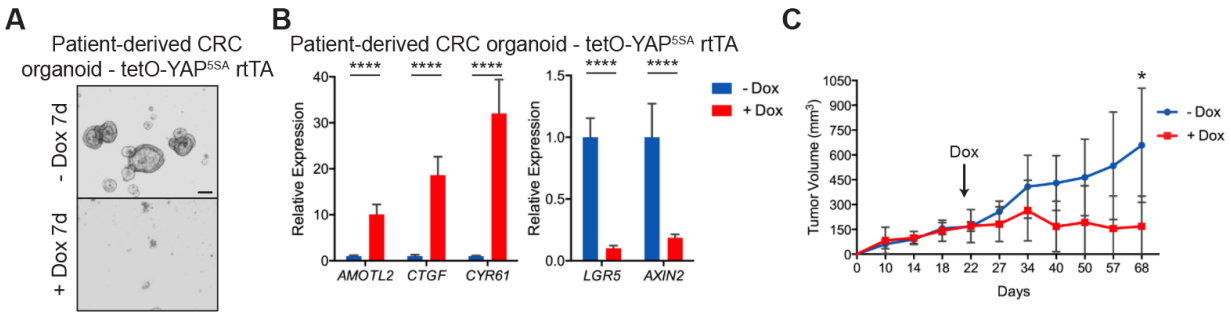

Figure 3.8. (A) Bright-field images of a patient-derived CRC organoid line with inducible YAP^{5SA} expression after 7 days in the presence or absence of doxycycline. The organoids were split on day 4. Scale bar, 200 µm. (B) RTq-PCR analysis of the indicated genes in patient-derived CRC organoids expressing YAP^{5SA}. Data are represented as mean ± SEM; n = 2 biological and 2 technical replicates. ****p < 0.0001. (C) Growth curve of subcutaneous tumors from patient-derived CRC organoids expressing YAP^{5SA} injected in the flanks of nude mice. The arrow indicates the day doxycycline treatment was started. Measurements were started one week after injection (shown as day 0 on the graph). *p < 0.05.

We also validated the role of YAP in human CRC as engineered inducible YAP^{5SA} expression leads to the reduction in growth of a patient-derived CRC organoid line (**Figure 3.8A**). This is accompanied by increased YAP target expression and strong downregulation of ISC and Wnt markers *LGR5* and *AXIN2* (**Figure 3.8B**). Additionally, expression of YAP in established human CRC xenografts leads to a statistically significant reduction in growth compared to their uninduced counterparts (**Figure 3.8B**). Taken together, our results indicate that YAP activation in CRC organoids leads to molecular reprogramming and proliferation arrest.

3.4.3 YAP suppresses cancer stemness in primary and metastatic tumor growth

We next tested the ability of YAP to suppress two critical features of malignant growth: tumor initiating capacity and metastatic potential. To measure tumor propagating capacity, we performed secondary transplantation of AKP colon organoids with and without YAP activation. After allowing the tumors to grow in mice for 6 weeks, we induced them with doxycycline for 2 days and isolated the EpCAM+ cells via FACS (**Figures 3.9A-B**). As before, we observed an increase in nuclear YAP and the YAP target *AmotL2* and a decrease in ISC and Wnt markers *Lgr5* and *Axin2* after only 2 days (**Figure 3.9C**). Equal numbers of uninduced and induced EpCAM+ tumor cells were transplanted subcutaneously into nude mice. While uninduced tumor cells grow dramatically over the course of 4 weeks, cells from doxycycline-induced tumors have virtually no capacity to reinitiate tumor growth (**Figures 3.9D-E**). Similarly, AKP organoids induced with doxycycline in culture for 4 days also exhibit a lack of growth following transplant compared to uninduced controls (**Figures 3.10A-C**), suggesting that YAP activation abolishes the tumor propagating potential of triple mutant AKP colon cancer cells.

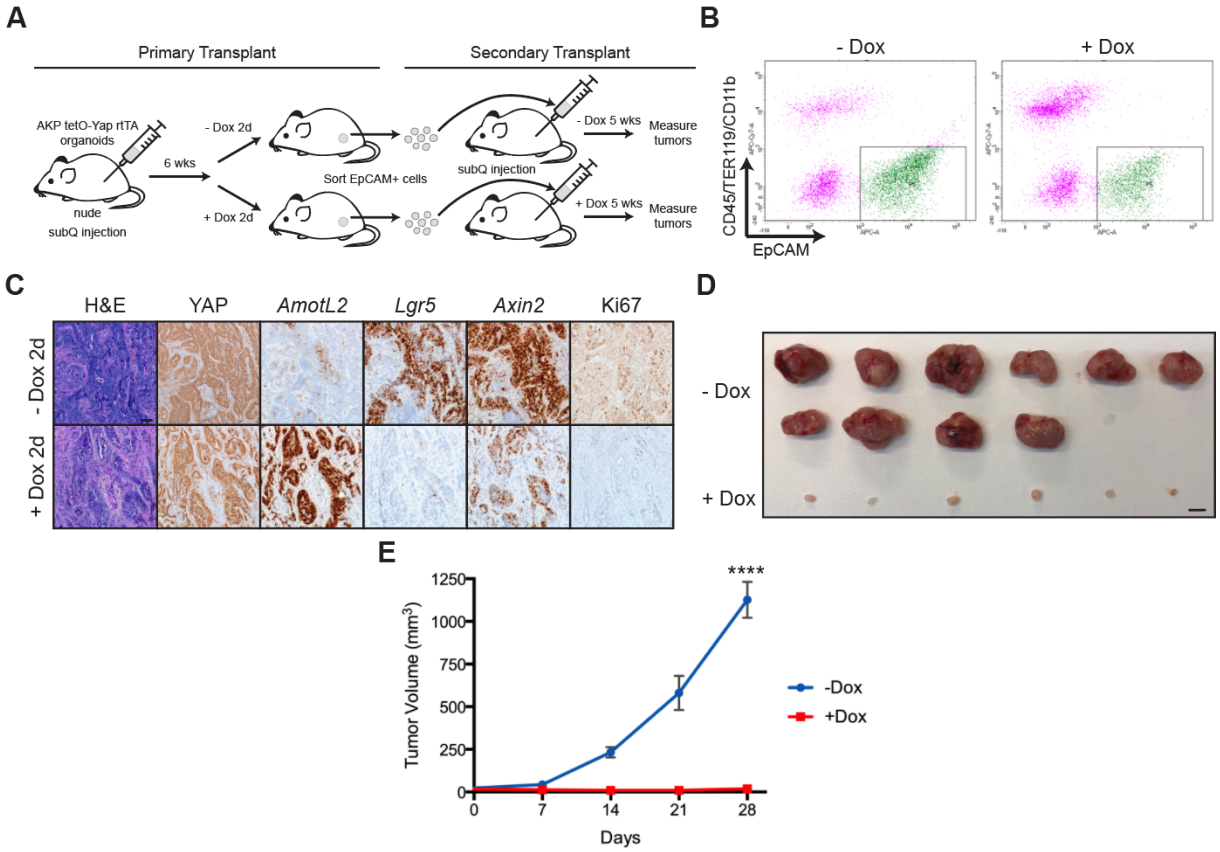

Figure 3.9. (A) Schematic of primary and secondary transplantation of *Apc*$^{-/-}$ *Kras*^{G12D} *p53*$^{-/-}$ tetO-YAP^{5SA} rtTA organoid cells into nude mice, including timeline of subcutaneous injections, doxycycline administration, and tumor isolation. (B) Gating strategy for isolation of *Apc*$^{-/-}$ *Kras*^{G12D} *p53*$^{-/-}$ tetO-YAP^{5SA} rtTA subcutaneous tumor cells by FACS. Tumor cells from control and doxycycline-treated mice were sorted on forward scatter and side scatter and subsequently by EpCAM+, Lin- (CD45, TER119, CD11b), and DAPI-. Sorted cells were then injected subcutaneously into nude mice for secondary transplants. (C) Histological analysis of *Apc*$^{-/-}$ *Kras*^{G12D} *p53*$^{-/-}$ tetO-YAP^{5SA} rtTA subcutaneous tumors 2 days after doxycycline administration: H&E stains, IHC for YAP and Ki67, and RNA-ISH for *AmotL2*, *Lgr5,* and *Axin2*. Scale bar, 50 μm. (D) Gross morphology of *Apc*$^{-/-}$ *Kras*^{G12D} *p53*$^{-/-}$ tetO-YAP^{5SA} rtTA secondary tumors harvested 5 weeks following transplant. Scale bar, 5 mm. (E) Growth curve of subcutaneous tumors from *Apc*$^{-/-}$ *Kras*^{G12D} *p53*$^{-/-}$ tetO-YAP^{5SA} rtTA organoid cells following secondary transplantation with or without doxycycline treatment. Measurements were started one week after injection (shown as day 0 on the plot). Data are represented as mean ± SEM; - dox: n = 10 tumors; + dox: n = 6 tumors. ****P < 0.0001.

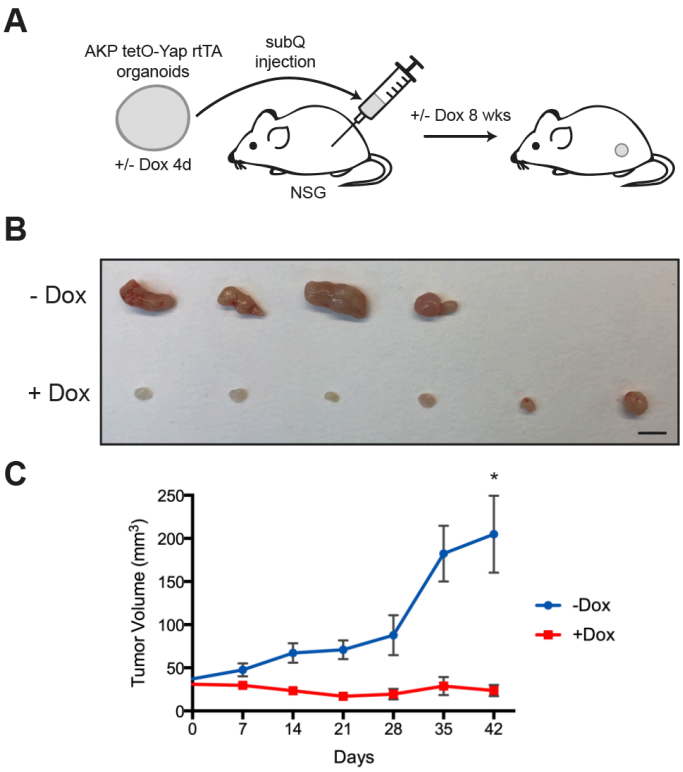

Figure 3.10. (A) Schematic of subcutaneous transplantation of control or doxycycline-treated *Apc*$^{-/-}$ *Kras*^{G12D} *p53*$^{-/-}$ tetO-YAP^{5SA} rtTA organoids into nude mice. (B) Gross morphology of subcutaneous tumors derived from control or doxycycline-treated *Apc*$^{-/-}$ *Kras*^{G12D} *p53*$^{-/-}$ tetO-YAP^{5SA} rtTA organoids 8 weeks following transplant. Scale bar, 5 mm. (C) Growth curve of subcutaneous tumors from control or doxycycline-treated *Apc*$^{-/-}$ *Kras*^{G12D} *p53*$^{-/-}$ tetO-YAP^{5SA} rtTA organoids injected into the flanks of nude mice. Measurements were started one week after injection (shown as day 0 on the graph). Data are represented as mean ± SEM; - dox, n = 6 tumors; + dox, n = 4 tumors. *$p < 0.05$.

To test the effect of YAP on metastatic potential, we engineered an additional *Smad4* mutation via CRISPR/Cas9 in AKP colon organoids to enhance their metastatic capacity (**Figures 3.11A-B**) (Fumagalli et al., 2017; Miyaki et al., 1999; B. Zhang et al., 2010). Strikingly, even in the presence of a fourth mutation, AKPS organoids with engineered YAP^{5SA} expression are not able to reform organoids by day 7 (**Figure 3.11C**). Similarly, these organoids also downregulate ISC and DCS markers as early as day 2 (**Figure 3.11D**). To test their metastatic potential *in vivo*, we injected control and doxycycline-induced AKPS organoids in the spleens of NSG mice (**Figures 3.12A**), which leads to formation of metastases in the liver (Fujii et al., 2016; O'Rourke et al., 2017). Five weeks post injection, we found that the livers of NSG mice injected with YAP-expressing AKPS organoids have a drastic and significant reduction in tumor burden (**Figures 3.12B-C**). Histological analysis of these livers reveals small metastatic foci compared to the extensive metastatic burden in livers with uninduced organoids (**Figure 3.12D**), suggesting YAP-expressing cancer cells are less able to seed and establish metastases in the liver.

To characterize the role of YAP on established liver metastases, we allowed AKPS organoids to grow in the livers of NSG mice for 5 weeks before administering doxycycline for 10 days. YAP activation has a drastic effect on the morphology of established metastatic tumors with obvious and large areas of necrosis (**Figure 3.13A**). Additionally, we observed the near complete elimination of *Lgr5*+ ISCs and a significant reduction in their proliferative index (**Figures 3.13B-C**). Altogether, our data point to the therapeutic role of activating YAP in preventing both the establishment and growth of liver metastases.

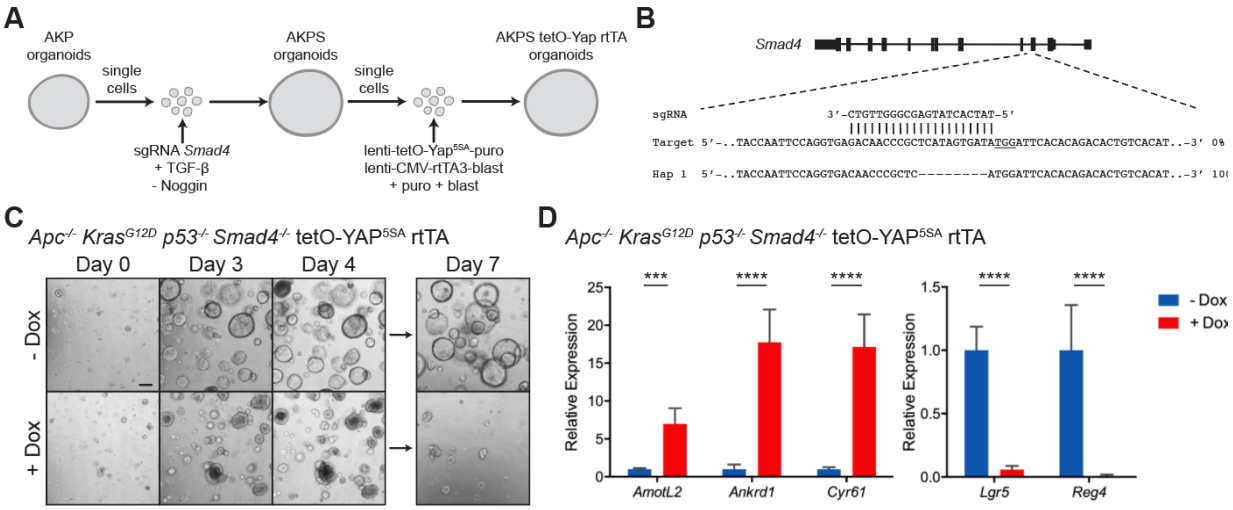

Figure 3.11. (A) Schematic for generating *Apc*$^{-/-}$ *Kras*^{G12D} *p53*$^{-/-}$ *Smad4*$^{-/-}$ tetO-YAP^{5SA} rtTA organoids. (B) Gene-targeting strategy for *Smad4*. The protospacer adjacent motif is underlined on the target sequence, and the allelic fraction of the haplotype identified is indicated. (C) Brightfield images of *Apc*$^{-/-}$ *Kras*^{G12D} *p53*$^{-/-}$ *Smad4*$^{-/-}$ tetO-YAP^{5SA} rtTA organoids on the indicated days in the presence or absence of doxycycline. The organoids were split on day 4. Scale bar, 200 μm. (D) RT-qPCR analysis of the indicated genes in *Apc*$^{-/-}$ *Kras*^{G12D} *p53*$^{-/-}$ *Smad4*$^{-/-}$ tetO-YAP^{5SA} rtTA organoids 2 days after induction with doxycycline. Data are represented as mean ± SEM; n = 3 biological and 2 technical replicates. ***P < 0.001 and ****P < 0.0001.

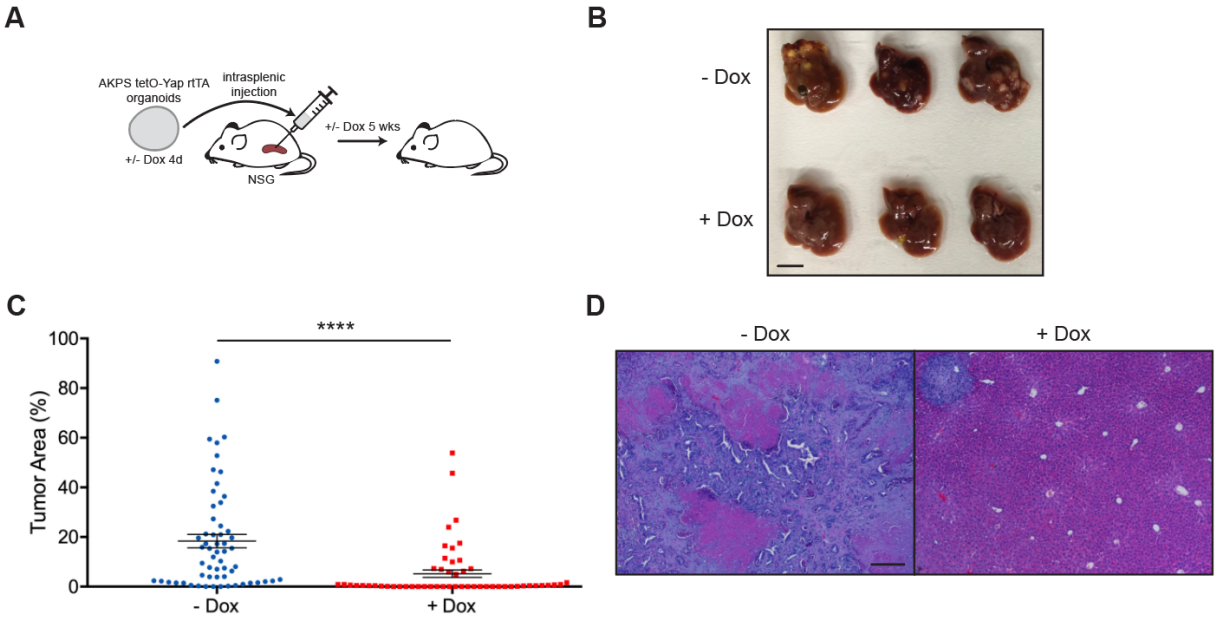

Figure 3.12. (A) Schematic of intrasplenic injection of uninduced and doxycycline-induced *Apc*$^{-/-}$ *Kras*^{G12D} *p53*$^{-/-}$ *Smad4*$^{-/-}$ tetO-YAP^{5SA} rtTA organoids into NSG mice. (B) Gross morphology of representative livers of NSG mice injected intrasplenically with *Apc*$^{-/-}$ *Kras*^{G12D} *p53*$^{-/-}$ *Smad4*$^{-/-}$ tetO-YAP^{5SA} rtTA organoids induced with or without doxycycline for 4 days in culture. Scale bar, 10 mm. (C) Quantification of tumor area per liver piece from Figure 6F. Dot plot is represented as mean ± SEM; - dox: n = 9-10 liver pieces per mouse, n = 6 mice; + dox: n = 9-10 liver pieces per mouse, n = 5 mice. ****P < 0.0001. (D) Representative H&E staining of livers from Figure 6F. Scale bar, 200 μm.

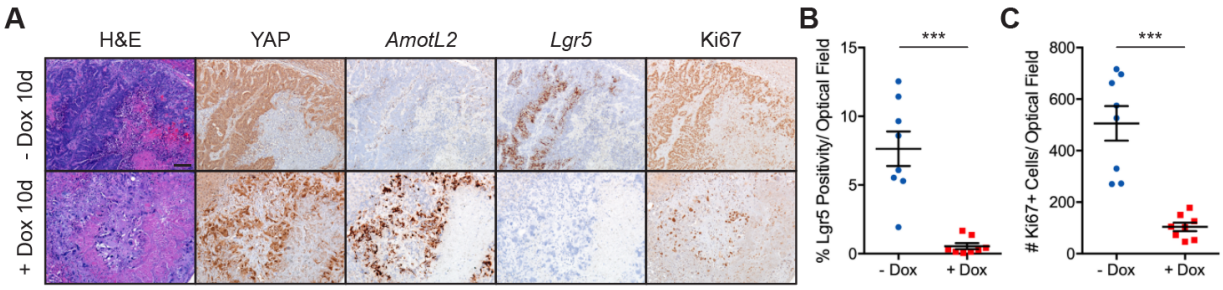

Figure 3.13. (A) Histological analysis of *Apc*$^{-/-}$ *Kras*^{G12D} *p53*$^{-/-}$ *Smad4*$^{-/-}$ tetO-YAP^{5SA} rtTA metastases 10 days after doxycycline administration: H&E stains, IHC for YAP and Ki67, and RNA-ISH for *AmotL2* and *Lgr5*. Scale bar, 100 μm. (B) Quantification of *Lgr5* positive staining in control and doxycycline-treated *Apc*$^{-/-}$ *Kras*^{G12D} *p53*$^{-/-}$ *Smad4*$^{-/-}$ tetO-YAP^{5SA} rtTA metastases from Figure S6I. Dot plot is represented as mean ± SEM; - dox, n = 4 optical fields per mouse, n = 2 mice; + dox, n = 2 optical fields per mouse, n = 4 mice. ***p < 0.001. (C) Quantification of Ki67+ cells per high powered optical field in control and doxycycline-treated *Apc*$^{-/-}$ *Kras*^{G12D} *p53*$^{-/-}$ *Smad4*$^{-/-}$ tetO-YAP^{5SA} rtTA metastases from Figure S6I. Dot plot is represented as mean ± SEM; - dox, n = 4 optical fields per mouse, n = 2 mice; + dox, n = 2 optical fields per mouse, n = 4 mice. ***p < 0.001.

3.4.4 Deletion of YAP/TAZ increases colon tumor growth

The data presented in this manuscript relating to YAP overactivation speak to a tumor suppressive role for YAP in CRC. However, other work has reported that YAP is required for intestinal and colonic tumor growth either in cell lines or in a mouse model of familial adenomatous polyposis (FAP), where one copy of *Apc* is mutated, and numerous tumors appear upon stochastic loss of the second copy (Cai et al., 2015; Gregorieff et al., 2015; Konsavage et al., 2012; Rosenbluh et al., 2012; Zhou et al., 2011). These experimental settings use a developmental deletion of YAP/TAZ and predominantly look at tumor formation in the small intestine. To test unbiasedly the effects of *Yap* and *Taz* knockout on the growth of discrete *Apc*-mutant tumors in the adult colon *in vivo*, we injected adenovirus expressing Cre recombinase in the colonic mucosa of $Apc^{fl/fl}$ and $Apc^{fl/fl}$ $Yap^{fl/fl}$ $Taz^{fl/fl}$ mice (**Figure 3.14A**) (Colnot et al., 2004; Schlegelmilch et al., 2011; Xin et al., 2013). While all mice at eight-weeks post injection develop tumors, $Apc^{fl/fl}$ $Yap^{fl/fl}$ $Taz^{fl/fl}$ mice present with higher tumor burden (**Figures 3.14 B-C**). We observed YAP deletion efficiency ranging from 40 to 100% in the tumors from $Apc^{fl/fl}$ $Yap^{fl/fl}$ $Taz^{fl/fl}$ mice and downregulation of the YAP target *AmotL2* in the YAP-deleted cells (**Figures 3.14D-E**). Furthermore, *Yap/Taz* knockout tumors have a significantly higher number of proliferating cells by phospho-histone H3 staining (**Figures 3.14F-G**), explaining the difference in tumor burden. Although these adenomas rarely become malignant, they grow until they obstruct the colonic lumen of the mice at which point the animals have to be euthanized. Taking this into account, we observed a significant decrease in survival in animals bearing *Yap/Taz* deleted tumors compared to their control counterparts (**Figure 3.14H**). Collectively, these results show

Figure 3.14. (A) Schematic of orthotopic injection of adenovirus expressing Cre recombinase (Ad-Cre) into mice of the indicated genotypes. (B) Colonoscopy images of mice of the indicated genotypes 8 weeks after injection with Ad-Cre in the colonic mucosa. (C) Volume of tumors from mice of the indicated genotypes harvested 8 weeks after injection with Ad-Cre in the colonic mucosa. Data are presented as mean ± SEM; n = 4 tumors per genotype. (D) Histological analysis of Ad-Cre injected *Apc*$^{fl/fl}$ and *Apc*$^{fl/fl}$ *Yap*$^{fl/fl}$ *Taz*$^{fl/fl}$ colonic tumors: H&E stains, YAP IHC, and *AmotL2* RNA-ISH. Scale bar, 20 μm. (E) IHC for YAP in tumors from *Apc*$^{fl/fl}$ *Yap*$^{fl/fl}$ *Taz*$^{fl/fl}$ mice injected with Ad-Cre. Scale bar, 200 μm. (F) IHC for 71hosphor-histone H3 (pH3) in Ad-Cre injected *Apc*$^{fl/fl}$ and *Apc*$^{fl/fl}$ *Yap*$^{fl/fl}$ *Taz*$^{fl/fl}$ colonic tumors. Scale bar, 100 μm. (G) Quantification of pH3+ cells per optical field in Ad-Cre injected *Apc*$^{fl/fl}$ and *Apc*$^{fl/fl}$ *Yap*$^{fl/fl}$ *Taz*$^{fl/fl}$ colonic tumors. Dot plot is represented as mean ± SEM; n = 2 measurements per mouse, n = 3 mice per group. $^{**}P < 0.01$. (H) Kaplan-Meier survival curve for mice of the indicated genotypes injected with Ad-Cre in the colonic mucosa. *Apc*$^{fl/fl}$: n = 9 mice; *Apc*$^{fl/fl}$ *Yap*$^{fl/fl}$ *Taz*$^{fl/fl}$: n = 10 mice. $^{***}P < 0.001$.

Figure 3.14 (Continued)

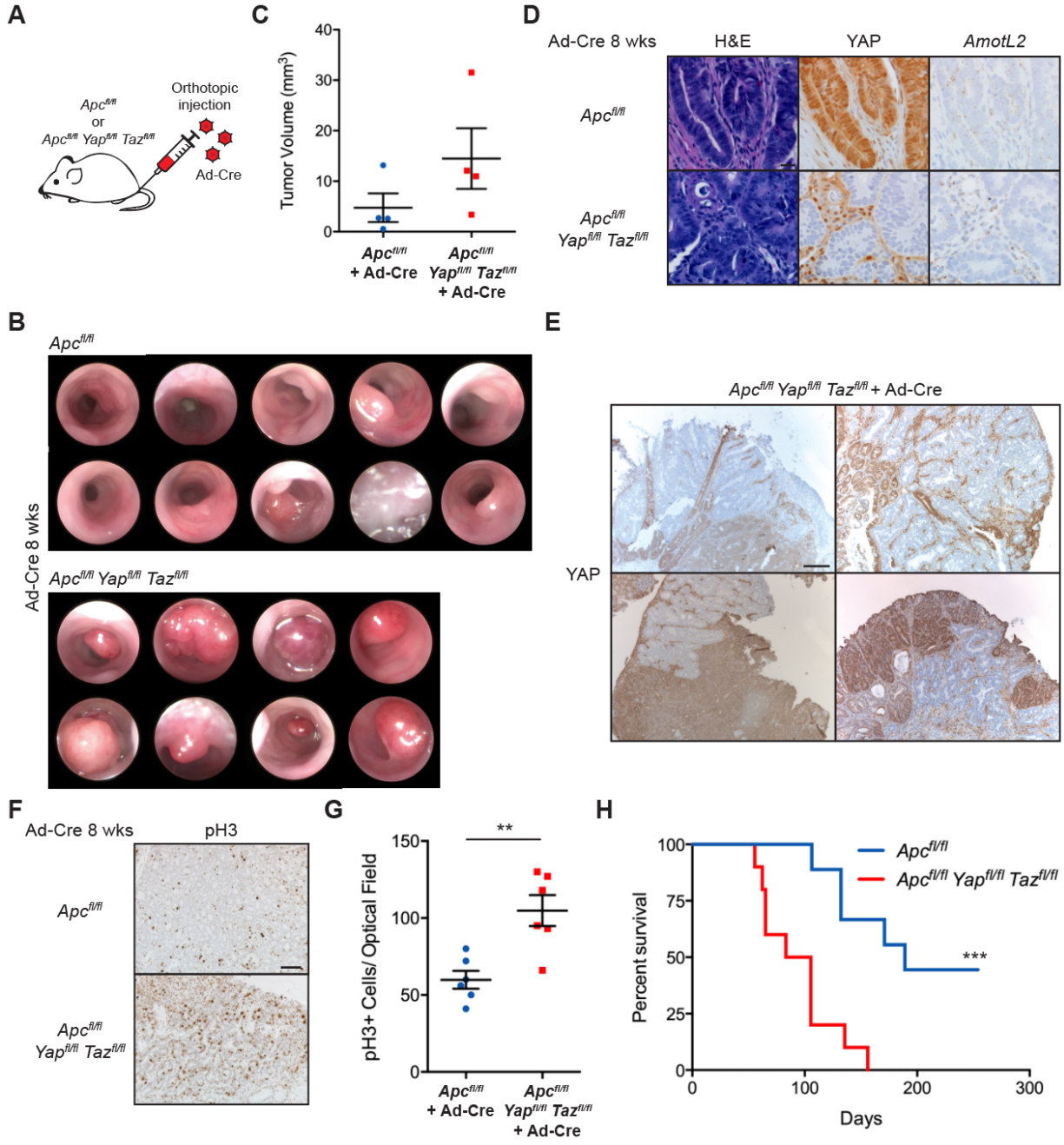

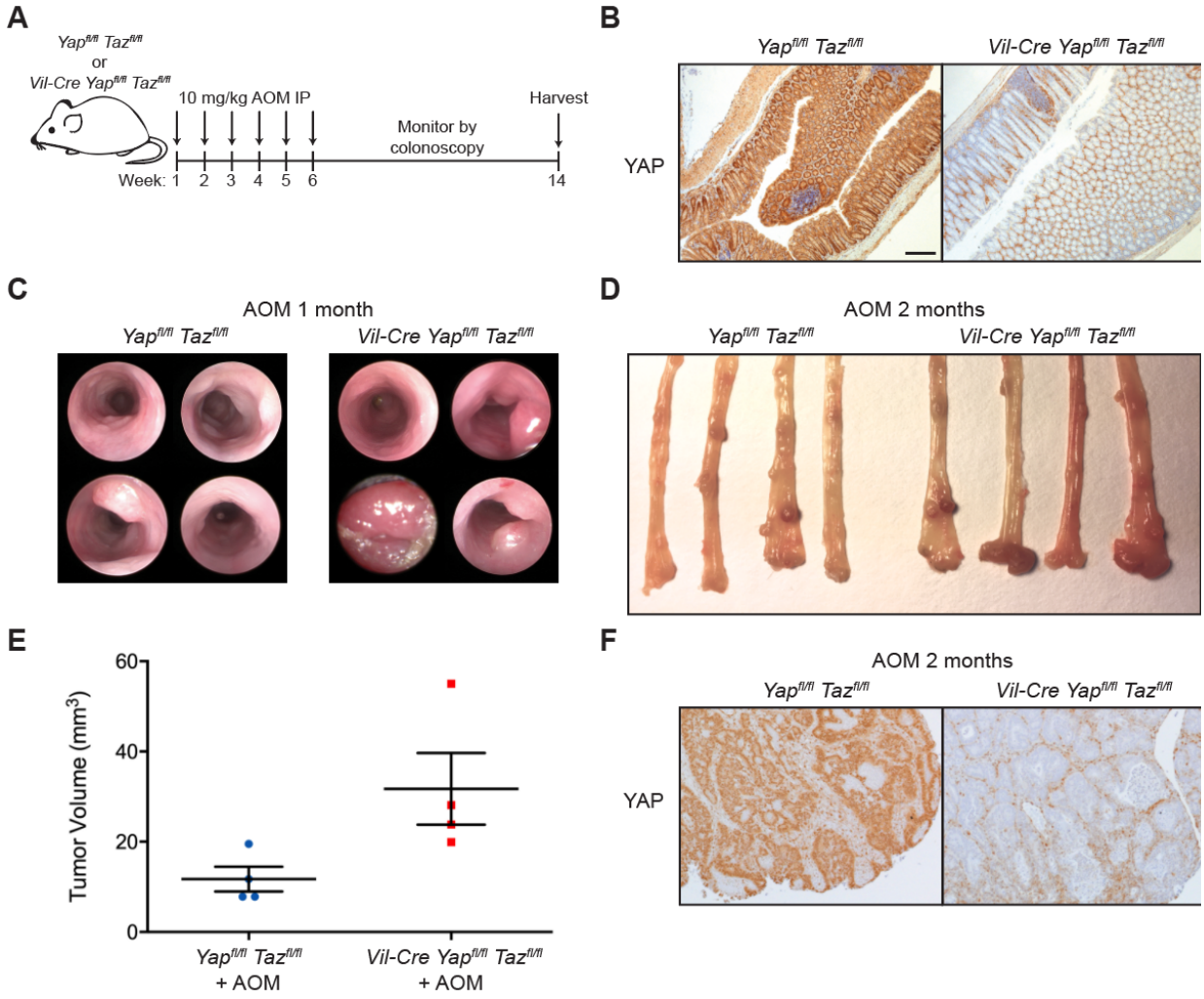

Figure 3.15. (A) Schematic of sporadic tumor formation in mice of the indicated genotypes, including timeline of azoxymethane (AOM) injection and tissue collection. (B) IHC for YAP in *Villin-Cre Yap$^{fl/fl}$ Taz$^{fl/fl}$* animals and control littermates. Scale bar, 200 μm. (C) Colonoscopy images of mice of the indicated genotypes one month after the last AOM injection. (D) Gross morphology of colons from mice of the indicated genotypes 2 months after the last AOM injection. (E) Quantification of tumor burden from *Yap$^{fl/fl}$ Taz$^{fl/fl}$* and *Villin-Cre Yap$^{fl/fl}$ Taz$^{fl/fl}$* mice after AOM-induced tumorigenesis. Data are presented as mean ± SEM; n = 4 tumors per genotype. (F) IHC for YAP in AOM-induced tumors from *Yap$^{fl/fl}$ Taz$^{fl/fl}$* and *Villin-Cre Yap$^{fl/fl}$ Taz$^{fl/fl}$* mice. Scale bar, 100 μm.

that *Yap/Taz* are not required for the growth of genetically defined colon tumors driven by Wnt but are rather inhibitory towards their growth.

We also tested the role of YAP/TAZ in sporadic tumor formation by inducing tumors in *Villin-Cre* $Yap^{fl/fl}$ $Taz^{fl/fl}$ mice and their $Yap^{fl/fl}$ $Taz^{fl/fl}$ littermates as controls with six weekly intraperitoneal injections of 10 mg/kg azoxymethane (AOM) carcinogen (**Figure 3.15A**) (Neufert et al., 2007). These conditional mouse knockouts lack YAP in the entire intestinal epithelium (**Figure 3.15B**). Colonoscopy imaging shows formation of tumors in both wildtype and *Yap/Taz* knockout mice 1 month after the last AOM injection (**Figure 3.15C**). Eight weeks after the last dose, we observed a higher tumor burden in the colons of *Yap/Taz* knockout mice than in their control littermates (**Figure 3.15D-E**). In this case, all epithelial cells of the tumors are fully deleted for *Yap/Taz* as are the cells of origin (**Figure 3.15F**). Altogether, our results not only establish YAP/TAZ as a *bona fide* tumor suppressor in *Apc* mutant colon tumors but also implicate YAP activation as a viable therapeutic strategy in this cellular context.

3.5 Discussion

Due to contrasting findings made by different groups, the role of Hippo/YAP signaling in the initiation and progression of CRC remains a matter debate (Azzolin et al., 2014; Barry et al., 2013; Cai et al., 2015; Gregorieff et al., 2015). Here we show that YAP antagonizes stemness and inhibits Wnt even in the presence of multiple oncogenic mutations, rendering *Lgr5*+ cancer stem cells non-proliferative and inducing tumor regression in mouse and patient-derived models of primary and metastatic CRC. On the other hand, YAP/TAZ depletion increases the growth and proliferation of colonic

adenomas. These data collectively suggest that this YAP-dependent regenerative program can be reactivated during CRC progression and be dominant over Wnt-driven outputs.

Interestingly, growth of certain CRC cell lines requires YAP, an observation that supports the idea of YAP as an oncogene in the colon as seen in other tissues (Konsavage et al., 2012; Rosenbluh et al., 2012; Zhou et al., 2011). However, it is possible that YAP dependence is a feature of *in vitro* culture and does not reflect physiological requirements of the *in vivo* intestine, where YAP deletion has no effect (Cai et al., 2010). Our data show that *in vivo* growth of *Apc* knockout adenomas is not only independent of YAP but is also favored upon YAP/TAZ depletion. Moreover, activation of YAP *in vivo* and *in vitro* hampers cancer growth by suppressing Wnt and antagonizing the stem cell state.

A few studies have also proposed an oncogenic role for YAP based on data from a mouse model of familial adenomatous polyposis, results of which might reflect a role of YAP in mitotic recombination as tumor outcome in this model depends on the loss of the second *Apc* allele (Cai et al., 2015; Gregorieff et al., 2015; Haigis & Dove, 2003; Haines et al., 2005). Furthermore, these experiments deplete YAP developmentally, which may not reproduce what occurs in an adult mutation. Additionally, the appearance of sporadic colon tumors through use of a chemical carcinogen does not require YAP, ruling out the role for YAP in tumor initiation. Altogether, our data using models of both YAP activation and depletion are consistent and strongly suggest that YAP functions as a tumor suppressor in the colon.

Multiple strategies are being developed to target solid tumor stem cells. Our study suggests that reprogramming of these cells into a regenerative state could be harnessed as a novel therapeutic approach. In this context, the cell state induced by YAP, marked by high *Klf6* expression during colonic regeneration, can be induced in CRC. Given that YAP

is negatively regulated by the upstream kinases LATS1/2 and MST1/2, our results indicate that Hippo kinase inhibitors could serve as potential therapeutic agents to combat CRC.

3.6 Materials and Methods

3.6.1 Mice

All animal protocols and procedures were approved by the respective local animal institutional committees. All mice used for this study were on a C57BL/6J background unless indicated otherwise.

Organoid transplantation experiments: Both male and female 2-3 months old nude mice were used for flank injections, and male and female 2-4 months old NSG mice were used for colon orthotopic and intrasplenic injections. Mice were administered doxycycline (2 mg/ml with 0.5% sucrose) in drinking water ad libitum either immediately upon transplantation or starting on the days indicated as specified in the figure legends.

Colon tumorigenesis: Both male and female $Apc^{fl/fl}$ and $Apc^{fl/fl}$ $Yap^{fl/fl}$ $Taz^{fl/fl}$ mice at 6-8 weeks old were used for injection of adenovirus expressing Cre recombinase. AOM-induced carcinogenesis was performed in *Villin-Cre* $Yap^{fl/fl}$ $Taz^{fl/fl}$ animals and their $Yap^{fl/fl}$ $Taz^{fl/fl}$ littermates as controls.

3.6.2 Azoxymethane-induced tumorigenesis

A stock solution of azoxymethane (AOM) was prepared at a concentration of 1 mg/mL. Colon tumorigenesis was induced by intraperitoneal injection of 10 mg/kg of AOM once weekly for six consecutive weeks into 8-week old mice of the indicated genotypes. Mice were harvested 2 months after the last injection for analysis.

3.6.3 Mouse colon organoid isolation and culturing

For colon epithelial cell isolation for organoid culture, a 2 cm piece of distal colon was extracted from 2-month old mice and incubated in 4 mM EDTA in PBS with mild agitation for 45 min at 4°C. The colon pieces were cut open, and colon crypts were scraped from the tissue with a coverslip. After washing with cold PBS and centrifugation at 1000 g for 5 min, crypts were resuspended in Matrigel and plated in 24-well plates (50 μL Matrigel/well). The Matrigel was allowed to solidify for 15-30 min in a 37°C incubator. 500 μL of organoid culture media was then overlaid onto the Matrigel and changed every 2-3 days. The organoid cultures were maintained at 37°C in fully humidified chambers containing 5% CO_2.

Colon organoids were prepared from animals with the following genotypes: *Col1a1*$^{tetO\text{-}YapS127A/+}$ *Rosa26*$^{LSL\text{-}rtTA/+}$, *Lrig1-CreERT2 Lats1*$^{fl/fl}$ *Lats2*$^{fl/fl}$, *Apc*$^{fl/fl}$ *Kras*$^{LSL\text{-}G12D}$ *p53*$^{fl/fl}$, and *Rosa26*$^{CAGs\text{-}rtTA3}$. Organoids were grown in conditioned media containing Wnt3a, R-Spondin, and noggin, generated as described previously from L-WRN cells (Miyoshi & Stappenbeck, 2013) and diluted 1:1 with Advanced DMEM/F-12 containing 1x N-2, 1x B-27, 1% Pen/Strep, and 2 mM L-glutamine. The growth media also contained 50 ng/mL EGF, 0.1 mg/mL primocin, 1 μM N-acety-L-cysteine, 10 mM HEPES, and 10 μM Y-27632 (added only upon passaging). Induction of *Lats1/2* knockout was performed by addition of 100 nM 4-OHT overnight whereas Yap overexpression was induced with 1 μg/mL doxycycline in the media.

To generate *tetO-Yap*^{S127A} *rtTA* organoids, organoids derived from *Col1a1*$^{tetO\text{-}YapS127A/+}$ *Rosa26*$^{LSL\text{-}rtTA/+}$ mice were transduced with a lentivirus expressing Cre recombinase (generated from Cre-IRES-PuroR, a gift from Darrell Kotton) to activate

rtTA expression (Somers et al., 2010). Three days after infection, organoids were selected by adding 1 μg/mL puromycin.

Knockout of *Apc* was performed by transfecting or transducing a plasmid or lentivirus, respectively, expressing Cas9 and a sgRNA against *Apc* (*Apc* sgRNA cloned into lentiCRISPR, a gift from Feng Zhang) (Schwank et al., 2013; Shalem et al., 2014). For organoids derived from $Col1a1^{tetO\text{-}YapS127A/+}$ $Rosa26^{LSL\text{-}rtTA/+}$ mice, the lentivirus additionally expressed Cre recombinase to activate rtTA (*Apc* sgRNA cloned into pSECC, a gift from Tyler Jacks) (Sanchez-Rivera et al., 2014). Three days after infection, organoids were selected by removing Wnt and R-Spondin from the media. These organoids were grown in the same media as wild-type organoids but did not contain conditioned media and were supplemented with 100 ng/mL noggin. $Apc^{-/-}$ *CAGs-rtTA3* organoids were infected with lentiviruses carrying inducible expression of mutant versions of YAP. Three days after infection, organoids were selected by adding 1 μg/mL puromycin for 3 days.

$Apc^{fl/fl}$ $Kras^{LSL\text{-}G12D}$ $p53^{fl/fl}$ organoids were infected with an adenovirus expressing Cre recombinase and GFP (Cat#VVC-U of Iowa-1174) and selected 3 days after infection for 1 week by adding 1 μM EGFR inhibitor gefitinib and 5 μM nutlin-3 to organoid media without Wnt, R-Spondin, or EGF. Growth media was the same as for wildtype organoids but did not contain conditioned media or EGF and was supplemented with 100 ng/mL noggin. Organoids with inducible Yap overexpression were obtained by infecting with a lentivirus overexpressing Yap in the pLVX-Tight-Puro system (Clonetech Cat#632162) followed by selection with 1 μg/mL puromycin (starting 3 days after infection) and subsequent infection with a lentivirus expressing rtTA (generated from pLenti CMV rtTA3

Blast (w756-1), a gift from Eric Campeau) and selection with 10 μg/mL blasticidin. We isolated 20 clones for which we tested YAP overexpression by western blot and used the clone that displayed higher levels of YAP expression for all the experiments shown in this manuscript.

Knockout of *Smad4* was performed by transfecting AKP organoids with a plasmid expressing Cas9 and a sgRNA against *Smad4* (*Smad4* sgRNA cloned into lentiCRISPR, a gift from Feng Zhang) (Shalem et al., 2014; Weber et al., 2015). The organoids were selected 3 days after transfection by removing noggin from the culture media for AKP organoids and supplementing with 10 ng/ml TGF-β (Matano et al., 2015). Selected clones were maintained in the same culture media as AKP organoids but without noggin.

3.6.4 Human colorectal cancer organoids

The collection of fresh human CRC specimens and the generation of organoid lines was described previously (Roper et al., 2017). The line used in this study is derived from a moderately differentiated liver metastasis from a MSS rectal adenocarcinoma and carries mutations in *KRAS*, *TP53*, and *PTCH1*. Human CRC organoids were grown in Matrigel and maintained in the same culture media as for AKP mouse organoids.

3.6.5 Murine colonoscopy and mucosal injection

Mouse colonoscopy was performed on anesthetized mice using Storz equipment. Injections were performed as described previously (Roper et al., 2017, 2018). We used a custom-made flexible steel needle, which was introduced through the working channel of the colonoscope. The injection was performed under observation by a very gentle mucosal penetration with the open side of the bevel heading up in a flat angle. A volume of 50-100

μL of virus or organoid solution was then injected into the colonic lamina propria. The viral titer of adenovirus expressing Cre recombinase (Cat#VVC-U of Iowa-5) was 10^9 pfu/ml with 3 injections per mouse at different locations.

Apc$^{-/-}$ *Kras*^{G12D} *p53*$^{-/-}$ tetO-YAP^{5SA} rtTA organoids were prepared for injection by mechanically resuspending the Matrigel and growth media with a pipette. They were dissociated by passing them 3 times through a syringe with a 25G needle followed by a cold PBS wash. They were resuspended in PBS containing 10% Matrigel and kept on ice before injection. Typically, one well of a 24-well plate containing 50 μL of Matrigel and grown to confluency (~100,000 cells) was resuspended in a volume of 250 μL for injection.

3.6.6 Subcutaneous transplantation of organoids

Apc$^{-/-}$ *Kras*^{G12D} *p53*$^{-/-}$ and human organoids expressing tetO-YAP^{5SA} and rtTA were injected subcutaneously in the flanks of nude mice. The organoids were prepared as described for colon injections but were resuspended in Matrigel diluted 1:1 in DMEM. Each flank was injected with organoids coming from three wells of a 24-well plate (~300,000 cells) resuspended in a volume of 100 μL. For secondary transplantation, 18,000 sorted EpCAM+ *Apc*$^{-/-}$ *Kras*^{G12D} *p53*$^{-/-}$ tetO-YAP^{5SA} rtTA tumor cells were transplanted into the flanks of nude mice.

3.6.7 Intrasplenic injection of organoids

Apc$^{-/-}$ *Kras*^{G12D} *p53*$^{-/-}$ *Smad4*$^{-/-}$ tetO-YAP^{5SA} rtTA organoids were prepared as single cells following a 20 min incubation in dispase supplemented with 10 μM Y-27632

at 37°C, subsequent incubation in 0.25% trypsin with 10 μM Y-27632 at 37°C for 10 min, and enzyme inactivation with Advanced DMEM/F12 (+1% Pen/Strep, 2 mM L-glutamine, 20% FBS). The cells were mechanically dissociated with a 25G needle, centrifuged, and resuspended in cold Advanced DMEM/F12. Mice were anesthetized with isoflurane, and under sterile conditions, the abdomens were depilated and sterilized. A small flank incision was made to expose the tip of the spleen, which was gently withdrawn from the abdomen with sterile tweezers and held in place with a sterile clamp by the fat tissue attached to the spleen. The bottom third of the spleen was loosely ligated using a non-absorbable Vicryl coated suture, and 300,000 cells in a 100 μL volume were injected with a 25G needle underneath the splenic capsule past the ligation. After needle withdrawal, the spleen was ligated to close the wound, and the incision was closed with sutures.

3.6.8 Lentivirus production

Lentiviruses were generated in 293X cells by transfecting backbone and packaging plasmids using TransIT reagent following manufacturer's instructions. 293X cells were maintained in DMEM (+10% FBS, 2 mM L-glutamine, 1% Pen/Strep). The supernatant containing the virus was collected 48 and 60-72 hours after transfection, concentrated by ultracentrifugation at 16,000 rpm for 90 min at 4°C, and resuspended in the remaining supernatant.

3.6.9 Organoid transfection and infection

2-3 days prior to transfection or infection, organoids were treated with 10 mM nicotinamide. Organoids were washed with PBS and treated with dispase to dissolve the Matrigel. They were passaged through a 25G syringe three times, spun down for 5 min at

1000 g and resuspended in 450 μL of culture media. The cell suspension was transferred to a 48-well plate, and 10 μL of a lentivirus solution (titer approximately 10^7 pfu/mL) or 50 μL of lipofectamine-DNA complex were added to the well. Cells were spinoculated for 1 hr at 30°C at 600 g. After a 4-6 h recovery at 37°C, the cells were resuspended, centrifuged in an Eppendorf tube, resuspended in 50 μL Matrigel, and cultured as described above.

3.6.10 Histology

Intestine, colon, and tumor samples were fixed overnight in 10% formalin, washed with PBS and 70% ethanol, and embedded in paraffin. Organoids grown in Matrigel were fixed in 4% paraformaldehyde/PBS, washed extensively with PBS and encapsulated in Histogel prior to embedding in paraffin. Livers were fixed 4% paraformaldehyde/PBS for 36-48 hours and cut into 9-10 pieces before embedding in paraffin. The paraffin blocks were cut into 5 μm sections using a microtome.

For immunohistochemistry, antigen retrieval for most epitopes was performed with citric-acid based pH 6.0 Antigen Unmasking Solution at 95°C in a pressure cooker for 1 hr. For epitopes requiring high pH, antigen retrieval was performed with tris-based pH 9.0 Antigen Unmasking Solution at 37°C for 10 min. The slides were blocked with 0.3% hydrogen peroxide and subsequently 2.5% donkey serum in PBS and incubated with primary antibody in blocking buffer overnight at 4°C. After washing with PBS three times, slides were incubated with biotinylated secondary antibodies in PBS for 1 hr. The signal was amplified with VectaStain ABC Reagent and developed with DAB. Harris modified

hematoxylin was used to counterstain nuclei and subsequently slides were washed, dehydrated, and mounted using VectaMount.

For immunofluorescence, following antigen retrieval, blocking, and primary antibody incubation, slides were incubated with appropriate fluorescent antibodies and 1 μg/ml DAPI for 1 hour and then mounted with Prolong Gold antifade with DAPI.

For RNA *in situ* hybridization, we used the RNAScope Brown HD 2.5 kit according to the manufacturer's instructions.

IHC and RNAScope images were taken using a Zeiss Axio Scope. IF images were obtained on a Zeiss AxioObserver Z1.

3.6.11 RNA isolation and RT-qPCR

RNA from organoids was extracted using Trizol reagent. cDNA was obtained using the cDNA Synthesis Kit and diluted 1:40 for RT-qPCR if starting from 500 ng of RNA. RT-qPCR was performed on a One Step plus Sequence Detection System (Applied Biosystems) using Fast SYBR® Green Master Mix (Life Technologies), and gene expression data was quantified using the DeltaDeltaCt method and normalized to *Gapdh*/*GADPH*.

3.6.12 Protein extraction and Western blot analyses

Organoids were washed in PBS, and the Matrigel was dissolved with dispase. After washing with PBS, the cells were lysed with RIPA buffer and quantified using Bradford Reagent. For western blot, 10 μg of total protein were loaded into each well of an SDS-PAGE gel.

3.6.13 Fluorescence-activated cell sorting

For isolation of tumor cells for FACS and subsequent secondary transplantation, tumors were chopped into small pieces in 300 U/ml collagenase IV in digestion buffer (1x HBSS, 10 mM HEPES, 1.25 mM $CaCl_2*2H_2O$, and 4 mM $MgCl_2*6H_2O$ in MilliQ H_2O) and subsequently incubated at 37°C for 30 min with occasional pipetting. The tumor pieces were then centrifuged and incubated in 0.25% trypsin at 37°C for 30 min with occasional pipetting followed by an addition of FBS to a 5% final concentration. The tumors cells were washed with cold PBS twice, filtered through 70 μm strainers, and stained in 2% FBS/PBS with fluorescent conjugated EpCAM, CD45, TER119, and CD11b antibodies diluted 1:100 for 30 min at 4°C.

All sorting was performed on a BD FACSAria II, using a 100 μm nozzle, and FlowJo (Tree Star) software was used for all flow cytometry analysis. The following combinations were used to isolate each of the respective populations: intestinal/colonic epithelial cells: EpCAM+CD45-TER119-; tumor epithelial cells: EpCAM+CD45-TER119-CD11b-. For all sorts, 4', 6-diamidino-2-phenylindole (DAPI) was used to eliminate dead cells.

3.6.14 Bulk RNA sequencing and analysis

RNA was isolated from organoids using the NucleoSpin RNA XS kit. The libraries for the RNA-seq analysis were prepared with 100 ng of RNA using the TruSeq RNA Library Preparation Kit v2 (Illumina) according to the manufacturer's protocol. All of the libraries were sequenced on an Illumina HiSeq 4000 using paired end 150 cycles kits at Novogene. Raw sequencing reads were aligned to a reference transcriptome generated from the Ensembl v98 database with Salmon v0.14.1 using options "--seqBias --useVBOpt --gcBias --numBootstraps 30 --validateMappings" (Patro et al., 2017). Length-scaled

transcripts per million were acquired using the tximport function, and log2 fold changes and false discovery rates were determined by DESeq2 in R (Love et al., 2014; Soneson et al., 2015). Shrunken log2 fold changes were determined with DESeq2, which were used to rank genes for GSEA of significant KEGG pathways by fgsea or of previously published gene signatures using the GSEA function (Kanehisa, 2000). In cases where there were duplicate gene symbols or Entrez IDs, the more significant gene was kept for the ranking. To identify the transcription factors differentially expressed, the differentially expressed genes at 72 hours with adjusted p-value < 0.05 and absolute log2 fold change > 1 were overlapped with the CIS-BP v2.00 database of mouse transcription factors (Weirauch et al., 2014). enrichGO in the clusterProfiler R package was used to identify significant GO biological processes overrepresented (G. Yu et al., 2012).

3.6.15 Image analysis

Quantification of tumor area was performed in ImageJ (Schneider et al., 2012). TIFF files were imported into ImageJ, and the scale for each image was set. Each liver piece was thresholded manually, which was used to calculate its area. The freehand selection tool was used to circle each tumor and calculate the area, which was summed for each liver piece to calculate the percent tumor burden.

For quantification of RNA-ISH images, digital morphometric analysis was performed using the Trainable Weka Segmentation (TWS) plugin in Fiji (Arganda-Carreras et al., 2017; Schindelin et al., 2012). TIFF files were imported into Fiji, and the TWS plugin was trained to produce a classifier, segmenting images into areas of background, nuclei, and probe. The same trained classifier was applied to all images, providing a percentage of positive staining for each image.

3.6.16 Quantification and statistical analysis

Data represented are expressed as mean ± standard error of mean unless otherwise specified. Data were analyzed using Prism Software 6.0 (GraphPad). Technical and biological replicates are specified for each experiment in the figure legends. P-values were determined by a two-tailed t test with Welch's correction unless otherwise indicated whereas p-values for the Kaplan-Meier survival curve were determined with the log rank test. The p-values are presented as follows: $*P < 0.05$, $**P < 0.01$, $***P < 0.001$, $****P < 0.0001$.

3.6.17 Data and code availability

The datasets generated in this study are available in the NCBI GEO database under GSE152376. Code to reproduce the analyses of the bulk RNA-seq datasets can be found at https://github.com/cheungpriscilla/CellStemCell_2020.

3.6.18 Antibodies

Antibody	Source	Identifier
Rabbit monoclonal anti-YAP (clone D8H1X)	Cell Signaling Technology	Cat#14074; RRID: AB_2650491
Rabbit polyclonal anti-human Lysozyme	Dako	Cat#A0099; RRID: AB_2341230
Rabbit monoclonal anti-Ki67 (clone SP6)	GeneTex	Cat#GTX16667; RRID: AB_422351
Rat monoclonal anti-mouse CD44	BD Biosciences	Cat#550538; RRID: AB_393732
Goat polyclonal anti-mCherry (tdTomato)	Sicgen	Cat#AB0040-200; RRID: AB_2333092

Rat monoclonal anti-Ki67 (clone SolA15)	Invitrogen	Cat#14-5698-82; RRID: AB_10854564
Rabbit monoclonal non-phospho (active) β-catenin (Ser33/37/Thr41) (clone D13A1)	Cell Signaling Technology	Cat#8814; RRID: AB_11127203
Rabbit monoclonal anti-phospho-histone H3 (Ser10) (clone E173)	Millipore	Cat#04-1093; RRID: AB_1977262
Rabbit monoclonal anti-HA-tag (clone C29F4)	Cell Signaling Technology	Cat#3724; RRID: AB_1549585
Rabbit monoclonal anti-GAPDH (clone 14C10) (HRP conjugated)	Cell Signaling Technology	Cat#3683; RRID: AB_1642205
APC rat monoclonal anti-mouse CD326 (Ep-CAM)	BioLegend	Cat#118214; RRID: AB_1134102
APC/Cy7 rat monoclonal anti-mouse TER-119	BioLegend	Cat#116223; RRID: AB_2137788
APC/Cy7 rat anti-mouse CD45 (clone 30-F11)	BD Biosciences	Cat#557659; RRID: AB_396774
APC/Cy7 rat anti-CD11b (clone M1/70)	BD Biosciences	Cat#557657; RRID: AB_396772
Biotinylated goat anti-rabbit IgG	Vector Laboratories	Cat#BA-1000; RRID: AB_2313606
Biotinylated goat anti-rat IgG	Vector Laboratories	Cat#BA-9400; RRID: AB_2336202
Donkey anti-rabbit IgG, Alexa Fluor 488	Thermo Fisher Scientific	Cat#A-21206; RRID: AB_2535792
Donkey anti-rat IgG, Alexa Fluor 594	Thermo Fisher Scientific	Cat#A-21209; RRID: AB_2535795

3.6.19 RT-qPCR primers

Gene	Direction	Sequence 5' to 3'	Source
Human AMOTL2	Forward	AGCTTCAATGAGGGTCTGCTC	Galli et al., 2015
	Reverse	CTGCTGAAGGACCTTGATCACT	

Human CYR61	Forward	CATTCCTCTGTGTCCCCAAGAA	Galli et al., 2015
	Reverse	TACTATCCTCGTCACAGACCCA	
Human GAPDH	Forward	CTGACTTCAACAGCGACACC	This paper
	Reverse	TAGCCAAATTCGTTGTCATACC	
Human LGR5	Forward	CTTCCAACCTCAGCGTCTTC	This paper
	Reverse	TTTCCCGCAAGACGTAACTC	
Mouse AmotL2	Forward	TGGAGACTGTACTGAGGGAGAA	Galli et al., 2015
	Reverse	GAGCCGCTGGATTTCATTTTCC	
Mouse Ankrd1	Forward	CATGATGCTGTGAGGCTGAAC	Galli et al., 2015
	Reverse	CATGATGCTGTGAGGCTGAAC	
Mouse Axin2	Forward	GCCAAGTGTCTCTACCTCATTT	This paper
	Reverse	TCCAGCTCCAGTTTCAGTTTC	
Mouse Cyr61	Forward	AGGTCTGCGCTAAACAACTCA	Galli et al., 2015
	Reverse	ATATTCACAGGGTCTGCCTTCT	
Mouse Gapdh	Forward	AGGTCGGTGTGAACGGATTTG	This paper
	Reverse	TGTAGACCATGTAGTTGAGGTCA	
Mouse Lgr5	Forward	CCTACTCGAAGACTTACCCAGT	This paper
	Reverse	GCATTGGGGTGAATGATAGCA	
Mouse Muc2	Forward	AGGGCTCGGAACTCCAGAAA	This paper
	Reverse	CCAGGGAATCGGTAGACATCG	
Mouse Reg4	Forward	CTGGAATCCCAGGACAAAGAGTG	Sasaki et al., 2016

3.6.20 RNAscope probes

Probe Name	**Source**	**Identifier**
RNAscope probe-Mm-AmotL2	Advanced Cell Diagnostics	Cat#515181
RNAscope probe-Mm-Lgr5	Advanced Cell Diagnostics	Cat#312171
RNAscope probe-Mm-Olfm4	Advanced Cell Diagnostics	Cat#311831
RNAscope probe-Mm-Axin2	Advanced Cell Diagnostics	Cat#400331

RNAscope probe-Mm-Reg4	Advanced Cell Diagnostics	Cat#409601
RNAscope probe-Mm-Klf6	Advanced Cell Diagnostics	Cat#426901

4

Pharmacological targeting of the LATS1/2 Hippo kinases in colorectal cancer

4.1 Abstract

We previously reported that genetic activation of the Hippo transcriptional coactivator YAP or equivalently inactivation of its upstream negative regulators LATS1 and LATS2 lead to a regenerative reprogramming of the colon cancer stem cells in Wnt-driven tumors. Here we describe our present efforts to develop, test, and characterize small molecule inhibitors of the LATS1/2 kinases. In collaboration with the NIH/NCATS, we performed an *in vitro* kinase screen and conducted a structure/activity/relationship campaign, identifying a panel of compounds with a diverse range of potency and selectivity against LATS1/2. YAP is activated upon LATS1/2 therapeutic inhibition in CRC organoid cultures, leading to decreased proliferation and stemness. We are currently testing and optimizing these small molecules for *in vivo* treatment with the goal of treating metastatic colorectal cancer in patients.

4.2 Attributions

Contributions to the work described in this chapter were made by Priscilla Cheung, Michele Ceribelli, Patrick Morris, Craig J. Thomas, and Fernando D. Camargo.

M.C., P.C., F.D.C., and C.J.T. conceived of the study. C.J.T. and F.D.C. supervised the study. M.C. and P.M. performed the screen, structure/activity/relationship studies, and cell-based assays. P.C. performed all organoid and mouse experiments. P.C. wrote the manuscript with contributions from M.C. and C.J.T.

4.3 Introduction

The Hippo signaling pathway is a highly conserved signal transduction cascade important in organ size control, tissue homeostasis, and cancer (F.-X. X. Yu et al., 2015). The major downstream transcriptional effectors of the pathway YAP/TAZ mediate the biological output of the pathway by regulating the transcription of genes involved in cell proliferation, anti-apoptosis, and stem cell self-renewal. In mammals, the LATS1 and LATS2 Hippo kinases directly regulate the activity of YAP/TAZ through phosphorylation, which leads to their cytoplasmic sequestration and eventual degradation, thereby inhibiting cell proliferation (Dong et al., 2007; Lei et al., 2008; Zhao et al., 2007, 2010). Indeed, activation of YAP or loss of its upstream negative regulators in mouse models have been shown to lead to the development of tumors (Harvey et al., 2013; Johnson & Halder, 2014).

Although the Hippo pathway acts as a *bona fide* tumor suppressor many tissues, recent works have identified a tumor suppressive role for YAP in colorectal cancer (CRC) (Barry et al., 2013; Cheung et al., 2020). Additionally, reports have highlighted the central role of YAP/TAZ activation in tissue regeneration in different organs, such as in liver and heart (Apte et al., 2009; Grijalva et al., 2014; Heallen et al., 2013; Leach et al., 2017; Lu et al., 2018; Pepe-Mooney et al., 2019; Xin et al., 2013). Despite the growing interest in the pharmacological modulation of this pathway for cancer prevention and regenerative medicine, only two targeted small-molecule modulators of this pathway have been reported to date - the MST1/2 inhibitor XMU-MP-1 (Fan et al., 2016) and YAP activator PY-60 (Shalhout et al., 2021).

Here in collaboration with the NIH/NCATS, we set out to develop novel selective inhibitors against the currently un-drugged LATS1 and LATS2 Hippo kinases. Following

a large-scale *in vitro* kinase screen, structure/activity/relationship studies, and validation via orthogonal cell-based assays, we identified the small molecule LATSi B3 as a potent inhibitor of CRC organoid growth.

4.4 Results

In collaboration with the NIH/NCATS, we developed several novel LATS1/2 inhibitors with a diverse range of potency and selectivity against LATS1/2. These were identified after a large-scale profiling of currently available kinases inhibitors against a panel of wild-type kinases, structure/activity/relationship efforts, and validation in orthogonal cell-based assays. We found these inhibitors to efficiently block LATS1/2-dependent YAP phosphorylation, induce YAP nuclear translocation under high cell-densities, and promote the transcription of YAP target genes. Consistent with the activation of a YAP-dependent transcriptional program, these inhibitors also promoted proliferation and regeneration in an *in vitro*, scratch-based wound-healing assay (data not shown), ultimately leading to the development of LATSi B3.

We then investigated whether LATSi B3 was capable of inhibiting LATS1/2 kinase activities within CRC organoids. We first performed a 1:3 dose titration starting from 10uM down to 1.5nM in *Apc*$^{-/-}$ *Kras*$^{G12D/+}$ *p53*$^{-/-}$ (AKP) cancer organoids and found that LATSi B3 was able to inhibit organoid growth as low as 1.11 uM (**Figure 4.1A**). Using an organoid-forming assay, we found that LATSi B3 at 1 uM prevented AKP organoids from reforming organoids upon passaging after treatment for 4 days (**Figure 4.1B**). These results were recapitulated in a different AKP clone as well as in an *Apc*$^{-/-}$ line (**Figure 4.1C**). Both AKP organoid lines treated with 1 uM LATSi B3 demonstrated upregulation of YAP target genes, confirming that the compound inhibits organoid growth in part

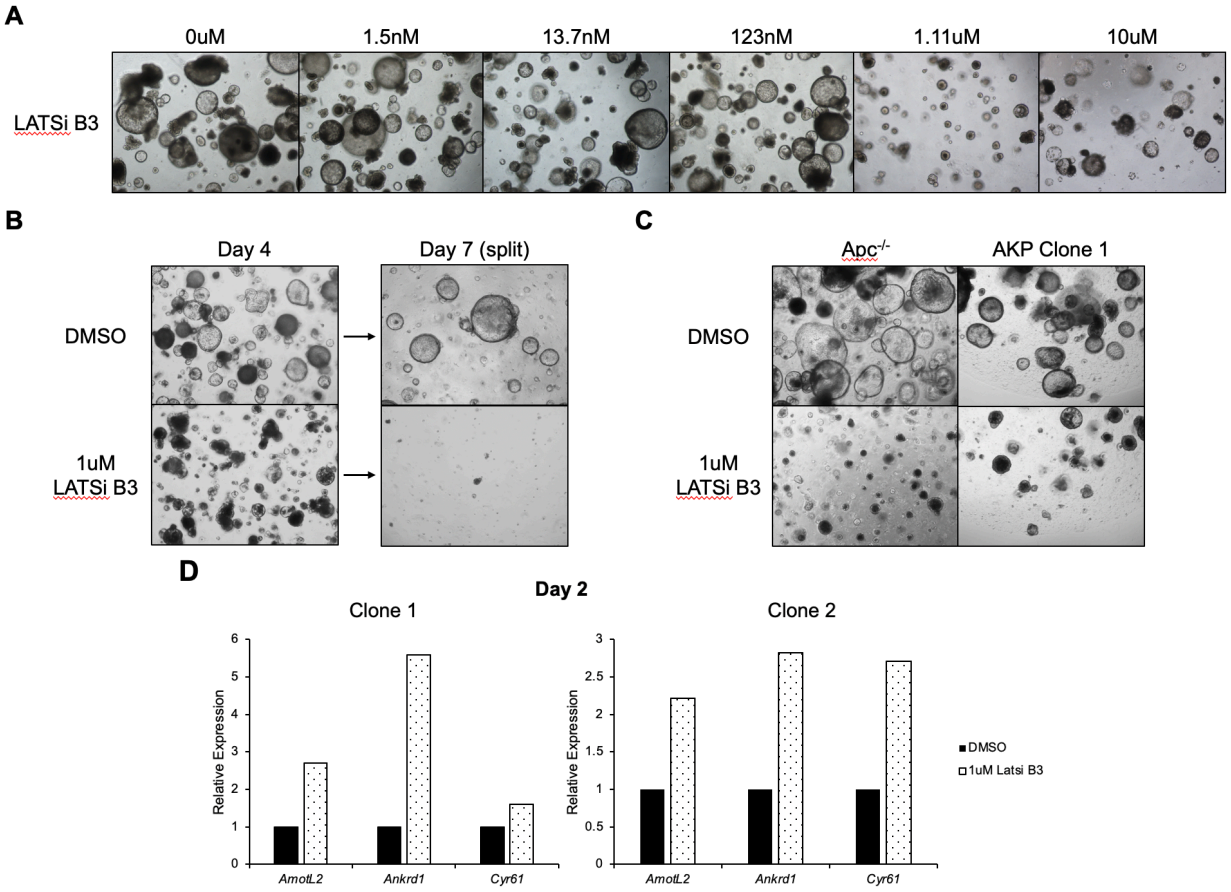

Figure 4.1. (A) Brightfield images of *Apc*$^{-/-}$ *Kras*^{G12D} *p53*$^{-/-}$ organoids treated with 1:3 serial dilutions of LATSiB3 starting from 10uM with 0uM as vehicle control. (B) Brightfield images of *Apc*$^{-/-}$ *Kras*^{G12D} *p53*$^{-/-}$ organoid clone 2 on the indicated days treated with 1uM LATSi B3 or vehicle control. The organoids were split on day 4. (C) Brightfield images of *Apc*$^{-/-}$ organoids and *Apc*$^{-/-}$ *Kras*^{G12D} *p53*$^{-/-}$ organoid clone 1 after 4 days on treatment with 1uM LATSi B3 or vehicle control. (D) RT-qPCR analysis of the indicated genes in *Apc*$^{-/-}$ *Kras*^{G12D} *p53*$^{-/-}$ organoid clones 1 and 2 after 2 days on treatment with 1uM LATSi B3 or vehicle control.

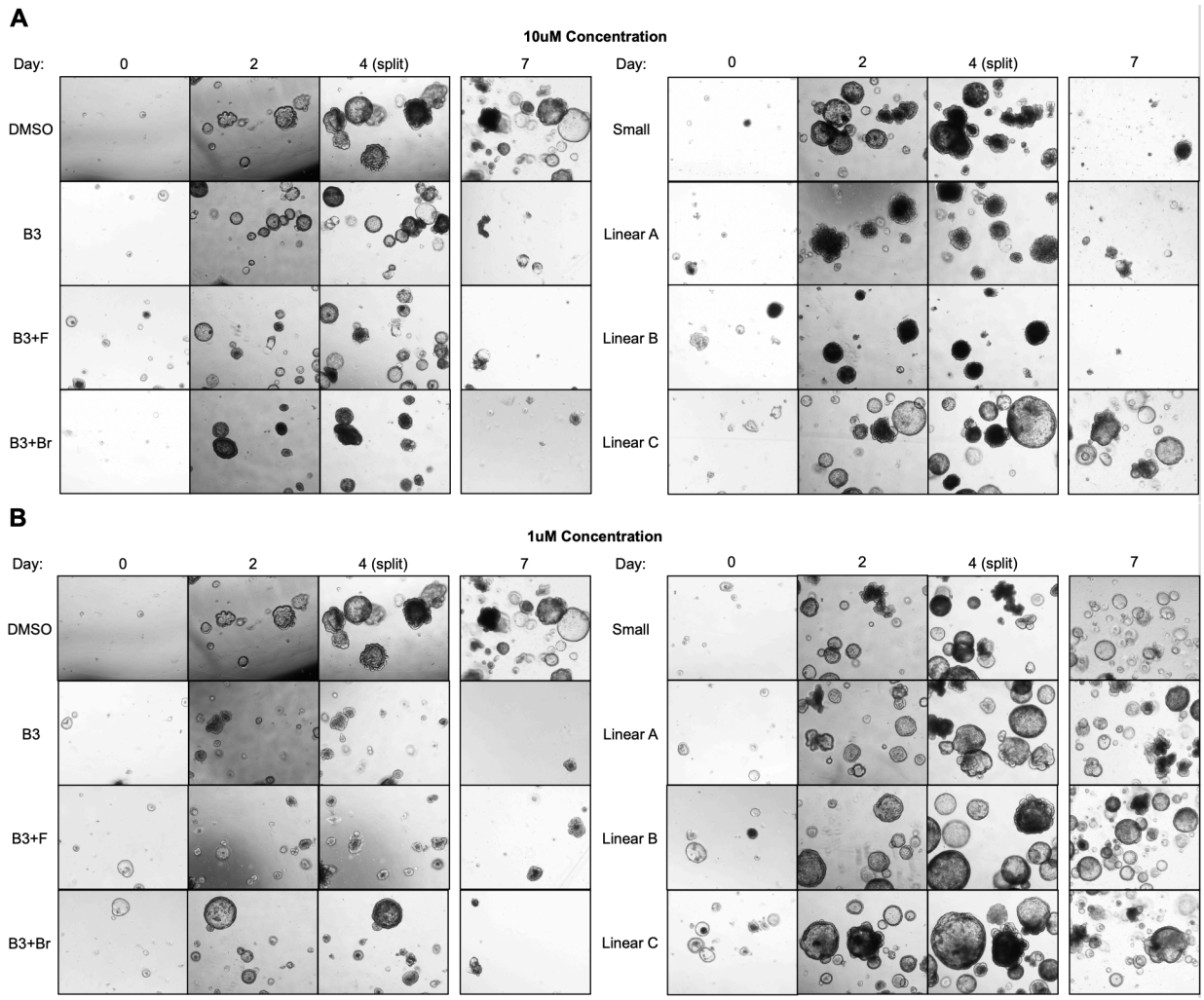

Figure 4.2. (A) Brightfield images of *Apc*$^{-/-}$ *Kras*^{G12D} *p53*$^{-/-}$ organoids treated with 10uM LATSiB3, its derivatives, or vehicle control for indicated days. The organoids were split on day 4. (B) Brightfield images of *Apc*$^{-/-}$ *Kras*^{G12D} *p53*$^{-/-}$ organoids treated with 1uM LATSiB3, its derivatives, or vehicle control for indicated days. The organoids were split on day 4.

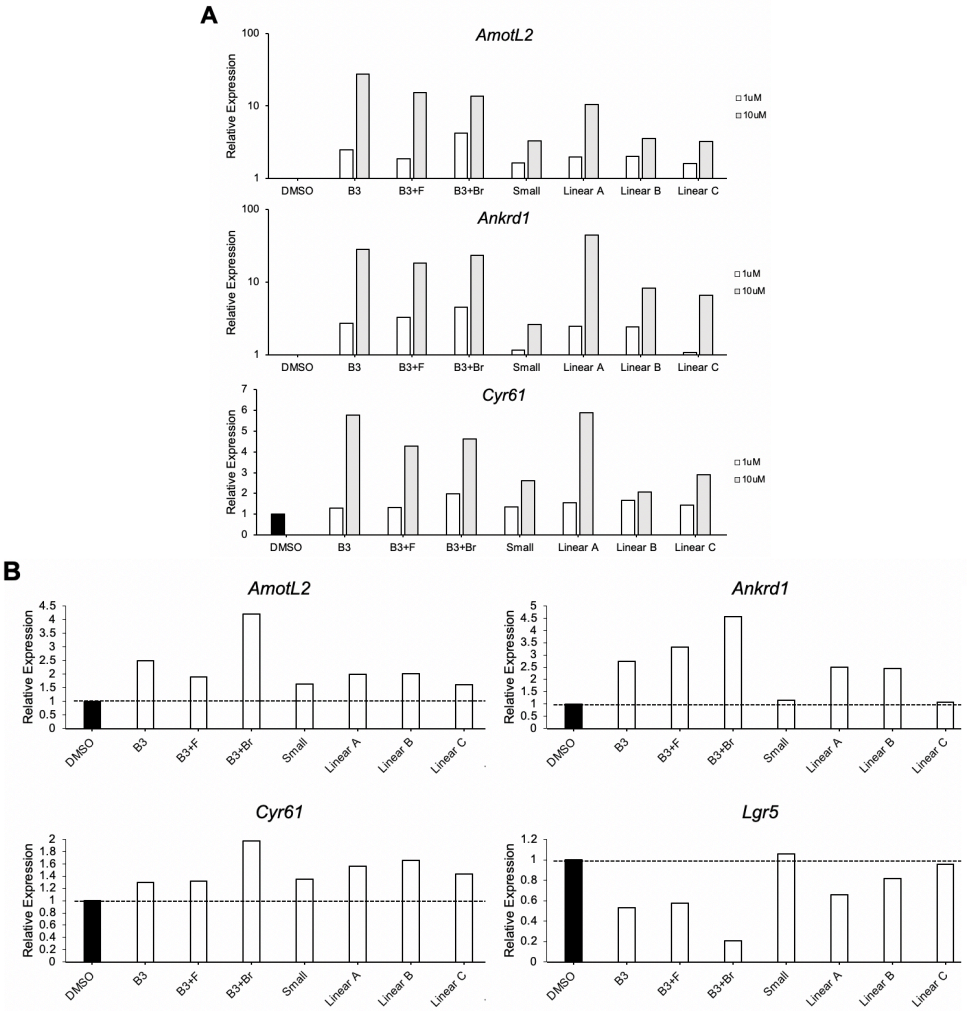

Figure 4.3. (A) RT-qPCR analysis of the indicated genes in *Apc*$^{-/-}$ *Kras*^{G12D} *p53*$^{-/-}$ organoids 2 days after treatment with 10 or 1uM LATSi B3 or vehicle control. (B) RT-qPCR analysis of the indicated genes in *Apc*$^{-/-}$ *Kras*^{G12D} *p53*$^{-/-}$ organoids 2 days after treatment with 1uM LATSi B3 or vehicle control.

through LATS1/2 inhibition (**Figure 4.1D**). Structure/activity/relationship analysis of LATSi B3 revealed that B3 derivatives were optimal for inhibiting growth in AKP organoids compared to the linear series, effects of which become apparent at 1 uM when compared to 10 uM (**Figures 4.2A-B and 4.3A**). At 1uM, treatment of the organoids with the linear series for the most part did not upregulate YAP targets or downregulate the intestinal stem cell marker *Lgr5* as well as the B3 series (**Figure 4.3B**).

Recently, YAP activation in CRC cells has been shown to suppress primary and metastatic colorectal cancer (Cheung et al., 2020). To investigate the effect of the compound on CRC growth, we treated nude mice with LATSi B3 at 5 mg/kg, the maximum non-lethal dose, daily 2 weeks following subcutaneous injection of mouse AKP CRC organoids (**Figure 4.4A**). We observed no difference in tumor growth compared to mice treated with vehicle (**Figure 4.4B**). To determine whether LATSi B3 can activate YAP and its downstream targets *in vivo*, we treated Cyr61-eGFP mice daily for 8 days and sacrificed the mice 2 and 4 hours after the last injection. We did not observe any upregulation of YAP target genes in the livers of these mice (**Figure 4.4C**), likely due to the high plasma binding property of LATSi B3 that is limiting the amount of free drug that can engaging LATS1/2 *in vivo*.

4.5 Discussion

Recent work indicate that Hippo kinases are targetable therapeutic vulnerabilities in CRC (Barry et al., 2013; Cheung et al., 2020). With this in mind, we identified a candidate LATS1/2 inhibitor that was able to suppress CRC organoid growth *in vitro* following an *in vitro* kinase screen, structure/activity/relationship efforts, and validation in cell-based assays. However, due the high plasma binding property of the compound,

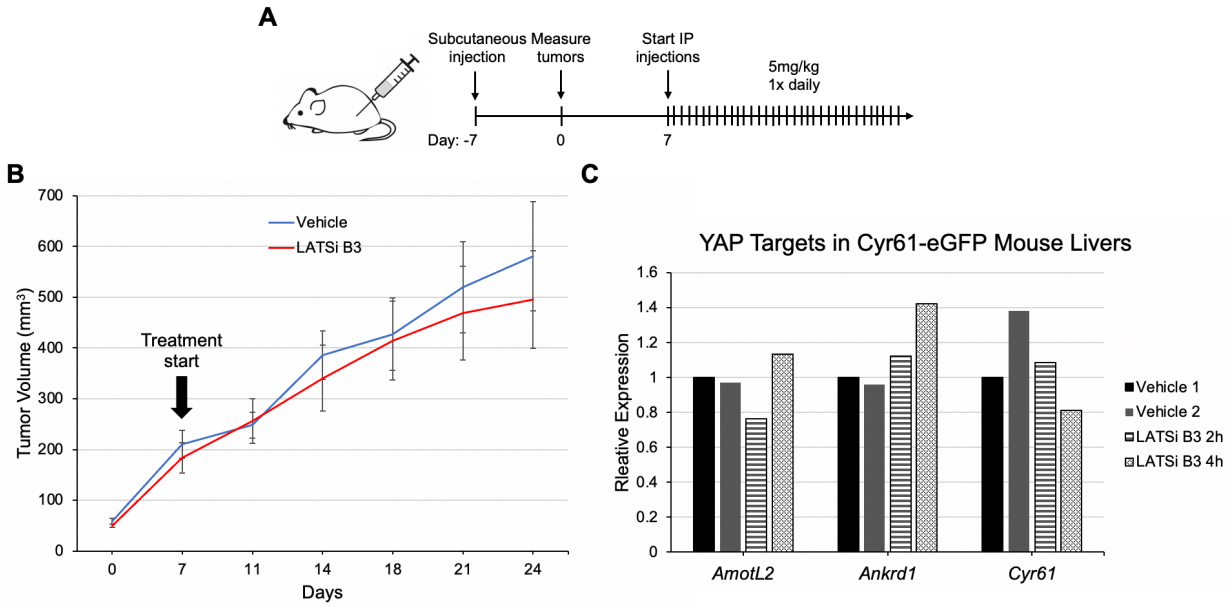

Figure 4.4. (A) Schematic of timeline for subcutaneous injection of *Apc*$^{-/-}$ *Kras*^{G12D} *p53*$^{-/-}$ organoids in the flanks of nude mice, tumor measurements, and treatment with LATSiB3 or vehicle control. (B) Growth curve of subcutaneous tumors from *Apc*$^{-/-}$ *Kras*^{G12D} *p53*$^{-/-}$ organoids injected in the flanks of nude mice. Measurements were started one week after injection (shown as day 0 on the plot). The arrow indicates the day doxycycline treatment was started. Data are represented as mean ± SD; n = 10 tumors per treatment group. (C) RT-qPCR analysis of the indicated genes in livers of Cyr61-eGFP mice treated with LATSi B3 or vehicle control for 8 days.

LATSi B3 was unable to activate YAP targets *in vivo* and therefore had no effect on tumor growth. Future work will require optimization of LATSi B3 to identify structural elements needed for high activity and engagement of LATS1/2 *in vivo*.

4.6 Materials and Methods

4.6.1 Intraperitoneal injection of LATSi B3 in mice

8–10-week-old nude or Cyr61-eGFP mice were treated once daily intraperitoneally for the indicated number of days consecutively with either vehicle only (20% 2-hydroxypropyl-β-cyclodextrin) or LATSi B3 (5mg/ml). In all models, animals were randomly assorted into groups of equal mean tumor volume or body weight before dosing. No animals were excluded from the analysis. The investigators were not blinded during group allocation or dosing. All animal studies were performed in compliance with protocols approved by the Boston Children's Hospital Institutional Animal Care and Use Committee.

4.6.2 Subcutaneous transplantation of organoids

Apc$^{-/-}$ *Kras*^{G12D} *p53*$^{-/-}$ organoids were injected subcutaneously in the flanks of nude mice. The organoids were prepared for injection by mechanically resuspending the Matrigel and growth media with a pipette. They were dissociated by passing them 3 times through a syringe with a 25G needle followed by a cold PBS wash. They were then resuspended in Matrigel diluted 1:1 in DMEM. Each flank was injected with organoids coming from three wells of a 24-well plate (~300,000 cells) resuspended in a volume of 100 μL.

4.6.3 Mouse colon organoid isolation and culturing

For colon epithelial cell isolation for organoid culture, a 2 cm piece of distal colon was extracted from 2-month-old mice and incubated in 4 mM EDTA in PBS with mild agitation for 45 min at 4°C. The colon pieces were cut open, and colon crypts were scraped from the tissue with a coverslip. After washing with cold PBS and centrifugation at 1000 g for 5 min, crypts were resuspended in Matrigel and plated in 24-well plates (50 μL Matrigel/well). The Matrigel was allowed to solidify for 15-30 min in a 37°C incubator. 500 μL of organoid culture media was then overlaid onto the Matrigel and changed every 2-3 days. The organoid cultures were maintained at 37°C in fully humidified chambers containing 5% CO_2.

Colon organoids were prepared from animals with the following genotypes: *Lrig1-CreERT2 Lats1*$^{fl/fl}$ *Lats2*$^{fl/fl}$ and *Apc*$^{fl/fl}$ *Kras*$^{LSL\text{-}G12D}$ *p53*$^{fl/fl}$. Organoids were grown in conditioned media containing Wnt3a, R-Spondin, and noggin, generated as described previously from L-WRN cells (Miyoshi & Stappenbeck, 2013) and diluted 1:1 with Advanced DMEM/F-12 containing 1x N-2, 1x B-27, 1% Pen/Strep, and 2 mM L-glutamine. The growth media also contained 50 ng/mL EGF, 0.1 mg/mL primocin, 1 μM N-acety-L-cysteine, 10 mM HEPES, and 10 μM Y-27632 (added only upon passaging).

Knockout of *Apc* was performed by transducing a lentivirus expressing Cas9 and a sgRNA against *Apc* (*Apc* sgRNA 5'-GTCTGCCATCCCTTCACGTT-3' cloned into lentiCRISPR, a gift from Feng Zhang) (Schwank et al., 2013; Shalem et al., 2014). Three days after infection, organoids were selected by removing Wnt and R-Spondin from the media. These organoids were grown in the same media as wild-type organoids but did not contain conditioned media and were supplemented with 100 ng/mL noggin.

Apc$^{fl/fl}$ *Kras*$^{LSL\text{-}G12D}$ *p53*$^{fl/fl}$ organoids were infected with an adenovirus expressing Cre recombinase and GFP (Cat#VVC-U of Iowa-1174) and selected 3 days after infection for 1 week by adding 1 μM EGFR inhibitor gefitinib and 5 μM nutlin-3 to organoid media without Wnt, R-Spondin, or EGF. Growth media was the same as for wildtype organoids but did not contain conditioned media or EGF and was supplemented with 100 ng/mL noggin.

4.6.4 Lentivirus production

Lentiviruses were generated in 293X cells by transfecting backbone and packaging plasmids using TransIT reagent following manufacturer's instructions. 293X cells were maintained in DMEM (+10% FBS, 2 mM L-glutamine, 1% Pen/Strep). The supernatant containing the virus was collected 48 and 60-72 hours after transfection, concentrated by ultracentrifugation at 16,000 rpm for 90 min at 4°C, and resuspended in the remaining supernatant.

4.6.5 Organoid infection

2-3 days prior to transfection or infection, organoids were treated with 10 mM nicotinamide. Organoids were washed with PBS and treated with dispase to dissolve the Matrigel. They were passaged through a 25G syringe three times, spun down for 5 min at 1000 g and resuspended in 450 μL of culture media. The cell suspension was transferred to a 48-well plate, and 10 μL of a lentivirus solution (titer approximately 10^7 pfu/mL) were added to the well. Cells were spinoculated for 1 hr at 30°C at 600 g. After a 4-6 h

recovery at 37°C, the cells were resuspended, centrifuged in an Eppendorf tube, resuspended in 50 μL Matrigel, and cultured as described above.

4.6.6 RNA isolation and RT-qPCR

RNA from organoids was extracted using Trizol reagent. cDNA was obtained using the cDNA Synthesis Kit and diluted 1:40 for RT-qPCR if starting from 500 ng of RNA. RT-qPCR was performed on a One Step plus Sequence Detection System (Applied Biosystems) using Fast SYBR® Green Master Mix (Life Technologies), and gene expression data was quantified using the DeltaDeltaCt method and normalized to *Gapdh*/*GADPH*.

4.6.7 RT-qPCR primers

Gene	Direction	Sequence 5' to 3'	Source
Mouse AmotL2	Forward	TGGAGACTGTACTGAGGGAGAA	Galli et al., 2015
	Reverse	GAGCCGCTGGATTTCATTTTCC	
Mouse Ankrd1	Forward	CATGATGCTGTGAGGCTGAAC	Galli et al., 2015
	Reverse	CATGATGCTGTGAGGCTGAAC	
Mouse Cyr61	Forward	AGGTCTGCGCTAAACAACTCA	Galli et al., 2015
	Reverse	ATATTCACAGGGTCTGCCTTCT	
Mouse Gapdh	Forward	AGGTCGGTGTGAACGGATTTG	This paper
	Reverse	TGTAGACCATGTAGTTGAGGTCA	
Mouse Lgr5	Forward	CCTACTCGAAGACTTACCCAGT	This paper
	Reverse	GCATTGGGGTGAATGATAGCA	

5

Conclusion

5.1 Overview of Results

Colorectal cancer (CRC) is a prevalent cancer in the United States with an estimated 150,000 new cases diagnosed and estimated 50,000 deaths in 2021. While diagnoses and therapies for patients with primary tumors are quite high, many CRC patients unfortunately succumb to metastatic disease and disease relapse, underscoring the need for better targeted therapies. Here we used single-cell RNA-sequencing (scRNA-seq) to elucidate a role for YAP in reprogramming intestinal stem cells into a wound-healing like cell state that is characterized by low Wnt activity and reduced stemness. This state can be induced via YAP to suppress both mouse and human tumor growth and metastatic seeding to the liver. Conversely, genetic deletion of YAP/TAZ leads to increased tumor growth, suggesting that YAP is indeed a tumor suppressor in the colon. Based on these findings, we have identified a small molecule inhibitor of the LATS1 and LATS2 Hippo kinases to activate YAP therapeutically for the treatment of this disease.

5.2 Discussion

5.2.1 Hippo inhibition reprograms intestinal stem cells to a regenerative cell state

The intestine has developed a remarkable ability to maintain its integrity and function amidst insults from the external environment through the highly proliferative capacity and self-renewal properties of the intestinal stem cell. This process of intestinal renewal is intricately regulated by crosstalk between the Hippo and Wnt signaling pathways. However, this cross-regulation between the Hippo and Wnt pathways has been a long-standing subject of debate (Barry et al., 2013; Cai et al., 2010; Gregorieff et al., 2015; Zhou et al., 2011). Using scRNA-seq, we demonstrate for the first time that Hippo

inhibition through knockout of LATS1/2 in intestinal stem cells leads to the reprogramming of these cells to a distinct cell state not found in the homeostatic intestine. This cell state, marked by expression of the transcription factor *Klf6*, is characterized by low Wnt signaling, confirming earlier findings that we and others have made (Barry et al., 2013; Gregorieff et al., 2015; Q. Li et al., 2020). Our work is consonant with a recent scRNA-seq study identifying a stem cell type enriched in YAP target genes (Ayyaz et al., 2019). In contrast to this work, our data suggest that this YAP-driven cell state does not exist in homeostasis, and it instead arises from the reprogramming of traditional intestinal stem cells. In fact, YAP overexpression in intestinal stem cells results in their loss from the intestinal epithelium. Furthermore, organoid-forming assays and lineage tracing data indicate that this cell state cannot self-renew, contrasting Gregorieff and colleagues' work demonstrating that YAP expands rare, quiescent stem cells to promote their survival and self-renewal upon injury (Ayyaz et al., 2019; Gregorieff et al., 2015). Interestingly, we find transcriptional similarities with that of the regenerating colon, suggesting this cell state represents a physiological equivalent of a transiently repairing cell type.

5.2.2 YAP as a tumor suppressive program in the adult colon

Based on our findings that YAP suppresses Wnt and stemness in the intestine, we reasoned that YAP activation could be leveraged for the treatment of CRC. We found that YAP expression can overcome Wnt hyperactivation downstream of *Apc* deletion as well as in the presence of additional cancer-driving mutations to inhibit the cancer stem cell state. By antagonizing *Lgr5*+ cancer stem cell content and activity, YAP hampered not only tumor growth and initiation but also metastatic seeding to the liver in both mouse

and patient-derived models of metastatic CRC. Conversely, we found that YAP is not required for and even restrains tumor growth in the context of an *Apc* deletion and sporadic tumor formation.

In many tissues, YAP is classically considered an oncogene. Interestingly, in some CRC cell lines, YAP depletion suppresses growth and invasion, providing evidence of its oncogenic role (Konsavage et al., 2012; Rosenbluh et al., 2012; Zhou et al., 2011). However, YAP is not required *in vivo* under normal homeostatic conditions (Cai et al., 2010). This dependence on YAP instead is likely a feature of *in vitro* growth as studies in intestinal organoids have revealed a requirement for YAP *in vitro*, the culture of which mimics features of the regenerating epithelium where YAP is required (Azzolin et al., 2014; Gregorieff et al., 2015; Serra et al., 2019). Furthermore, the genetic background of these CRC cell lines could be a contributing factor as recent work has identified one mouse CRC cell line with a dependency on LATS1/2 for growth (Pan et al., 2019). Our data show that *in vivo* in the context of an *Apc* deletion and sporadic tumor formation, YAP is not required for and even restrains tumor growth. Consistent with these results, we find that YAP activation suppresses Wnt and the cancer stem cell state *in vivo* and *in vitro* thereby inhibiting tumor progression, initiation, and metastatic seeding. These observations are supported by recent data demonstrating transient stages of YAP activation during organoid formation, where YAP activity is negatively correlated with the presence of *Lgr5*+ stem cells (Serra et al., 2019). In contrast to our findings, this work and others showed that YAP activation promotes the survival of organoids *in vitro* (Gregorieff et al., 2015; Serra et al., 2019), which might be reflective of tissue differences from which these organoids were derived (e.g., small intestine versus colon in our work).

Interestingly, some studies have shown that YAP depletion suppresses tumor growth in mouse models of familial adenomatous polyposis, which carry a germline mutation in one allele of *Apc* (Cai et al., 2015; Gregorieff et al., 2015). However, tumor progression in this model depends on the loss of the second *Apc* allele (Haigis & Dove, 2003; Haines et al., 2005), which could reflect a role of YAP in mitotic recombination rather than in tumor growth. Furthermore, these experiments were performed in the context of developmental YAP deletions and might not be informative of what would occur in an adult mutation. Additionally, as tumors in these mice form in the small intestine, these models do not recapitulate what occur in CRC patients. Therefore, the use of an acute adult and colon-specific manipulation of YAP as done here represents the most relevant model to study the role of YAP in adenoma growth. Furthermore, our results demonstrating YAP is not required for the formation of sporadic tumors eliminate the possibility that YAP functions in tumor initiation. Altogether, our data using models of both YAP activation and depletion specifically in the colon suggest that YAP functions as a tumor suppressor in this context.

5.2.3 Pharmacological inhibition of LATS1/2 inhibits colorectal cancer organoid growth

Given that YAP is negatively regulated by the upstream kinases LATS1/2 and MST1/2, our results indicate that Hippo kinase inhibitors could serve as potential therapeutic agents to combat CRC. However, only two small molecules targeting the Hippo pathway have been reported to date with none targeting LATS1/2 (Fan et al., 2016; Shalhout et al., 2021). In collaboration with the NIH/NCATS, we identified LATSi B3, a candidate small molecule inhibitor of the LATS1/2 Hippo kinases, to suppress CRC organoid growth, following an *in vitro* kinase screen and a structure/activity/ relationship

campaign. These results are consistent with data from our genetic models of LATS1/2 inactivation, suggesting that LATS1/2 are indeed oncogenic in this context. While this compound activated YAP downstream targets and downregulated intestinal stem cells *in vitro*, this inhibitor did not have any effect on YAP target gene expression *in vivo*, explaining the minimal effect observed on tumor growth. This lack of effect *in vivo* could be explained by the high protein plasma binding properties of the compound, which is likely limiting the amount of free drug available to engage LATS1/2 *in vivo*. Ongoing work to modify structural elements of our current LATSi B3 compound could improve tissue access of this inhibitor for therapeutic activation of YAP *in vivo*. A future challenge of this work is to determine how we can pharmacologically modulate LATS1/2 specifically for treatment of CRC without affecting other tissues where YAP is pro-proliferative.

5.3 Future Directions

5.3.1 Mechanism of YAP inhibition of Wnt signaling

As is evident from many studies including ours, Hippo and Wnt signaling crosstalk intricately regulate intestinal homeostasis. However, the mechanism of this cross-regulation remains unclear as different models have been proposed for how the Hippo pathway interacts with Wnt signaling in the intestine. Numerous studies have suggested a cytoplasmic role of YAP for inhibiting Wnt, including incorporation of YAP/TAZ into the APC destruction complex to sequester β-catenin (Azzolin et al., 2014; Imajo et al., 2012) and interaction with a Wnt positive regulator Dishevelled (Barry et al., 2013; Varelas et al., 2010). Recent work suggested a YAP/TAZ dependent but TEAD independent role for Wnt inhibition in the intestine (Q. Li et al., 2020), which is in

contrast to our data demonstrating that this inhibition is mediated by the TEAD-dependent transcriptional activity of YAP through the use of a TEAD-binding mutant. One caveat of their study is that the conclusion of those experiments was derived from the use of a small molecule inhibitor of TEAD, which could have off-targets confounding the results of the experiments.

As transcription factors are the main drivers of reprogramming, one potential mechanism is YAP-mediated induction of transcription factors involved in this phenotype. It is interesting to note that in our study, KLF6, a zinc finger transcription factor known to be an immediate early gene in response to injury and reported to be a tumor suppressor in CRC (Inuzuka et al., 1999; Kojima et al., 2000; Ratziu et al., 1998; Reeves et al., 2004), upon knockout in the context of YAP overexpression did not rescue the phenotype in organoids (data not shown). One possibility is that this transcription factor is only positively correlated with this YAP-mediated phenotype or that more than one transcription factor is required for this. Future work would require identification of candidate transcription factors upregulated upon YAP overexpression in organoids via genetic screening. Deconvoluting this mechanism would not only unveil putative targets for the development of tailored therapies but also prognostic markers for CRC patients.

5.3.2 Translational application of therapeutically activating YAP in CRC

CRC is a highly heterogeneous disease with different consensus molecular subtypes as well as underlying differences in genetic mutations (Cancer Genome Atlas Network, 2012; Linnekamp et al., 2015; Wood et al., 2007). In our work, we focus on CRC associated with the traditional adenoma-carcinoma sequence, relying primarily on the deletion of the *Apc* tumor suppressor as the initial driver in many of our murine models

of the disease. However, only ~50-60% of CRCs follow this sequence as the remaining CRC follow other routes of CRC development, such as the serrated pathway (IJspeert et al., 2015) and colitis-associated CRC (Leedham et al., 2009; Punt et al., 2016). It remains to be seen whether the therapeutic activation of YAP may translate in the context of other cancer-driving mutations or chronic inflammation. Interestingly, of the two human CRC lines we tested, only one responded to YAP activation (**Chapter 3** and data not shown), indicating that the genetic background of CRC must be considered when using YAP activation as a therapy. Confounding mutations in the non-responsive line could likely be responsible for this difference that are yet to be elucidated. Future work on understanding the genetic vulnerabilities underlying sensitivity to YAP activation would have tremendous implications for precision medicine in this disease.

5.4 Conclusion

In summary, this work provides new insight into the role of Hippo-Wnt crosstalk in intestinal homeostasis and CRC progression. Using scRNA-seq, we identified a distinct regenerative cell state that emerges upon YAP-mediated reprogramming of intestinal stem cells. Moreover, we are able to leverage YAP activation to reprogram cancer stem cells to suppress both primary and metastatic CRC. Further work needs to be done to translate our findings to clinically tractable modalities and in the context of other cancer-driving mutations.

References

Aberle, H., Bauer, A., Stappert, J., Kispert, A., & Kemler, R. (1997). beta-catenin is a target for the ubiquitin-proteasome pathway. *The EMBO Journal*, *16*(13), 3797–3804. https://doi.org/10.1093/emboj/16.13.3797

Alessandrì, L., Cordero, F., Beccuti, M., Arigoni, M., Olivero, M., Romano, G., Rabellino, S., Licheri, N., De Libero, G., Pace, L., & Calogero, R. A. (2019). RCASC: Reproducible classification analysis of single-cell sequencing data. *GigaScience*. https://doi.org/10.1093/gigascience/giz105

Almendro, V., Marusyk, a, & Polyak, K. (2013). Cellular heterogeneity and molecular evolution in cancer. *Annu Rev Pathol*, *8*, 277–302. https://doi.org/10.1146/annurev-pathol-020712-163923

Amit, S., Hatzubai, A., Birman, Y., Andersen, J. S., Ben-Shushan, E., Mann, M., Ben-Neriah, Y., & Alkalay, I. (2002). Axin-mediated CKI phosphorylation of beta-catenin at Ser 45: a molecular switch for the Wnt pathway. *Genes & Development*, *16*(9), 1066–1076. https://doi.org/10.1101/gad.230302

Apte, U., Gkretsi, V., Bowen, W. C., Mars, W. M., Luo, J.-H., Donthamsetty, S., Orr, A., Monga, S. P. S., Wu, C., & Michalopoulos, G. K. (2009). Enhanced liver regeneration following changes induced by hepatocyte-specific genetic ablation of integrin-linked kinase. *Hepatology (Baltimore, Md.)*, *50*(3), 844–851. https://doi.org/10.1002/hep.23059

Arganda-Carreras, I., Kaynig, V., Rueden, C., Eliceiri, K. W., Schindelin, J., Cardona, A., & Seung, H. S. (2017). Trainable Weka Segmentation: A machine learning tool for microscopy pixel classification. *Bioinformatics*. https://doi.org/10.1093/bioinformatics/btx180

Ayyaz, A., Kumar, S., Sangiorgi, B., Ghoshal, B., Gosio, J., Ouladan, S., Fink, M., Barutcu, S., Trcka, D., Shen, J., Chan, K., Wrana, J. L., & Gregorieff, A. (2019). Single-cell transcriptomes of the regenerating intestine reveal a revival stem cell. *Nature*. https://doi.org/10.1038/s41586-019-1154-y

Azzolin, L., Panciera, T., Soligo, S., Enzo, E., Bicciato, S., Dupont, S., Bresolin, S., Frasson, C., Basso, G., Guzzardo, V., Fassina, A., Cordenonsi, M., & Piccolo, S.

(2014). YAP/TAZ incorporation in the β-catenin destruction complex orchestrates the Wnt response. *Cell*, *158*(1), 157–170. https://doi.org/10.1016/j.cell.2014.06.013

Azzolin, L., Zanconato, F., Bresolin, S., Forcato, M., Basso, G., Bicciato, S., Cordenonsi, M., & Piccolo, S. (2012). Role of TAZ as mediator of wnt signaling. *Cell*. https://doi.org/10.1016/j.cell.2012.11.027

Barker, N., Van Es, J. H., Kuipers, J., Kujala, P., Van Den Born, M., Cozijnsen, M., Haegebarth, A., Korving, J., Begthel, H., Peters, P. J., & Clevers, H. (2007). Identification of stem cells in small intestine and colon by marker gene Lgr5. *Nature*, *449*(7165), 1003–1007. https://doi.org/10.1038/nature06196

Barry, E. R., Morikawa, T., Butler, B. L., Shrestha, K., De La Rosa, R., Yan, K. S., Fuchs, C. S., Magness, S. T., Smits, R., Ogino, S., Kuo, C. J., & Camargo, F. D. (2013). Restriction of intestinal stem cell expansion and the regenerative response by YAP. *Nature*, *493*(7430), 106–110. https://doi.org/10.1038/nature11693

Behrens, J., Jerchow, B. A., Würtele, M., Grimm, J., Asbrand, C., Wirtz, R., Kühl, M., Wedlich, D., & Birchmeier, W. (1998). Functional interaction of an axin homolog, conductin, with beta-catenin, APC, and GSK3beta. *Science (New York, N.Y.)*, *280*(5363), 596–599. https://doi.org/10.1126/science.280.5363.596

Behrens, J., von Kries, J. P., Kühl, M., Bruhn, L., Wedlich, D., Grosschedl, R., & Birchmeier, W. (1996). Functional interaction of beta-catenin with the transcription factor LEF-1. *Nature*, *382*(6592), 638–642. https://doi.org/10.1038/382638a0

Bhanot, P., Brink, M., Samos, C. H., Hsieh, J. C., Wang, Y., Macke, J. P., Andrew, D., Nathans, J., & Nusse, R. (1996). A new member of the frizzled family from Drosophila functions as a Wingless receptor. *Nature*, *382*(6588), 225–230. https://doi.org/10.1038/382225a0

Butler, A., Hoffman, P., Smibert, P., Papalexi, E., & Satija, R. (2018). Integrating single-cell transcriptomic data across different conditions, technologies, and species. *Nature Biotechnology*. https://doi.org/10.1038/nbt.4096

Cai, J., Maitra, A., Anders, R. A., Taketo, M. M., & Pan, D. (2015). β-catenin destruction complex-independent regulation of Hippo-YAP signaling by APC in intestinal tumorigenesis. *Genes and Development*, *29*(14), 1493–1506. https://doi.org/10.1101/gad.264515.115

Cai, J., Zhang, N., Zheng, Y., De Wilde, R. F., Maitra, A., & Pan, D. (2010). The Hippo signaling pathway restricts the oncogenic potential of an intestinal regeneration program. *Genes and Development*, *24*(21), 2383–2388. https://doi.org/10.1101/gad.1978810

Callus, B. A., Verhagen, A. M., & Vaux, D. L. (2006). Association of mammalian sterile twenty kinases, Mst1 and Mst2, with hSalvador via C-terminal coiled-coil domains, leads to its stabilization and phosphorylation. *FEBS Journal*, *273*(18), 4264–4276.

https://doi.org/10.1111/j.1742-4658.2006.05427.x

Camargo, F. D., Gokhale, S., Johnnidis, J. B., Fu, D., Bell, G. W., Jaenisch, R., & Brummelkamp, T. R. (2007). YAP1 Increases Organ Size and Expands Undifferentiated Progenitor Cells. *Current Biology*, *17*(23), 2054–2060. https://doi.org/10.1016/j.cub.2007.10.039

Cancer Genome Atlas Network. (2012). Comprehensive molecular characterization of human colon and rectal cancer. *Nature*, *487*(7407), 330–337. https://doi.org/10.1038/nature11252

Carmon, K. S., Gong, X., Lin, Q., Thomas, A., & Liu, Q. (2011). R-spondins function as ligands of the orphan receptors LGR4 and LGR5 to regulate Wnt/beta-catenin signaling. *Proceedings of the National Academy of Sciences of the United States of America*, *108*(28), 11452–11457. https://doi.org/10.1073/pnas.1106083108

Cavallo, R. A., Cox, R. T., Moline, M. M., Roose, J., Polevoy, G. A., Clevers, H., Peifer, M., & Bejsovec, A. (1998). Drosophila Tcf and Groucho interact to repress Wingless signalling activity. *Nature*, *395*(6702), 604–608. https://doi.org/10.1038/26982

Chan, E. H. Y., Nousiainen, M., Chalamalasetty, R. B., Schäfer, A., Nigg, E. A., & Sillje, H. H. W. (2005). The Ste20-like kinase Mst2 activates the human large tumor suppressor kinase Lats1. *Oncogene*, *24*(12), 2076–2086. https://doi.org/10.1038/sj.onc.1208445

Cheung, P., Xiol, J., Dill, M. T., Yuan, W. C., Panero, R., Roper, J., Osorio, F. G., Maglic, D., Li, Q., Gurung, B., Calogero, R. A., Yilmaz, Ö. H., Mao, J., & Camargo, F. D. (2020). Regenerative Reprogramming of the Intestinal Stem Cell State via Hippo Signaling Suppresses Metastatic Colorectal Cancer. *Cell Stem Cell*. https://doi.org/10.1016/j.stem.2020.07.003

Clevers, H. (2006). Wnt/beta-catenin signaling in development and disease. *Cell*, *127*(3), 469–480. https://doi.org/10.1016/j.cell.2006.10.018

Colnot, S., Niwa-Kawakita, M., Hamard, G., Godard, C., Le Plenier, S., Houbron, C., Romagnolo, B., Berrebi, D., Giovannini, M., & Perret, C. (2004). Colorectal cancers in a new mouse model of familial adenomatous polyposis: Influence of genetic and environmental modifiers. *Laboratory Investigation*, *84*(12), 1619–1630. https://doi.org/10.1038/labinvest.3700180

Cortina, C., Turon, G., Stork, D., Hernando-Momblona, X., Sevillano, M., Aguilera, M., Tosi, S., Merlos-Suárez, A., Stephan-Otto Attolini, C., Sancho, E., & Batlle, E. (2017). A genome editing approach to study cancer stem cells in human tumors. *EMBO Molecular Medicine*. https://doi.org/10.15252/emmm.201707550

Dalerba, P, Dylla, S., Park, I., & Liu, R. (2007). Phenotypic characterization of human colorectal cancer stem cells. *Proceedings of The*. http://www.pnas.org/content/104/24/10158.short

Dalerba, Piero, Kalisky, T., Sahoo, D., Rajendran, P. S., Rothenberg, M. E., Leyrat, A. A., Sim, S., Okamoto, J., Johnston, D. M., Qian, D., Zabala, M., Bueno, J., Neff, N. F., Wang, J., Shelton, A. A., Visser, B., Hisamori, S., Shimono, Y., Van De Wetering, M., … Quake, S. R. (2011). Single-cell dissection of transcriptional heterogeneity in human colon tumors. *Nature Biotechnology*, *29*(12), 1120–1127. https://doi.org/10.1038/nbt.2038

Darwich, A. S., Aslam, U., Ashcroft, D. M., & Rostami-Hodjegan, A. (2014). Meta-analysis of the turnover of intestinal epithelia in preclinical animal species and humans. *Drug Metabolism and Disposition: The Biological Fate of Chemicals*, *42*(12), 2016–2022. https://doi.org/10.1124/dmd.114.058404

de Lau, W., Barker, N., Low, T. Y., Koo, B.-K., Li, V. S. W., Teunissen, H., Kujala, P., Haegebarth, A., Peters, P. J., van de Wetering, M., Stange, D. E., van Es, J. E., Guardavaccaro, D., Schasfoort, R. B. M., Mohri, Y., Nishimori, K., Mohammed, S., Heck, A. J. R., & Clevers, H. (2011). Lgr5 homologues associate with Wnt receptors and mediate R-spondin signalling. *Nature*, *476*(7360), 293–297. https://doi.org/10.1038/nature10337

De Sousa E Melo, F., Kurtova, A. V., Harnoss, J. M., Kljavin, N., Hoeck, J. D., Hung, J., Anderson, J. E., Storm, E. E., Modrusan, Z., Koeppen, H., Dijkgraaf, G. J. P., Piskol, R., De Sauvage, F. J., Sousa, F. De, Antonina, V., Harnoss, J. M., Kljavin, N., Hoeck, J. D., Hung, J., … Sauvage, F. J. De. (2017). A distinct role for Lgr5 + stem cells in primary and metastatic colon cancer. *Nature*, *543*(7647), 676–680. https://doi.org/10.1038/nature21713

Del Re, D. P., Yang, Y., Nakano, N., Cho, J., Zhai, P., Yamamoto, T., Zhang, N., Yabuta, N., Nojima, H., Pan, D., & Sadoshima, J. (2013). Yes-associated protein isoform 1 (Yapl) promotes cardiomyocyte survival and growth to protect against myocardial ischemic injury. *Journal of Biological Chemistry*, *288*(6), 3977–3988. https://doi.org/10.1074/jbc.M112.436311

Dong, J., Feldmann, G., Huang, J., Wu, S., Zhang, N., Comerford, S. A., Gayyed, M. F., Anders, R. A., Maitra, A., & Pan, D. (2007). Elucidation of a Universal Size-Control Mechanism in Drosophila and Mammals. *Cell*, *130*(6), 1120–1133. https://doi.org/10.1016/j.cell.2007.07.019

Dupont, S., Morsut, L., Aragona, M., Enzo, E., Giulitti, S., Cordenonsi, M., Zanconato, F., Le Digabel, J., Forcato, M., Bicciato, S., Elvassore, N., & Piccolo, S. (2011). Role of YAP/TAZ in mechanotransduction. *Nature*, *474*(7350), 179–184. https://doi.org/10.1038/nature10137

El Marjou, F., Janssen, K. P., Chang, B. H. J., Li, M., Hindie, V., Chan, L., Louvard, D., Chambon, P., Metzger, D., & Robine, S. (2004). Tissue-specific and inducible Cre-mediated recombination in the gut epithelium. *Genesis*. https://doi.org/10.1002/gene.20042

Fan, F., He, Z., Kong, L. L., Chen, Q., Yuan, Q., Zhang, S., Ye, J., Liu, H., Sun, X., Geng,

J., Yuan, L., Hong, L., Xiao, C., Zhang, W., Sun, X., Li, Y., Wang, P., Huang, L., Wu, X., … Zhou, D. (2016). Pharmacological targeting of kinases MST1 and MST2 augments tissue repair and regeneration. *Science Translational Medicine*. https://doi.org/10.1126/scitranslmed.aaf2304

Fearon, E. R. (2011). Molecular genetics of colorectal cancer. *Annu. Rev. Pathol.*, *6*, 479–507. https://doi.org/10.1146/annurev-pathol-011110-130235

Fearon, E. R., & Vogelstein, B. (1990). A genetic model for colorectal tumorigenesis. *Cell*, *61*(5), 759–767. https://doi.org/10.1016/0092-8674(90)90186-I

Fevr, T., Robine, S., Louvard, D., & Huelsken, J. (2007). Wnt/ -Catenin Is Essential for Intestinal Homeostasis and Maintenance of Intestinal Stem Cells. *Molecular and Cellular Biology*. https://doi.org/10.1128/mcb.01034-07

Fujii, M., Shimokawa, M., Date, S., Takano, A., Matano, M., Nanki, K., Ohta, Y., Toshimitsu, K., Nakazato, Y., Kawasaki, K., Uraoka, T., Watanabe, T., Kanai, T., & Sato, T. (2016). A Colorectal Tumor Organoid Library Demonstrates Progressive Loss of Niche Factor Requirements during Tumorigenesis. *Cell Stem Cell*. https://doi.org/10.1016/j.stem.2016.04.003

Fumagalli, A., Drost, J., Suijkerbuijk, S. J. E., Boxtel, R. Van, & De, J. (2017). *Genetic dissection of colorectal cancer progression by orthotopic transplantation of engineered cancer organoids*. 1–19. https://doi.org/10.1073/pnas.1701219114

Fumagalli, A., Oost, K. C., Kester, L., Morgner, J., Bornes, L., Bruens, L., Spaargaren, L., Azkanaz, M., Schelfhorst, T., Beerling, E., Heinz, M. C., Postrach, D., Seinstra, D., Sieuwerts, A. M., Martens, J. W. M., van der Elst, S., van Baalen, M., Bhowmick, D., Vrisekoop, N., … van Rheenen, J. (2020). Plasticity of Lgr5-Negative Cancer Cells Drives Metastasis in Colorectal Cancer. *Cell Stem Cell*. https://doi.org/10.1016/j.stem.2020.02.008

Galli, G. G., Carrara, M., Yuan, W. C., Valdes-Quezada, C., Gurung, B., Pepe-Mooney, B., Zhang, T., Geeven, G., Gray, N. S., de Laat, W., Calogero, R. a., & Camargo, F. D. (2015). YAP Drives Growth by Controlling Transcriptional Pause Release from Dynamic Enhancers. *Molecular Cell*, *60*(2), 328–337. https://doi.org/10.1016/j.molcel.2015.09.001

Gehart, H., & Clevers, H. (2019). Tales from the crypt: new insights into intestinal stem cells. *Nature Reviews. Gastroenterology & Hepatology*, *16*(1), 19–34. https://doi.org/10.1038/s41575-018-0081-y

Gerstung, M., Jolly, C., Leshchiner, I., Dentro, S. C., Gonzalez, S., Rosebrock, D., Mitchell, T. J., Rubanova, Y., Anur, P., Yu, K., Tarabichi, M., Deshwar, A., Wintersinger, J., Kleinheinz, K., Vázquez-García, I., Haase, K., Jerman, L., Sengupta, S., Macintyre, G., … Van Loo, P. (2020). The evolutionary history of 2,658 cancers. *Nature*. https://doi.org/10.1038/s41586-019-1907-7

Goto, N., Fukuda, A., Yamaga, Y., Yoshikawa, T., Maruno, T., Maekawa, H., Inamoto, S., Kawada, K., Sakai, Y., Miyoshi, H., Taketo, M. M., Chiba, T., & Seno, H. (2019). Lineage tracing and targeting of IL17RB+ tuft cell-like human colorectal cancer stem cells. *Proceedings of the National Academy of Sciences of the United States of America*. https://doi.org/10.1073/pnas.1900251116

Gregorieff, A., & Clevers, H. (2005). Wnt signaling in the intestinal epithelium: From endoderm to cancer. In *Genes and Development*. https://doi.org/10.1101/gad.1295405

Gregorieff, A., Liu, Y., Inanlou, M. R., Khomchuk, Y., & Wrana, J. L. (2015). Yap-dependent reprogramming of Lgr5+ stem cells drives intestinal regeneration and cancer. *Nature*, *526*(7575), 715–718. https://doi.org/10.1038/nature15382

Grijalva, J. L., Huizenga, M., Mueller, K., Rodriguez, S., Brazzo, J., Camargo, F., Sadri-Vakili, G., & Vakili, K. (2014). Dynamic alterations in Hippo signaling pathway and YAP activation during liver regeneration. *American Journal of Physiology-Gastrointestinal and Liver Physiology*, *307*(2), G196–G204. https://doi.org/10.1152/ajpgi.00077.2014

Hafemeister, C., & Satija, R. (2019). Normalization and variance stabilization of single-cell RNA-seq data using regularized negative binomial regression. *Genome Biology*. https://doi.org/10.1186/s13059-019-1874-1

Haigis, K. M., & Dove, W. F. (2003). A Robertsonian translocation suppresses a somatic recombination pathway to loss of heterozygosity. *Nature Genetics*. https://doi.org/10.1038/ng1055

Haines, J., Johnson, V., Pack, K., Suraweera, N., Slijepcevic, P., Cabuy, E., Coster, M., Ilyas, M., Wilding, J., Sieber, O., Bodmer, W., Tomlinson, I., & Silver, A. (2005). Genetic basis of variation in adenoma multiplicity in ApcMin/+ Mom1S mice. *Proceedings of the National Academy of Sciences*, *102*(8), 2868–2873. https://doi.org/10.1073/pnas.0500039102

Hao, H.-X., Xie, Y., Zhang, Y., Charlat, O., Oster, E., Avello, M., Lei, H., Mickanin, C., Liu, D., Ruffner, H., Mao, X., Ma, Q., Zamponi, R., Bouwmeester, T., Finan, P. M., Kirschner, M. W., Porter, J. A., Serluca, F. C., & Cong, F. (2012). ZNRF3 promotes Wnt receptor turnover in an R-spondin-sensitive manner. *Nature*, *485*(7397), 195–200. https://doi.org/10.1038/nature11019

Hart, M., Concordet, J. P., Lassot, I., Albert, I., del los Santos, R., Durand, H., Perret, C., Rubinfeld, B., Margottin, F., Benarous, R., & Polakis, P. (1999). The F-box protein beta-TrCP associates with phosphorylated beta-catenin and regulates its activity in the cell. *Current Biology : CB*, *9*(4), 207–210. https://doi.org/10.1016/s0960-9822(99)80091-8

Harvey, K. F., Pfleger, C. M., & Hariharan, I. K. (2003). The Drosophila Mst ortholog, hippo, restricts growth and cell proliferation and promotes apoptosis. *Cell*, *114*(4),

457–467. https://doi.org/10.1016/S0092-8674(03)00557-9

Harvey, K. F., Zhang, X., & Thomas, D. M. (2013). The Hippo pathway and human cancer. *Nature Reviews. Cancer*, *13*(4), 246–257. https://doi.org/10.1038/nrc3458

Heallen, T., Morikawa, Y., Leach, J., Tao, G., Willerson, J. T., Johnson, R. L., & Martin, J. F. (2013). Hippo signaling impedes adult heart regeneration. *Development (Cambridge, England)*, *140*(23), 4683–4690. https://doi.org/10.1242/dev.102798

Heallen, T., Zhang, M., Wang, J., Bonilla-Claudio, M., Klysik, E., Johnson, R. L., & Martin, J. F. (2011). Hippo pathway inhibits wnt signaling to restrain cardiomyocyte proliferation and heart size. *Science*, *332*(6028), 458–461. https://doi.org/10.1126/science.1199010

Heitzer, E., Auer, M., Gasch, C., Pichler, M., Ulz, P., Hoffmann, E. M., Lax, S., Waldispuehl-Geigl, J., Mauermann, O., Lackner, C., Höfler, G., Eisner, F., Sill, H., Samonigg, H., Pantel, K., Riethdorf, S., Bauernhofer, T., Geigl, J. B., & Speicher, M. R. (2013). Complex tumor genomes inferred from single circulating tumor cells by array-CGH and next-generation sequencing. *Cancer Research*, *73*(10), 2965–2975. https://doi.org/10.1158/0008-5472.CAN-12-4140

Hong, A. W., Meng, Z., & Guan, K. L. (2016). The Hippo pathway in intestinal regeneration and disease. In *Nature Reviews Gastroenterology and Hepatology*. https://doi.org/10.1038/nrgastro.2016.59

Huang, E. H., Hynes, M. J., Zhang, T., Ginestier, C., Dontu, G., Appelman, H., Fields, J. Z., Wicha, M. S., & Boman, B. M. (2009). Aldehyde dehydrogenase 1 is a marker for normal and malignant human colonic stem cells (SC) and tracks SC overpopulation during colon tumorigenesis. *Cancer Research*. https://doi.org/10.1158/0008-5472.CAN-08-4418

Huang, J., Wu, S., Barrera, J., Matthews, K., & Pan, D. (2005). The Hippo signaling pathway coordinately regulates cell proliferation and apoptosis by inactivating Yorkie, the Drosophila homolog of YAP. *Cell*, *122*(3), 421–434. https://doi.org/10.1016/j.cell.2005.06.007

Huch, M., Dorrell, C., Boj, S. F., Van Es, J. H., Li, V. S. W., Van De Wetering, M., Sato, T., Hamer, K., Sasaki, N., Finegold, M. J., Haft, A., Vries, R. G., Grompe, M., & Clevers, H. (2013). In vitro expansion of single Lgr5 + liver stem cells induced by Wnt-driven regeneration. *Nature*. https://doi.org/10.1038/nature11826

Humphries, A., Cereser, B., Gay, L. J., Miller, D. S. J., Das, B., Gutteridge, A., Elia, G., Nye, E., Jeffery, R., Poulsom, R., Novelli, M. R., Rodriguez-Justo, M., McDonald, S. a C., Wright, N. a, & Graham, T. a. (2013). Lineage tracing reveals multipotent stem cells maintain human adenomas and the pattern of clonal expansion in tumor evolution. *Proceedings of the National Academy of Sciences of the United States of America*, *110*(27), E2490-9. https://doi.org/10.1073/pnas.1220353110

IJspeert, J. E. G., Vermeulen, L., Meijer, G. A., & Dekker, E. (2015). Serrated neoplasia-role in colorectal carcinogenesis and clinical implications. *Nature Reviews. Gastroenterology & Hepatology*, *12*(7), 401–409. https://doi.org/10.1038/nrgastro.2015.73

Imajo, M., Miyatake, K., Iimura, A., Miyamoto, A., & Nishida, E. (2012). A molecular mechanism that links Hippo signalling to the inhibition of Wnt/β-catenin signalling. *EMBO Journal*, *31*(5), 1109–1122. https://doi.org/10.1038/emboj.2011.487

Inuzuka, H., Wakao, H., Masuho, Y., Muramatsu, M. aki, Tojo, H., & Nanbu-Wakao, R. (1999). cDNA cloning and expression analysis of mouse zf9, a Kruppel-like transcription factor gene that is induced by adipogenic hormonal stimulation in 3T3-L1 cells. *Biochimica et Biophysica Acta - Gene Structure and Expression*. https://doi.org/10.1016/S0167-4781(99)00161-X

Jeon, Y. K., Kim, S. H., Choi, S. H., Kim, K. H., Yoo, B. C., Ku, J. L., & Park, J. G. (2010). Promoter hypermethylation and loss of CD133 gene expression in colorectal cancers. *World Journal of Gastroenterology*. https://doi.org/10.3748/wjg.v16.i25.3153

Jia, J., Zhang, W., Wang, B., Trinko, R., & Jiang, J. (2003). The Drosophila Ste20 family kinase dMST functions as a tumor suppressor by restricting cell proliferation and promoting apoptosis. *Genes and Development*, *17*(20), 2514–2519. https://doi.org/10.1101/gad.1134003

Jiao, S., Wang, H., Shi, Z., Dong, A., Zhang, W., Song, X., He, F., Wang, Y., Zhang, Z., Wang, W., Wang, X., Guo, T., Li, P., Zhao, Y., Ji, H., Zhang, L., & Zhou, Z. (2014). A Peptide Mimicking VGLL4 Function Acts as a YAP Antagonist Therapy against Gastric Cancer. *Cancer Cell*, *25*(2), 166–180. https://doi.org/10.1016/j.ccr.2014.01.010

Johnson, R., & Halder, G. (2014). The two faces of Hippo: targeting the Hippo pathway for regenerative medicine and cancer treatment. *Nature Reviews. Drug Discovery*, *13*(1), 63–79. https://doi.org/10.1038/nrd4161

Justice, R. W., Zilian, O., Woods, D. F., Noll, M., & Bryant, P. J. (1995). The Drosophila tumor suppressor gene warts encodes a homolog of human myotonic dystrophy kinase and is required for the control of cell shape and proliferation. *Genes and Development*, *9*(5), 534–546. https://doi.org/10.1101/gad.9.5.534

Kahn, M. (2014). Can we safely target the WNT pathway? In *Nature Reviews Drug Discovery*. https://doi.org/10.1038/nrd4233

Kanehisa, M. (2000). KEGG: Kyoto Encyclopedia of Genes and Genomes. *Nucleic Acids Research*. https://doi.org/10.1093/nar/28.1.27

Kango-Singh, M. (2002). Shar-pei mediates cell proliferation arrest during imaginal

disc growth in Drosophila. *Development*, *129*(24), 5719–5730. https://doi.org/10.1242/dev.00168

Kemper, K., Prasetyanti, P. R., De Lau, W., Rodermond, H., Clevers, H., & Medema, J. P. (2012). Monoclonal antibodies against Lgr5 identify human colorectal cancer stem cells. *Stem Cells*. https://doi.org/10.1002/stem.1233

Kemper, K., Versloot, M., Cameron, K., Colak, S., De Sousa E Melo, F., De Jong, J. H., Bleackley, J., Vermeulen, L., Versteeg, R., Koster, J., & Medema, J. P. (2012). Mutations in the Ras-Raf axis underlie the prognostic value of CD133 in colorectal cancer. *Clinical Cancer Research*. https://doi.org/10.1158/1078-0432.CCR-11-3066

Kim, K. A., Kakitani, M., Zhao, J., Oshima, T., Tang, T., Binnerts, M., Liu, Y., Boyle, B., Park, E., Emtage, P., Funk, W. D., & Tomizuka, K. (2005). Medicine: Mitogenic influence of human R-spondin1 on the intestinal epithelium. *Science*. https://doi.org/10.1126/science.1112521

Kim, T. M., Jung, S. H., An, C. H., Lee, S. H., Baek, I. P., Kim, M. S., Park, S. W., Rhee, J. K., Lee, S. H., & Chung, Y. J. (2015). Subclonal genomic architectures of primary and metastatic colorectal cancer based on intratumoral genetic heterogeneity. *Clinical Cancer Research*, *21*(19), 4461–4472. https://doi.org/10.1158/1078-0432.CCR-14-2413

Kimelman, D., & Xu, W. (2006). beta-catenin destruction complex: insights and questions from a structural perspective. *Oncogene*, *25*(57), 7482–7491. https://doi.org/10.1038/sj.onc.1210055

Kojima, S., Hayashi, S., Shimokado, K., Suzuki, Y., Shimada, J., Crippa, M. P., & Friedman, S. L. (2000). Transcriptional activation of urokinase by the Kruppel-like factor Zf9/COPEB activates latent TGF-β1 in vascular endothelial cells. *Blood*.

Konsavage, W. M., Kyler, S. L., Rennoll, S. A., Jin, G., & Yochum, G. S. (2012). Wnt/β-catenin signaling regulates yes-associated protein (YAP) gene expression in colorectal carcinoma cells. *Journal of Biological Chemistry*. https://doi.org/10.1074/jbc.M111.327767

Koo, B.-K., Spit, M., Jordens, I., Low, T. Y., Stange, D. E., van de Wetering, M., van Es, J. H., Mohammed, S., Heck, A. J. R., Maurice, M. M., & Clevers, H. (2012). Tumour suppressor RNF43 is a stem-cell E3 ligase that induces endocytosis of Wnt receptors. *Nature*, *488*(7413), 665–669. https://doi.org/10.1038/nature11308

Korinek, V., Barker, N., Moerer, P., Van Donselaar, E., Huls, G., Peters, P. J., & Clevers, H. (1998). Depletion of epithelial stem-cell compartments in the small intestine of mice lacking Tcf-4. *Nature Genetics*. https://doi.org/10.1038/1270

Kreso, a, O'Brien, C. a, van Galen, P., Gan, O. I., Notta, F., Brown, a M., Ng, K., Ma, J., Wienholds, E., Dunant, C., Pollett, a, Gallinger, S., McPherson, J., Mullighan, C. G.,

Shibata, D., & Dick, J. E. (2013). Variable clonal repopulation dynamics influence chemotherapy response in colorectal cancer. *Science*, *339*(6119), 543–548. https://doi.org/science.1227670 [pii]\r10.1126/science.1227670

Kuhnert, F., Davis, C. R., Wang, H. T., Chu, P., Lee, M., Yuan, J., Nusse, R., & Kuo, C. J. (2004). Essential requirement for Wnt signaling in proliferation of adult small intestine and colon revealed by adenoviral expression of Dickkopf-1. *Proceedings of the National Academy of Sciences of the United States of America*. https://doi.org/10.1073/pnas.2536800100

Lai, Z.-C. C., Wei, X., Shimizu, T., Ramos, E., Rohrbaugh, M., Nikolaidis, N., Ho, L.-L. L., & Li, Y. (2005). Control of cell proliferation and apoptosis by mob as tumor suppressor, mats. *Cell*, *120*(5), 675–685. https://doi.org/10.1016/j.cell.2004.12.036

Lam-Himlin, D. M., Daniels, J. A., Gayyed, M. F., Dong, J., Maitra, A., Pan, D., Montgomery, E. A., & Anders, R. A. (2006). The hippo pathway in human upper gastrointestinal dysplasia and carcinoma: A novel oncogenic pathway. *International Journal of Gastrointestinal Cancer*. https://doi.org/10.1007/s12029-007-0010-8

Lamprecht, S., Schmidt, E. M., Blaj, C., Hermeking, H., Jung, A., Kirchner, T., & Horst, D. (2017). Multicolor lineage tracing reveals clonal architecture and dynamics in colon cancer. *Nature Communications*. https://doi.org/10.1038/s41467-017-00976-9

Langmead, B., Trapnell, C., Pop, M., & Salzberg, S. L. (2009). Ultrafast and memory-efficient alignment of short DNA sequences to the human genome. *Genome Biology*. https://doi.org/10.1186/gb-2009-10-3-r25

Lapidot, T., Sirard, C., Vormoor, J., Murdoch, B., Hoang, T., Caceres-Cortes, J., Minden, M., Paterson, B., Caligiuri, M. A., & Dick, J. E. (1994). A cell initiating human acute myeloid leukaemia after transplantation into SCID mice. *Nature*. https://doi.org/10.1038/367645a0

Leach, J. P., Heallen, T., Zhang, M., Rahmani, M., Morikawa, Y., Hill, M. C., Segura, A., Willerson, J. T., & Martin, J. F. (2017). Hippo pathway deficiency reverses systolic heart failure after infarction. *Nature*, *550*(7675), 260–264. https://doi.org/10.1038/nature24045

Leedham, S. J., Graham, T. A., Oukrif, D., McDonald, S. A. C., Rodriguez-Justo, M., Harrison, R. F., Shepherd, N. A., Novelli, M. R., Jankowski, J. A. Z., & Wright, N. A. (2009). Clonality, founder mutations, and field cancerization in human ulcerative colitis-associated neoplasia. *Gastroenterology*, *136*(2), 542-50.e6. https://doi.org/10.1053/j.gastro.2008.10.086

Lei, Q.-Y., Zhang, H., Zhao, B., Zha, Z.-Y., Bai, F., Pei, X.-H., Zhao, S., Xiong, Y., & Guan, K.-L. (2008). TAZ Promotes Cell Proliferation and Epithelial-Mesenchymal Transition and Is Inhibited by the Hippo Pathway. *Molecular and Cellular Biology*,

28(7), 2426–2436. https://doi.org/10.1128/MCB.01874-07

Lenos, K. J., Miedema, D. M., Lodestijn, S. C., Nijman, L. E., van den Bosch, T., Romero Ros, X., Lourenço, F. C., Lecca, M. C., van der Heijden, M., van Neerven, S. M., van Oort, A., Leveille, N., Adam, R. S., de Sousa E Melo, F., Otten, J., Veerman, P., Hypolite, G., Koens, L., Lyons, S. K., … Vermeulen, L. (2018). Stem cell functionality is microenvironmentally defined during tumour expansion and therapy response in colon cancer. *Nature Cell Biology*. https://doi.org/10.1038/s41556-018-0179-z

Li, B., & Dewey, C. N. (2011). RSEM: Accurate transcript quantification from RNA-Seq data with or without a reference genome. *BMC Bioinformatics*. https://doi.org/10.1186/1471-2105-12-323

Li, H., Handsaker, B., Wysoker, A., Fennell, T., Ruan, J., Homer, N., Marth, G., Abecasis, G., & Durbin, R. (2009). The Sequence Alignment/Map format and SAMtools. *Bioinformatics*. https://doi.org/10.1093/bioinformatics/btp352

Li, Q., Sun, Y., Jarugumilli, G. K., Liu, S., Dang, K., Cotton, J. L., Xiol, J., Chan, P. Y., DeRan, M., Ma, L., Li, R., Zhu, L. J., Li, J. H., Leiter, A. B., Ip, Y. T., Camargo, F. D., Luo, X., Johnson, R. L., Wu, X., & Mao, J. (2020). Lats1/2 Sustain Intestinal Stem Cells and Wnt Activation through TEAD-Dependent and Independent Transcription. *Cell Stem Cell*. https://doi.org/10.1016/j.stem.2020.03.002

Lian, I., Kim, J., Okazawa, H., Zhao, J., Zhao, B., Yu, J., Chinnaiyan, A., Israel, M. A., Goldstein, L. S. B., Abujarour, R., Ding, S., & Guan, K. L. (2010). The role of YAP transcription coactivator in regulating stem cell self-renewal and differentiation. *Genes and Development*, *24*(11), 1106–1118. https://doi.org/10.1101/gad.1903310

Lin, Z., Von Gise, A., Zhou, P., Gu, F., Ma, Q., Jiang, J., Yau, A. L., Buck, J. N., Gouin, K. A., Van Gorp, P. R. R., Zhou, B., Chen, J., Seidman, J. G., Wang, D. Z., & Pu, W. T. (2014). Cardiac-specific YAP activation improves cardiac function and survival in an experimental murine MI model. *Circulation Research*, *115*(3), 354–363. https://doi.org/10.1161/CIRCRESAHA.115.303632

Linnekamp, J. F., Wang, X., Medema, J. P., & Vermeulen, L. (2015). Colorectal cancer heterogeneity and targeted therapy: A case for molecular disease subtypes. *Cancer Research*, *75*(2), 245–249. https://doi.org/10.1158/0008-5472.CAN-14-2240

Liu, C., Li, Y., Semenov, M., Han, C., Baeg, G. H., Tan, Y., Zhang, Z., Lin, X., & He, X. (2002). Control of beta-catenin phosphorylation/degradation by a dual-kinase mechanism. *Cell*, *108*(6), 837–847. https://doi.org/10.1016/s0092-8674(02)00685-2

Lotti, F., Jarrar, A. M., Pai, R. K., Hitomi, M., Lathia, J., Mace, A., Gantt, G. A., Sukhdeo, K., DeVecchio, J., Vasanji, A., Leahy, P., Hjelmeland, A. B., Kalady, M. F., & Rich, J. N. (2013). Chemotherapy activates cancer-associated fibroblasts to maintain colorectal cancer-initiating cells by IL-17A. *Journal of Experimental Medicine*.

https://doi.org/10.1084/jem.20131195

Love, M. I., Huber, W., & Anders, S. (2014). Moderated estimation of fold change and dispersion for RNA-seq data with DESeq2. *Genome Biology*. https://doi.org/10.1186/s13059-014-0550-8

Lu, L., Finegold, M. J., & Johnson, R. L. (2018). Hippo pathway coactivators Yap and Taz are required to coordinate mammalian liver regeneration. *Experimental & Molecular Medicine*, *50*(1), e423. https://doi.org/10.1038/emm.2017.205

MacDonald, B. T., Tamai, K., & He, X. (2009). Wnt/beta-catenin signaling: components, mechanisms, and diseases. *Developmental Cell*, *17*(1), 9–26. https://doi.org/10.1016/j.devcel.2009.06.016

Madison, B. B., Dunbar, L., Qiao, X. T., Braunstein, K., Braunstein, E., & Gumucio, D. L. (2002). cis elements of the villin gene control expression in restricted domains of the vertical (crypt) and horizontal (duodenum, cecum) axes of the intestine. *Journal of Biological Chemistry*. https://doi.org/10.1074/jbc.M204935200

Marusyk, A., Almendro, V., & Polyak, K. (2012). Intra-tumour heterogeneity: a looking glass for cancer? *Nature Reviews. Cancer*, *12*(5), 323–334. https://doi.org/10.1038/nrc3261

Matano, M., Date, S., Shimokawa, M., Takano, A., Fujii, M., Ohta, Y., Watanabe, T., Kanai, T., & Sato, T. (2015). Modeling colorectal cancer using CRISPR-Cas9–mediated engineering of human intestinal organoids. *Nature Medicine*, *21*(3), 256–262. https://doi.org/10.1038/nm.3802

McDavid, A., Finak, G., Chattopadyay, P. K., Dominguez, M., Lamoreaux, L., Ma, S. S., Roederer, M., & Gottardo, R. (2013). Data exploration, quality control and testing in single-cell qPCR-based gene expression experiments. *Bioinformatics*. https://doi.org/10.1093/bioinformatics/bts714

McGranahan, N., & Swanton, C. (2015). Biological and therapeutic impact of intratumor heterogeneity in cancer evolution. *Cancer Cell*, *27*(1), 15–26. https://doi.org/10.1016/j.ccell.2014.12.001

McInnes, L., Healy, J., Saul, N., & Großberger, L. (2018). UMAP: Uniform Manifold Approximation and Projection. *Journal of Open Source Software*. https://doi.org/10.21105/joss.00861

Merlos-Suárez, A., Barriga, F. M., Jung, P., Iglesias, M., Céspedes, M. V., Rossell, D., Sevillano, M., Hernando-Momblona, X., Da Silva-Diz, V., Muñoz, P., Clevers, H., Sancho, E., Mangues, R., & Batlle, E. (2011). The intestinal stem cell signature identifies colorectal cancer stem cells and predicts disease relapse. *Cell Stem Cell*, *8*(5), 511–524. https://doi.org/10.1016/j.stem.2011.02.020

Miyaki, M., Iijima, T., Konishi, M., Sakai, K., Ishii, A., Yasuno, M., Hishima, T., Koike,

M., Shitara, N., Iwama, T., Utsunomiya, J., Kuroki, T., & Mori, T. (1999). Higher frequency of Smad4 gene mutation in human colorectal cancer with distant metastasis. *Oncogene*. https://doi.org/10.1038/sj.onc.1202642

Miyoshi, H., & Stappenbeck, T. S. (2013). In vitro expansion and genetic modification of gastrointestinal stem cells in spheroid culture. *Nature Protocols*, *8*(12), 2471–2482. https://doi.org/10.1038/nprot.2013.153

Molenaar, M., van de Wetering, M., Oosterwegel, M., Peterson-Maduro, J., Godsave, S., Korinek, V., Roose, J., Destrée, O., & Clevers, H. (1996). XTcf-3 transcription factor mediates beta-catenin-induced axis formation in Xenopus embryos. *Cell*, *86*(3), 391–399. https://doi.org/10.1016/s0092-8674(00)80112-9

Morral, C., Stanisavljevic, J., Hernando-Momblona, X., Mereu, E., Álvarez-Varela, A., Cortina, C., Stork, D., Slebe, F., Turon, G., Whissell, G., Sevillano, M., Merlos-Suárez, A., Casanova-Martí, À., Moutinho, C., Lowe, S. W., Dow, L. E., Villanueva, A., Sancho, E., Heyn, H., & Batlle, E. (2020). Zonation of Ribosomal DNA Transcription Defines a Stem Cell Hierarchy in Colorectal Cancer. *Cell Stem Cell*. https://doi.org/10.1016/j.stem.2020.04.012

Muñoz, J., Stange, D. E., Schepers, A. G., Van De Wetering, M., Koo, B. K., Itzkovitz, S., Volckmann, R., Kung, K. S., Koster, J., Radulescu, S., Myant, K., Versteeg, R., Sansom, O. J., Van Es, J. H., Barker, N., Van Oudenaarden, A., Mohammed, S., Heck, A. J. R., & Clevers, H. (2012). The Lgr5 intestinal stem cell signature: Robust expression of proposed quiescent ′ +4′ cell markers. *EMBO Journal*. https://doi.org/10.1038/emboj.2012.166

Nakanishi, Y., Seno, H., Fukuoka, A., Ueo, T., Yamaga, Y., Maruno, T., Nakanishi, N., Kanda, K., Komekado, H., Kawada, M., Isomura, A., Kawada, K., Sakai, Y., Yanagita, M., Kageyama, R., Kawaguchi, Y., Taketo, M. M., Yonehara, S., & Chiba, T. (2013). Dclk1 distinguishes between tumor and normal stem cells in the intestine. *Nature Genetics*, *45*(1), 98–103. https://doi.org/10.1038/ng.2481

Neufert, C., Becker, C., & Neurath, M. F. (2007). An inducible mouse model of colon carcinogenesis for the analysis of sporadic and inflammation-driven tumor progression. *Nature Protocols*. https://doi.org/10.1038/nprot.2007.279

Nowell, P. C. (1976). The clonal evolution of tumor cell populations. *Science*, *194*(4260), 23–28. https://doi.org/10.1126/science.959840

Nusse, Y. M., Savage, A. K., Marangoni, P., Rosendahl-Huber, A. K. M., Landman, T. A., De Sauvage, F. J., Locksley, R. M., & Klein, O. D. (2018). Parasitic helminths induce fetal-like reversion in the intestinal stem cell niche. *Nature*. https://doi.org/10.1038/s41586-018-0257-1

O'Brien, C. A., Pollett, A., Gallinger, S., Gallinger, S., Dick, J. E., Brien, C. A. O., Pollett, A., Gallinger, S., Dick, J. E., & O'Brien, C. A. (2007). A human colon cancer cell capable of initiating tumour growth in immunodeficient mice. *Nature*,

445(January), 111–115. https://doi.org/10.1038/nature05372

O'Rourke, K. P., Loizou, E., Livshits, G., Schatoff, E. M., Baslan, T., Manchado, E., Simon, J., Romesser, P. B., Leach, B., Han, T., Pauli, C., Beltran, H., Rubin, M. A., Dow, L. E., & Lowe, S. W. (2017). Transplantation of engineered organoids enables rapid generation of metastatic mouse models of colorectal cancer. *Nature Biotechnology*. https://doi.org/10.1038/nbt.3837

Ootani, A., Li, X., Sangiorgi, E., Ho, Q. T., Ueno, H., Toda, S., Sugihara, H., Fujimoto, K., Weissman, I. L., Capecchi, M. R., & Kuo, C. J. (2009). Sustained in vitro intestinal epithelial culture within a Wnt-dependent stem cell niche. *Nature Medicine*. https://doi.org/10.1038/nm.1951

Ordóñez-Morán, P., Dafflon, C., Imajo, M., Nishida, E., & Huelsken, J. (2015). HOXA5 Counteracts Stem Cell Traits by Inhibiting Wnt Signaling in Colorectal Cancer. *Cancer Cell*. https://doi.org/10.1016/j.ccell.2015.11.001

Pan, W. W., Moroishi, T., Koo, J. H., & Guan, K. L. (2019). Cell type-dependent function of LATS1/2 in cancer cell growth. *Oncogene*. https://doi.org/10.1038/s41388-018-0610-8

Pantalacci, S., Tapon, N., & Léopold, P. (2003). The salvador partner Hippo promotes apoptosis and cell-cycle exit in Drosophila. *Nature Cell Biology*, *5*(10), 921–927. https://doi.org/10.1038/ncb1051

Park, H. W., Kim, Y. C., Yu, B., Moroishi, T., Mo, J. S., Plouffe, S. W., Meng, Z., Lin, K. C., Yu, F. X., Alexander, C. M., Wang, C. Y., & Guan, K. L. (2015). Alternative Wnt Signaling Activates YAP/TAZ. *Cell*, *162*(4), 780–794. https://doi.org/10.1016/j.cell.2015.07.013

Patro, R., Duggal, G., Love, M. I., Irizarry, R. A., & Kingsford, C. (2017). Salmon provides fast and bias-aware quantification of transcript expression. *Nature Methods*. https://doi.org/10.1038/nmeth.4197

Pepe-Mooney, B. J., Dill, M. T., Alemany, A., Ordovas-Montanes, J., Matsushita, Y., Rao, A., Sen, A., Miyazaki, M., Anakk, S., Dawson, P. A., Ono, N., Shalek, A. K., van Oudenaarden, A., & Camargo, F. D. (2019). Single-Cell Analysis of the Liver Epithelium Reveals Dynamic Heterogeneity and an Essential Role for YAP in Homeostasis and Regeneration. *Cell Stem Cell*, *25*(1), 23-38.e8. https://doi.org/10.1016/j.stem.2019.04.004

Peterson, L. W., & Artis, D. (2014). Intestinal epithelial cells: Regulators of barrier function and immune homeostasis. In *Nature Reviews Immunology*. https://doi.org/10.1038/nri3608

Pinson, K. I., Brennan, J., Monkley, S., Avery, B. J., & Skarnes, W. C. (2000). An LDL-receptor-related protein mediates Wnt signalling in mice. *Nature*, *407*(6803), 535–538. https://doi.org/10.1038/35035124

Pinto, D., Gregorieff, A., Begthel, H., & Clevers, H. (2003). Canonical Wnt signals are essential for homeostasis of the intestinal epithelium. *Genes and Development*. https://doi.org/10.1101/gad.267103

Piskol, R., & de Sousa e Melo, F. (2020). Colon Cancer Heterogeneity: Welcome to the RiboZone. *Cell Stem Cell*. https://doi.org/10.1016/j.stem.2020.05.005

Powell, A. E., Wang, Y., Li, Y., Poulin, E. J., Means, A. L., Washington, M. K., Higginbotham, J. N., Juchheim, A., Prasad, N., Levy, S. E., Guo, Y., Shyr, Y., Aronow, B. J., Haigis, K. M., Franklin, J. L., & Coffey, R. J. (2012). The pan-ErbB negative regulator lrig1 is an intestinal stem cell marker that functions as a tumor suppressor. *Cell*. https://doi.org/10.1016/j.cell.2012.02.042

Praskova, M., Xia, F., & Avruch, J. (2008). MOBKL1A/MOBKL1B Phosphorylation by MST1 and MST2 Inhibits Cell Proliferation. *Current Biology*, *18*(5), 311–321. https://doi.org/10.1016/j.cub.2008.02.006

Premsrirut, P. K., Dow, L. E., Kim, S. Y., Camiolo, M., Malone, C. D., Miething, C., Scuoppo, C., Zuber, J., Dickins, R. A., Kogan, S. C., Shroyer, K. R., Sordella, R., Hannon, G. J., & Lowe, S. W. (2011). A rapid and scalable system for studying gene function in mice using conditional RNA interference. *Cell*, *145*(1), 145–158. https://doi.org/10.1016/j.cell.2011.03.012

Punt, C. J. A. A., Koopman, M., & Vermeulen, L. (2016). From tumour heterogeneity to advances in precision treatment of colorectal cancer. *Nature Reviews Clinical Oncology*, *14*(4), 235–246. https://doi.org/10.1038/nrclinonc.2016.171

Ratziu, V., Lalazar, A., Wong, L., Dang, Q., Collins, C., Shaulian, E., Jensen, S., & Friedman, S. L. (1998). Zf9, a Kruppel-like transcription factor up-regulated in vivo during early hepatic fibrosis. *Proceedings of the National Academy of Sciences of the United States of America*. https://doi.org/10.1073/pnas.95.16.9500

Reeves, H. L., Narla, G., Ogunbiyi, O., Haq, A. I., Katz, A., Benzeno, S., Hod, E., Harpaz, N., Goldberg, S., Tal-Kremer, S., Eng, F. J., Arthur, M. J. P., Martignetti, J. A., & Friedman, S. L. (2004). Kruppel-Like Factor 6 (KLF6) Is a Tumor-Suppressor Gene Frequently Inactivated in Colorectal Cancer. *Gastroenterology*. https://doi.org/10.1053/j.gastro.2004.01.005

Ricci-Vitiani, L., Lombardi, D. G., Pilozzi, E., Biffoni, M., Todaro, M., Peschle, C., & De Maria, R. (2007). Identification and expansion of human colon-cancer-initiating cells. *Nature*, *445*(7123), 111–115. https://doi.org/10.1038/nature05384

Roose, J., Molenaar, M., Peterson, J., Hurenkamp, J., Brantjes, H., Moerer, P., van de Wetering, M., Destrée, O., & Clevers, H. (1998). The Xenopus Wnt effector XTcf-3 interacts with Groucho-related transcriptional repressors. *Nature*, *395*(6702), 608–612. https://doi.org/10.1038/26989

Roper, J., Tammela, T., Akkad, A., Almeqdadi, M., Santos, S. B., Jacks, T., & Yilmaz, Ö.

H. (2018). Colonoscopy-based colorectal cancer modeling in mice with CRISPR-Cas9 genome editing and organoid transplantation. *Nature Protocols*. https://doi.org/10.1038/nprot.2017.136

Roper, J., Tammela, T., Cetinbas, N. M., Akkad, A., Roghanian, A., Rickelt, S., Almeqdadi, M., Wu, K., Oberli, M. A., Sánchez-Rivera, F., Park, Y. K., Liang, X., Eng, G., Taylor, M. S., Azimi, R., Kedrin, D., Neupane, R., Beyaz, S., Sicinska, E. T., … Yilmaz, Ö. H. (2017). In vivo genome editing and organoid transplantation models of colorectal cancer and metastasis. *Nature Biotechnology*. https://doi.org/10.1038/nbt.3836

Rosenbluh, J., Nijhawan, D., Cox, A. G., Li, X., Neal, J. T., Schafer, E. J., Zack, T. I., Wang, X., Tsherniak, A., Schinzel, A. C., Shao, D. D., Schumacher, S. E., Weir, B. A., Vazquez, F., Cowley, G. S., Root, D. E., Mesirov, J. P., Beroukhim, R., Kuo, C. J., … Hahn, W. C. (2012). β-Catenin-driven cancers require a YAP1 transcriptional complex for survival and tumorigenesis. *Cell*, *151*(7), 1457–1473. https://doi.org/10.1016/j.cell.2012.11.026

Sanchez-Rivera, F. J., Papagiannakopoulos, T., Romero, R., Tammela, T., Bauer, M. R., Bhutkar, A., Joshi, N. S., Subbaraj, L., Bronson, R. T., Xue, W., & Jacks, T. (2014). Rapid modelling of cooperating genetic events in cancer through somatic genome editing. *Nature*. https://doi.org/10.1038/nature13906

Sasaki, N., Sachs, N., Wiebrands, K., Ellenbroek, S. I. J., Fumagalli, A., Lyubimova, A., Begthel, H., van den Born, M., van Es, J. H., Karthaus, W. R., Li, V. S. W., López-Iglesias, C., Peters, P. J., van Rheenen, J., van Oudenaarden, A., & Clevers, H. (2016). Reg4+ deep crypt secretory cells function as epithelial niche for Lgr5+ stem cells in colon. *Proceedings of the National Academy of Sciences of the United States of America*, *4*, 201607327. https://doi.org/10.1073/pnas.1607327113

Sato, T., Van Es, J. H., Snippert, H. J., Stange, D. E., Vries, R. G., Van Den Born, M., Barker, N., Shroyer, N. F., Van De Wetering, M., & Clevers, H. (2011). Paneth cells constitute the niche for Lgr5 stem cells in intestinal crypts. *Nature*. https://doi.org/10.1038/nature09637

Schepers, A. G., Snippert, H. J., Stange, D. E., Van Den Born, M., Van Es, J. H., Van De Wetering, M., Clevers, H., & Schepers, A. G., Snippert, H. J., Stange, D. E., Born, M. van den, Es, J. H. van, Wetering, M. van de, and Clevers, H. (2012). Lineage Tracing Reveals Lgr5+ Stem Cell Activity in Mouse Intestinal Adenomas. *Science*, *337*(6095), 730–735. https://doi.org/10.1126/science.1224676

Schindelin, J., Arganda-Carreras, I., Frise, E., Kaynig, V., Longair, M., Pietzsch, T., Preibisch, S., Rueden, C., Saalfeld, S., Schmid, B., Tinevez, J. Y., White, D. J., Hartenstein, V., Eliceiri, K., Tomancak, P., & Cardona, A. (2012). Fiji: An open-source platform for biological-image analysis. In *Nature Methods*. https://doi.org/10.1038/nmeth.2019

Schlegelmilch, K., Mohseni, M., Kirak, O., Pruszak, J., Rodriguez, J. R., Zhou, D.,

Kreger, B. T., Vasioukhin, V., Avruch, J., Brummelkamp, T. R., & Camargo, F. D. (2011). Yap1 acts downstream of α-catenin to control epidermal proliferation. *Cell*, *144*(5), 782–795. https://doi.org/10.1016/j.cell.2011.02.031

Schneider, C. A., Rasband, W. S., & Eliceiri, K. W. (2012). NIH Image to ImageJ: 25 years of image analysis. In *Nature Methods*. https://doi.org/10.1038/nmeth.2089

Schwank, G., Koo, B. K., Sasselli, V., Dekkers, J. F., Heo, I., Demircan, T., Sasaki, N., Boymans, S., Cuppen, E., Van Der Ent, C. K., Nieuwenhuis, E. E. S., Beekman, J. M., & Clevers, H. (2013). Functional repair of CFTR by CRISPR/Cas9 in intestinal stem cell organoids of cystic fibrosis patients. *Cell Stem Cell*. https://doi.org/10.1016/j.stem.2013.11.002

Seno, H., Miyoshi, H., Brown, S. L., Geske, M. J., Colonna, M., & Stappenbeck, T. S. (2009). Efficient colonic mucosal wound repair requires Trem2 signaling. *Proceedings of the National Academy of Sciences of the United States of America*. https://doi.org/10.1073/pnas.0803343106

Sergushichev, A. A. (2016). An algorithm for fast preranked gene set enrichment analysis using cumulative statistic calculation. *BioRxiv*. https://doi.org/10.1101/060012

Serra, D., Mayr, U., Boni, A., Lukonin, I., Rempfler, M., Challet Meylan, L., Stadler, M. B., Strnad, P., Papasaikas, P., Vischi, D., Waldt, A., Roma, G., & Liberali, P. (2019). Self-organization and symmetry breaking in intestinal organoid development. *Nature*. https://doi.org/10.1038/s41586-019-1146-y

Shalem, O., Sanjana, N. E., Hartenian, E., Shi, X., Scott, D. A., Mikkelsen, T. S., Heckl, D., Ebert, B. L., Root, D. E., Doench, J. G., & Zhang, F. (2014). Genome-scale CRISPR-Cas9 knockout screening in human cells. *Science*, *343*(6166), 84–87. https://doi.org/10.1126/science.1247005

Shalhout, S. Z., Yang, P. Y., Grzelak, E. M., Nutsch, K., Shao, S., Zambaldo, C., Iaconelli, J., Ibrahim, L., Stanton, C., Chadwick, S. R., Chen, E., DeRan, M., Li, S., Hull, M., Wu, X., Chatterjee, A. K., Shen, W., Camargo, F. D., Schultz, P. G., & Bollong, M. J. (2021). YAP-dependent proliferation by a small molecule targeting annexin A2. *Nature Chemical Biology*. https://doi.org/10.1038/s41589-021-00755-0

Shimokawa, M., Ohta, Y., Nishikori, S., Matano, M., Takano, A., Fujii, M., Date, S., Sugimoto, S., Kanai, T., & Sato, T. (2017). Visualization and targeting of LGR5 + human colon cancer stem cells. *Nature*, 1–21. https://doi.org/10.1038/nature22081

Shmelkov, S. V., Butler, J. M., Hooper, A. T., Hormigo, A., Kushner, J., Milde, T., St Clair, R., Baljevic, M., White, I., Jin, D. K., Chadburn, A., Murphy, A. J., Valenzuela, D. M., Gale, N. W., Thurston, G., Yancopoulos, G. D., D'Angelica, M., Kemeny, N., Lyden, D., & Rafii, S. (2008). CD133 expression is not restricted to stem cells, and both CD133 + and CD133- metastatic colon cancer cells initiate tumors. *Journal of*

Clinical Investigation. https://doi.org/10.1172/JCI34401

Siegel, R. L., Miller, K. D., Goding Sauer, A., Fedewa, S. A., Butterly, L. F., Anderson, J. C., Cercek, A., Smith, R. A., & Jemal, A. (2020). Colorectal cancer statistics, 2020. *CA: A Cancer Journal for Clinicians*. https://doi.org/10.3322/caac.21601

Siegel, R. L., Miller, K. D., & Jemal, A. (2020). Cancer statistics, 2020. *CA: A Cancer Journal for Clinicians*. https://doi.org/10.3322/caac.21590

Siegmund, K., & Marjoram, P. (2009). Inferring clonal expansion and cancer stem cell dynamics from DNA methylation patterns in colorectal cancers. *Proceedings of the National Academy of Sciences*, *106*(12), 4828–4833. http://www.pnas.org/content/106/12/4828.short

Siravegna, G., Mussolin, B., Buscarino, M., Corti, G., Cassingena, A., Crisafulli, G., Ponzetti, A., Cremolini, C., Amatu, A., Lauricella, C., Lamba, S., Hobor, S., Avallone, A., Valtorta, E., Rospo, G., Medico, E., Motta, V., Antoniotti, C., Tatangelo, F., … Bardelli, A. (2015). Clonal evolution and resistance to EGFR blockade in the blood of colorectal cancer patients. *Nature Medicine*, *21*(7), 795–801. https://doi.org/10.1038/nm.3870

Somers, A., Jean, J. C., Sommer, C. A., Omari, A., Ford, C. C., Mills, J. A., Ying, L., Sommer, A. G., Jean, J. M., Smith, B. W., Lafyatis, R., Demierre, M. F., Weiss, D. J., French, D. L., Gadue, P., Murphy, G. J., Mostoslavsky, G., & Kotton, D. N. (2010). Generation of transgene-free lung disease-specific human induced pluripotent stem cells using a single excisable lentiviral stem cell cassette. *Stem Cells*. https://doi.org/10.1002/stem.495

Soneson, C., Love, M. I., & Robinson, M. D. (2015). Differential analyses for RNA-seq: transcript-level estimates improve gene-level inferences. *F1000Research*. https://doi.org/10.12688/f1000research.7563.1

Sottoriva, A., Kang, H., Ma, Z., Graham, T. a, Salomon, M. P., Zhao, J., Marjoram, P., Siegmund, K., Press, M. F., Shibata, D., & Curtis, C. (2015). A Big Bang model of human colorectal tumor growth. *Nature Genetics*, *47*(3), 209–216. https://doi.org/10.1038/ng.3214

Sottoriva, A., Spiteri, I., Shibata, D., Curtis, C., & Tavaré, S. (2013). Single-molecule genomic data delineate patient-specific tumor profiles and cancer stem cell organization. *Cancer Research*, *73*(1), 41–49. https://doi.org/10.1158/0008-5472.CAN-12-2273

Stein, C., Bardet, A. F., Roma, G., Bergling, S., Clay, I., Ruchti, A., Agarinis, C., Schmelzle, T., Bouwmeester, T., Schübeler, D., & Bauer, A. (2015). YAP1 Exerts Its Transcriptional Control via TEAD-Mediated Activation of Enhancers. *PLoS Genetics*, *11*(8). https://doi.org/10.1371/journal.pgen.1005465

Steinhardt, A. A., Gayyed, M. F., Klein, A. P., Dong, J., Maitra, A., Pan, D., Montgomery,

E. A., & Anders, R. A. (2008). Expression of Yes-associated protein in common solid tumors. *Human Pathology*, *39*(11), 1582–1589. https://doi.org/10.1016/j.humpath.2008.04.012

Tamai, K, Semenov, M., Kato, Y., Spokony, R., Liu, C., Katsuyama, Y., Hess, F., Saint-Jeannet, J. P., & He, X. (2000). LDL-receptor-related proteins in Wnt signal transduction. *Nature*, *407*(6803), 530–535. https://doi.org/10.1038/35035117

Tamai, Keiko, Zeng, X., Liu, C., Zhang, X., Harada, Y., Chang, Z., & He, X. (2004). A mechanism for Wnt coreceptor activation. *Molecular Cell*, *13*(1), 149–156. https://doi.org/10.1016/s1097-2765(03)00484-2

Tapon, N., Harvey, K. F., Bell, D. W., Wahrer, D. C. R., Schiripo, T. A., Haber, D. A., & Hariharan, I. K. (2002). salvador promotes both cell cycle exit and apoptosis in Drosophila and is mutated in human cancer cell lines. *Cell*, *110*(4), 467–478. https://doi.org/10.1016/S0092-8674(02)00824-3

Tauriello, D. V. F., Jordens, I., Kirchner, K., Slootstra, J. W., Kruitwagen, T., Bouwman, B. A. M., Noutsou, M., Rüdiger, S. G. D., Schwamborn, K., Schambony, A., & Maurice, M. M. (2012). Wnt/β-catenin signaling requires interaction of the Dishevelled DEP domain and C terminus with a discontinuous motif in Frizzled. *Proceedings of the National Academy of Sciences of the United States of America*, *109*(14), E812-20. https://doi.org/10.1073/pnas.1114802109

Thompson, B. J., & Cohen, S. M. (2006). The Hippo Pathway Regulates the bantam microRNA to Control Cell Proliferation and Apoptosis in Drosophila. *Cell*. https://doi.org/10.1016/j.cell.2006.07.013

Todaro, M., Gaggianesi, M., Catalano, V., Benfante, A., Iovino, F., Biffoni, M., Apuzzo, T., Sperduti, I., Volpe, S., Cocorullo, G., Gulotta, G., Dieli, F., De Maria, R., & Stassi, G. (2014). CD44v6 is a marker of constitutive and reprogrammed cancer stem cells driving colon cancer metastasis. *Cell Stem Cell*. https://doi.org/10.1016/j.stem.2014.01.009

Udan, R. S., Kango-Singh, M., Nolo, R., Tao, C., & Halder, G. (2003). Hippo promotes proliferation arrest and apoptosis in the Salvador/Warts pathway. *Nature Cell Biology*, *5*(10), 914–920. https://doi.org/10.1038/ncb1050

van Es, J. H., Haegebarth, A., Kujala, P., Itzkovitz, S., Koo, B.-K., Boj, S. F., Korving, J., van den Born, M., van Oudenaarden, A., Robine, S., & Clevers, H. (2012). A Critical Role for the Wnt Effector Tcf4 in Adult Intestinal Homeostatic Self-Renewal. *Molecular and Cellular Biology*. https://doi.org/10.1128/mcb.06288-11

Varelas, X., Miller, B. W., Sopko, R., Song, S., Gregorieff, A., Fellouse, F. A., Sakuma, R., Pawson, T., Hunziker, W., McNeill, H., Wrana, J. L., & Attisano, L. (2010). The Hippo Pathway Regulates Wnt/β-Catenin Signaling. *Developmental Cell*, *18*(4), 579–591. https://doi.org/10.1016/j.devcel.2010.03.007

Vermeulen, L., De Sousa E Melo, F., van der Heijden, M., Cameron, K., de Jong, J. H., Borovski, T., Tuynman, J. B., Todaro, M., Merz, C., Rodermond, H., Sprick, M. R., Kemper, K., Richel, D. J., Stassi, G., & Medema, J. P. (2010). Wnt activity defines colon cancer stem cells and is regulated by the microenvironment. *Nature Cell Biology*, *12*(5), 468–476. https://doi.org/10.1038/ncb2048

von Gise, A., Lin, Z., Schlegelmilch, K., Honor, L. B., Pan, G. M., Buck, J. N., Ma, Q., Ishiwata, T., Zhou, B., Camargo, F. D., & Pu, W. T. (2012). YAP1, the nuclear target of Hippo signaling, stimulates heart growth through cardiomyocyte proliferation but not hypertrophy. *Proceedings of the National Academy of Sciences*, *109*(7), 2394–2399. https://doi.org/10.1073/pnas.1116136109

Wallingford, J. B., & Habas, R. (2005). The developmental biology of Dishevelled: an enigmatic protein governing cell fate and cell polarity. *Development (Cambridge, England)*, *132*(20), 4421–4436. https://doi.org/10.1242/dev.02068

Walther, A., Johnstone, E., Swanton, C., Midgley, R., Tomlinson, I., & Kerr, D. (2009). Genetic prognostic and predictive markers in colorectal cancer. In *Nature Reviews Cancer*. https://doi.org/10.1038/nrc2645

Wang, L., Shi, S., Guo, Z., Zhang, X., Han, S., Yang, A., Wen, W., & Zhu, Q. (2013). Overexpression of YAP and TAZ Is an Independent Predictor of Prognosis in Colorectal Cancer and Related to the Proliferation and Metastasis of Colon Cancer Cells. *PLoS ONE*. https://doi.org/10.1371/journal.pone.0065539

Weber, J., Öllinger, R., Friedrich, M., Ehmer, U., Barenboim, M., Steiger, K., Heid, I., Mueller, S., Maresch, R., Engleitner, T., Gross, N., Geumann, U., Fu, B., Segler, A., Yuan, D., Lange, S., Strong, A., Rosa, J. D. La, Esposito, I., … Rad, R. (2015). CRISPR/Cas9 somatic multiplex-mutagenesis for high-Throughput functional cancer genomics in mice. *Proceedings of the National Academy of Sciences of the United States of America*. https://doi.org/10.1073/pnas.1512392112

Wehrli, M., Dougan, S. T., Caldwell, K., O'Keefe, L., Schwartz, S., Vaizel-Ohayon, D., Schejter, E., Tomlinson, A., & DiNardo, S. (2000). arrow encodes an LDL-receptor-related protein essential for Wingless signalling. *Nature*, *407*(6803), 527–530. https://doi.org/10.1038/35035110

Wei, X., Shimizu, T., & Lai, Z. C. (2007). Mob as tumor suppressor is activated by Hippo kinase for growth inhibition in Drosophila. *EMBO Journal*, *26*(7), 1772–1781. https://doi.org/10.1038/sj.emboj.7601630

Weirauch, M. T., Yang, A., Albu, M., Cote, A. G., Montenegro-Montero, A., Drewe, P., Najafabadi, H. S., Lambert, S. A., Mann, I., Cook, K., Zheng, H., Goity, A., van Bakel, H., Lozano, J. C., Galli, M., Lewsey, M. G., Huang, E., Mukherjee, T., Chen, X., … Hughes, T. R. (2014). Determination and inference of eukaryotic transcription factor sequence specificity. *Cell*. https://doi.org/10.1016/j.cell.2014.08.009

Wersto, R. P., Liblit, R. L., Deitch, D., & Koss, L. G. (1991). Variability in DNA

measurements in multiple tumor samples of human colonic carcinoma. *Cancer*, *67*(1), 106–115. https://doi.org/10.1002/1097-0142(19910101)67:1<106::AID-CNCR2820670120>3.0.CO;2-I

Wood, L. D., Parsons, D. W., Jones, S., Lin, J., Sjöblom, T., Leary, R. J., Shen, D., Boca, S. M., Barber, T., Ptak, J., Silliman, N., Szabo, S., Dezso, Z., Ustyanksky, V., Nikolskaya, T., Nikolsky, Y., Karchin, R., Wilson, P. A., Kaminker, J. S., … Vogelstein, B. (2007). The genomic landscapes of human breast and colorectal cancers. *Science (New York, N.Y.)*, *318*(5853), 1108–1113. https://doi.org/10.1126/science.1145720

Wu, S., Huang, J., Dong, J., & Pan, D. (2003). hippo encodes a Ste-20 family protein kinase that restricts cell proliferation and promotes apoptosis in conjunction with salvador and warts. *Cell*, *114*(4), 445–456. https://doi.org/10.1016/S0092-8674(03)00549-X

Wu, S., Liu, Y., Zheng, Y., Dong, J., & Pan, D. (2008). The TEAD/TEF family protein Scalloped mediates transcriptional output of the Hippo growth-regulatory pathway. *Developmental Cell*. https://doi.org/10.1016/j.devcel.2008.01.007

Xin, M., Kim, Y., Sutherland, L. B., Murakami, M., Qi, X., McAnally, J., Porrello, E. R., Mahmoud, A. I., Tan, W., Shelton, J. M., Richardson, J. A., Sadek, H. A., Bassel-Duby, R., & Olson, E. N. (2013). Hippo pathway effector Yap promotes cardiac regeneration. *Proceedings of the National Academy of Sciences*, *110*(34), 13839–13844. https://doi.org/10.1073/pnas.1313192110

Xin, M., Kim, Y., Sutherland, L. B., Qi, X., McAnally, J., Schwartz, R. J., Richardson, J. A., Bassel-Duby, R., & Olson, E. N. (2011). Development: Regulation of insulin-like growth factor signaling by Yap governs cardiomyocyte proliferation and embryonic heart size. *Science Signaling*, *4*(196). https://doi.org/10.1126/scisignal.2002278

Xu, T., Wang, W., Zhang, S., Stewart, R. A., & Yu, W. (1995). Identifying tumor suppressors in genetic mosaics: the Drosophila lats gene encodes a putative protein kinase. *Development*, *121*(4), 1053–1063. https://doi.org/10.1101/gad.3.9.1273

Yagi, R., Chen, L. F., Shigesada, K., Murakami, Y., & Ito, Y. (1999). A WW domain-containing Yes-associated protein (YAP) is a novel transcriptional co-activator. *EMBO Journal*. https://doi.org/10.1093/emboj/18.9.2551

Yimlamai, D., Christodoulou, C., Galli, G. G., Yanger, K., Pepe-Mooney, B., Gurung, B., Shrestha, K., Cahan, P., Stanger, B. Z., & Camargo, F. D. (2014). Hippo pathway activity influences liver cell fate. *Cell*, *157*(6), 1324–1338. https://doi.org/10.1016/j.cell.2014.03.060

Yin, F., Yu, J., Zheng, Y., Chen, Q., Zhang, N., & Pan, D. (2013). XSpatial organization of hippo signaling at the plasma membrane mediated by the tumor suppressor merlin/NF2. *Cell*, *154*(6). https://doi.org/10.1016/j.cell.2013.08.025

Yu, C., Yu, J., Yao, X., Wu, W. K., Lu, Y., Tang, S., Li, X., Bao, L., Li, X., Hou, Y., Wu, R., Jian, M., Chen, R., Zhang, F., Xu, L., Fan, F., He, J., Liang, Q., Wang, H., … Wang, J. (2014). Discovery of biclonal origin and a novel oncogene SLC12A5 in colon cancer by single-cell sequencing. *Cell Research*, *24*(6), 701–712. https://doi.org/10.1038/cr.2014.43

Yu, F.-X. X., Zhao, B., & Guan, K.-L. L. (2015). Hippo Pathway in Organ Size Control, Tissue Homeostasis, and Cancer. *Cell*, *163*(4), 811–828. https://doi.org/10.1016/j.cell.2015.10.044

Yu, G., Wang, L. G., Han, Y., & He, Q. Y. (2012). ClusterProfiler: An R package for comparing biological themes among gene clusters. *OMICS A Journal of Integrative Biology*. https://doi.org/10.1089/omi.2011.0118

Yuen, H. F., McCrudden, C. M., Huang, Y. H., Tham, J. M., Zhang, X., Zeng, Q., Zhang, S. D., & Hong, W. J. (2013). TAZ Expression as a Prognostic Indicator in Colorectal Cancer. *PLoS ONE*. https://doi.org/10.1371/journal.pone.0054211

Yui, S., Azzolin, L., Maimets, M., Pedersen, M. T., Fordham, R. P., Hansen, S. L., Larsen, H. L., Guiu, J., Alves, M. R. P., Rundsten, C. F., Johansen, J. V., Li, Y., Madsen, C. D., Nakamura, T., Watanabe, M., Nielsen, O. H., Schweiger, P. J., Piccolo, S., & Jensen, K. B. (2018). YAP/TAZ-Dependent Reprogramming of Colonic Epithelium Links ECM Remodeling to Tissue Regeneration. *Cell Stem Cell*, *22*(1), 35-49.e7. https://doi.org/10.1016/j.stem.2017.11.001

Zanconato, F., Forcato, M., Battilana, G., Azzolin, L., Quaranta, E., Bodega, B., Rosato, A., Bicciato, S., Cordenonsi, M., & Piccolo, S. (2015). Genome-wide association between YAP/TAZ/TEAD and AP-1 at enhancers drives oncogenic growth. *Nature Cell Biology*, *17*(9), 1218–1227. https://doi.org/10.1038/ncb3216

Zhang, B., Halder, S. K., Kashikar, N. D., Cho, Y. J., Datta, A., Gorden, D. L., & Datta, P. K. (2010). Antimetastatic Role of Smad4 Signaling in Colorectal Cancer. *Gastroenterology*. https://doi.org/10.1053/j.gastro.2009.11.004

Zhang, N., Bai, H., David, K. K., Dong, J., Zheng, Y., Cai, J., Giovannini, M., Liu, P., Anders, R. A., & Pan, D. (2010). The Merlin/NF2 Tumor Suppressor Functions through the YAP Oncoprotein to Regulate Tissue Homeostasis in Mammals. *Developmental Cell*, *19*(1), 27–38. https://doi.org/10.1016/j.devcel.2010.06.015

Zhang, W., Gao, Y., Li, P., Shi, Z., Guo, T., Li, F., Han, X., Feng, Y., Zheng, C., Wang, Z., Li, F., Chen, H., Zhou, Z., Zhang, L., & Ji, H. (2014). VGLL4 functions as a new tumor suppressor in lung cancer by negatively regulating the YAP-TEAD transcriptional complex. *Cell Research*, *24*(3), 331–343. https://doi.org/10.1038/cr.2014.10

Zhao, B., Kim, J., Ye, X., Lai, Z. C., & Guan, K. L. (2009). Both TEAD-binding and WW domains are required for the growth stimulation and oncogenic transformation activity of yes-associated protein. *Cancer Research*. https://doi.org/10.1158/0008-

5472.CAN-08-2997

Zhao, B., Li, L., Lu, Q., Wang, L. H., Liu, C. Y., Lei, Q., & Guan, K. L. (2011). Angiomotin is a novel Hippo pathway component that inhibits YAP oncoprotein. *Genes and Development*, *25*(1), 51–63. https://doi.org/10.1101/gad.2000111

Zhao, B., Li, L., Tumaneng, K., Wang, C. Y., & Guan, K. L. (2010). A coordinated phosphorylation by Lats and CK1 regulates YAP stability through SCFβ-TRCP. *Genes and Development*, *24*(1), 72–85. https://doi.org/10.1101/gad.1843810

Zhao, B., Li, L., Wang, L., Wang, C. Y., Yu, J., & Guan, K. L. (2012). Cell detachment activates the Hippo pathway via cytoskeleton reorganization to induce anoikis. *Genes and Development*, *26*(1), 54–68. https://doi.org/10.1101/gad.173435.111

Zhao, B., Wei, X., Li, W., Udan, R. S., Yang, Q., Kim, J., Xie, J., Ikenoue, T., Yu, J., Li, L. L., Zheng, P., Ye, K., Chinnaiyan, A., Halder, G., Lai, Z. C. Z.-C., Guan, K.-L. K. L. K.-L. K.-L., Zhao, B., Wei, X., Wei, X., … Guan, K.-L. K. L. K.-L. K.-L. (2007). Inactivation of YAP oncoprotein by the Hippo pathway is involved in cell contact inhibition and tissue growth control. *Genes & Development*, *21*(21), 2747–2761. https://doi.org/10.1101/gad.1602907

Zhao, B., Ye, X., Yu, J. J., Li, L., Li, W., Li, S., Yu, J. J., Lin, J. D., Wang, C. Y., Chinnaiyan, A. M., Lai, Z. C., & Guan, K. L. (2008). TEAD mediates YAP-dependent gene induction and growth control. *Genes and Development*, *22*(14), 1962–1971. https://doi.org/10.1101/gad.1664408

Zhou, D., Conrad, C., Xia, F., Park, J. S., Payer, B., Yin, Y., Lauwers, G. Y., Thasler, W., Lee, J. T., Avruch, J., & Bardeesy, N. (2009). Mst1 and Mst2 Maintain Hepatocyte Quiescence and Suppress Hepatocellular Carcinoma Development through Inactivation of the Yap1 Oncogene. *Cancer Cell*, *16*(5), 425–438. https://doi.org/10.1016/j.ccr.2009.09.026

Zhou, D., Zhang, Y., Wu, H., Barryg, E., Yin, Y. Y., Lawrence, E., Dawson, D., Willis, J. E., Markowitz, S. D., Camargo, F. D., Avruch, J., Barry, E., Yin, Y. Y., Lawrence, E., Dawson, D., Willis, J. E., Markowitz, S. D., Camargo, F. D., & Avruch, J. (2011). Mst1 and Mst2 protein kinases restrain intestinal stem cell proliferation and colonic tumorigenesis by inhibition of Yes-associated protein (Yap) overabundance. *Proceedings of the National Academy of Sciences of the United States of America*, *108*(49), 1312–1320. https://doi.org/10.1073/pnas.1110428108

Zilionis, R., Nainys, J., Veres, A., Savova, V., Zemmour, D., Klein, A. M., & Mazutis, L. (2017). Single-cell barcoding and sequencing using droplet microfluidics. *Nature Protocols*, *12*(1), 44–73. https://doi.org/10.1038/nprot.2016.154